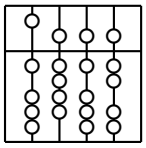

Institut für Informatik

der Technischen Universität München

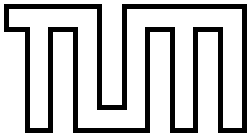

A Computer-Aided System for Planning and Performing Accurate Osteotomies of the Proximal Femur

Dissertation

Heiko Gottschling

Institut für Informatik
der Technischen Universität München

A Computer-Aided System for Planning and Performing Accurate Osteotomies of the Proximal Femur

Heiko Gottschling

Vollständiger Abdruck der von der Fakultät für Informatik der Technischen Universität München zur Erlangung des akademischen Grades eines

Doktors der Naturwissenschaften (Dr. rer. nat.)

genehmigten Dissertation.

Vorsitzender: Univ.-Prof. Dr. Rüdiger Westermann

Prüfer der Dissertation:

1. Univ.-Prof. Dr. Bernd Radig
2. Univ.-Prof. Dr. Achim Schweikard, Universität zu Lübeck

Die Dissertation wurde am 26.01.2006 bei der Technischen Universität München eingereicht und durch die Fakultät für Informatik am 28.06.2006 angenommen.

Abstract

Intertrochanteric osteotomy of the proximal femur is a surgical procedure which aims at realigning the proximal part of the femur (long bone of the thigh) in relation to its distal part through the removal of a bone wedge between the two fragments. In contrast to hip arthroplasty, which is a total replacement of the hip joint, intertrochanteric osteotomy is a joint-saving procedure. Indications for this kind of intervention are numerous especially among young patients, who are to be spared a total hip replacement as long as possible. Due to the complex nature of the realignment, which may involve a correction with up to six degrees of freedom (three rotations and three translations in 3D), this intervention is technically highly demanding for the surgeon.

This thesis presents a novel approach to planning and performing this kind of intervention with the help of a computer-aided navigation system. The FEMOS (FEMur OSteotomy) system, which was developed for this thesis, allows the repositioning of the proximal fragment to be planned with all six degrees of freedom, based solely on two calibrated fluoroscopic images acquired intraoperatively. Using a primitive 3D model reconstructed from these images, the system determines all parameters essential for the procedure, such as the location of the planes forming the bone wedge to be excised and the position of an insertion channel for the fixation plate, with which the fragments are held together after the operation. During the interactive planning phase, the surgeon has full control over the predicted outcome of the intervention, including the effects on the biomechanical axis of the leg and the position of the plate, a visualization of which is overlaid to the fluoroscopic images. Specifying the location of the fixation plate is made especially intuitive through the use of a custom-designed tool, tracked by the localizer, which allows the surgeon to adjust this position for optimal fit directly on the bone surface. Furthermore, by using a special template system, the portion of the procedure during which position tracking is required is minimized. In particular, the critical steps of the intervention, the cutting of the excision planes and the gouging of the channel for the implant, can be performed without the tracking system.

The system was evaluated in a number of in-vitro test series, including a comparison with

the results obtained with the conventional operating method under identical conditions, and a test series conducted with "traditional" navigation techniques (without the special template system). The analysis of the results has shown a noticeable increase in accuracy and reproducibility when using the FEMOS system in comparison to the other methods.

Kurzfassung

Die intertrochantäre Umstellungsosteotomie ist ein chirurgischer Eingriff am Femur (Oberschenkelknochen), in dem die Stellung des proximalen (körpernahen) Fragments in Bezug auf das distale (körperferne) Fragment durch Entnahme eines Knochenkeils verändert werden soll. Im Gegensatz zum künstlichen Hüftgelenkersatz, bei dem das komplette Gelenk ersetzt wird, handelt es sich bei der intertrochantären Osteotomie um einen gelenkerhaltenden Eingriff. Es existieren zahlreiche Indikationen für diesen Eingriff, insbesondere bei jungen Patienten, denen man ein künstliches Hüftgelenk so lange wie möglich ersparen möchte. Da eine solche Umstellung mit bis zu sechs zu beachtenden Freiheitsgraden (drei Rotationen und drei Translationen im Raum) sehr komplex werden kann, erfordert diese Operation großes Geschick vom Operateur.

Die vorliegende Arbeit präsentiert einen neuartigen Ansatz zur Planung und Durchführung einer solchen Operation mithilfe eines computergestützten Navigationssystems. Das für diese Arbeit entwickelte FEMOS -System (FEMur OSteotomy) ermöglicht die Planung der Umstellung des proximalen Fragments in allen sechs Freiheitsgraden. Als Grundlage für die Planung dienen lediglich zwei intraoperativ erstellte kalibrierte Fluoroskopieaufnahmen, aus denen ein einfaches 3D-Modell des Knochens gewonnen wird. Mit diesem Modell kann das System die für die Ausführung des Eingriffs notwendigen Parameter bestimmen, z.B. die Lage der Schnittebenen die den Keil bilden, oder die Position des Kanals, in den die Klinge des zur Fixation der Fragmente verwendeten Implantats eingeführt wird. Während der interaktiven Planungsphase hat der Chirurg volle Kontrolle über das zu erwartende Ergebnis der Operation, darunter die Auswirkungen auf die biomechanischen Beinachse oder die Positionierung der Platte, die in die fluoroskopischen Aufnahmen eingeblendet wird. Die Festlegung der gewünschten Plattenposition wurde durch ein speziell entwickeltes, positionsgetracktes Instrument vereinfacht, das die Anpassung der Platte für optimalen Sitz direkt am Knochen erlaubt. Desweiteren konnte durch Verwendung eines Führungssystems die Phase des Eingriffs, in dem das Trackingsystem verwendet werden muss, soweit minimiert werden, dass die kritischen Schritte ohne dieses durchgeführt werden können. Dies betrifft unter anderem

die Sägeschnitte entlang der Keilebenen, und das Erzeugen des Implantatkanals durch einen Knochenmeißel.

Das System wurde in einer Reihe von in-vitro-Tests ausgewertet, einschließlich eines Vergleichs mit der konventionellen Operationsmethode bei gleichen Bedingungen, und einer Testserie unter Verwendung ”traditioneller” Navigationstechniken (d.h. ohne das spezielle Führungssystem). Die Ergebnisse zeigen, verglichen mit anderen Methoden, einen deutlichen Zuwachs an Genauigkeit und Reproduzierbarkeit bei Verwendung des FEMOS -Systems.

Danksagung

Die vorliegende Arbeit entstand während meiner Arbeit am Lehrstuhl für Bildverstehen und wissensbasierte Systeme der Technischen Universität München.

Meinem Doktorvater Prof. Dr. Achim Schweikard danke ich für die Aufgabenstellung und dafür, dass er mir durch die Aufnahme in seine Arbeitsgruppe ermöglicht hat, dieses interessante Thema zu bearbeiten.

Weiterhin danke ich Prof. Dr. Bernd Radig dafür, dass er mir die Gelegenheit gegeben hat, meine Arbeit am Lehrstuhl nach Prof. Schweikards Weggang nach Lübeck weiterzuführen.

Mein besonderer Dank gilt Dr. Rainer Burgkart vom Klinikum rechts der Isar, der die eigentliche Idee für diese Arbeit hatte. Ohne die enge Zusammenarbeit mit ihm wäre dieses Projekt nicht durchführbar gewesen. Insbesondere danke ich ihm für seine stete Diskussionsbereitschaft und sein motivierendes Engagement, und nicht zuletzt für die Durchsicht dieser Arbeit nach medizinischen Gesichtspunkten.

Desweiteren danke ich meinem Kollegen Dr. Michael Roth, der mir während der ganzen Zeit als kompetenter Gesprächspartner zur Verfügung stand, für die zahlreichen wichtigen Diskussionen im Zusammenhang mit dieser Arbeit und die große Unterstützung bei allen Versuchen im Klinikum, die im Rahmen des Projekts durchgeführt wurden.

Ebenso bedanke ich mich bei meinen Kollegen, allen voran meinen Zimmergenossen und Freunden Kajetan Berlinger und Freek Stulp, aber genauso Ernst Bartels, Suat Gedikli, Simone Hämmerle, Matthias Wimmer und allen anderen für die sehr angenehme Arbeitsatmosphäre am Lehrstuhl und die nicht immer rein fachlichen Diskussionen, die sich in den vier Jahren ergeben haben :-)

Schließlich danke ich Markus Molitor, der die Arbeit in sprachlicher Hinsicht überprüft hat, für die zahlreichen Hinweise und Verbesserungsvorschläge, die nach meiner Meinung deutlich zur Lesbarkeit beigetragen haben.

München, Januar 2006

Contents

Chapter 1 Introduction

This thesis focuses on a surgical procedure called *intertrochanteric femur osteotomy*, through which deformities and misalignments of the hip joint can be corrected. It presents a novel approach to performing the intervention with the aid of a computer, so that the accuracy and reproducibility as compared to the conventional method are greatly enhanced.

1.1 Motivation

An osteotomy[1] is a surgical intervention involving the cutting of a bone, which is normally employed to realign a bone in relation to a joint. In particular, intertrochanteric femur osteotomy is a procedure in which a bone wedge situated between the trochanters of the femur (long bone of the thigh) is removed, thus causing a realignment of the proximal part of the femur. This is done by first cutting through the entire width of the femur, which yields a proximal and a distal fragment. Then, a second cut is made in the proximal fragment, which in combination with the previous cut forms the wedge which is to be removed. The two fragments can now be shifted and rotated relative to each other until the target position has been reached. Finally, they are fixed together in the new position using a metal implant by inserting the implant's blade into the femur neck and screwing its shaft to the diaphysis of the distal part (see Figure 1.1).

In contrast to a hip-alloarthroplasty, which is a complete replacement of the hip joint with an artificial implant, the femur osteotomy is a joint-saving procedure, since the actual hip joint is left intact. In spite of great advances in total hip replacement, indications for joint-saving procedures are still numerous especially among young patients who are to be spared a total hip replacement as long as possible [Bur05].

[1] From Greek *osteon* (bone) and *tomos* (cut)

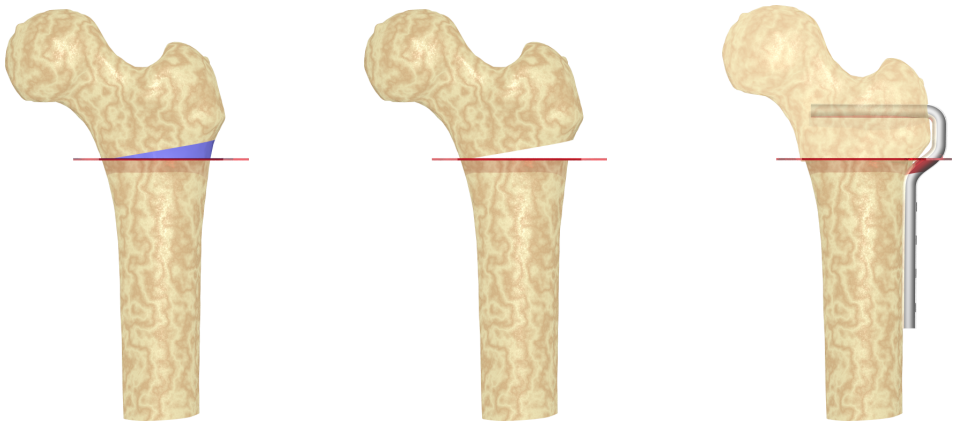

(a) The wedge to be excised

(b) After wedge removal

(c) The metal implant used for fixation of the realigned fragments

Figure 1.1. The femur bone before and after the intervention. The blue bone wedge is removed, and the rearranged fragments are fixed with a metal implant.

1.1.1 Indications

A common indication for intertrochanteric femur osteotomy is a condition called *slipped capital femoral epiphysis* (SCFE), in which the femoral head slips off in posterior direction along the femoral neck. The disease typically affects adolescent children 11 to 16 years of age and is the most common cause of hip disease among this age group [Kor00]. Consequences include pain in the hip, decreased range of motion in the joint and the risk of developing degenerative hip arthritis.

SCFE presents a complex three-dimensional deformity, for the correction of which a variety of techniques are available. Several kinds of osteotomies, applied to various parts of the femur, have been proposed by different authors. These methods include intertrochanteric [Imh57], subcapital [Nis89] and base-of-neck [Kra76] osteotomies. The most common among these is the intertrochanteric variant [Imh57], which is the topic of this thesis.

Various other indications for performing an intertrochanteric osteotomy exist [Bau86]:

- Correction of a hip dysplasia (coxa valga antetorta)
- Aseptic necrosis of the femoral head
- Rotational misalignment of the femur, following a fracture of the femoral shaft or neck
- Painful, early-stage coxarthrosis

1.1.2 Challenges of the Conventional Technique

Performing an intervention of this kind is complex, and requires considerable skills on part of the surgeon. The main points to be considered are:

Implant channel To be able to insert the blade of the metal implant after the osteotomy, a channel must be gouged into the femoral neck. For reasons of stability, this must happen *before* the osteotomy is performed. The difficulty consists in finding the correct position for the channel in the intact femur, so that the implant aligns well with the femoral shaft *after* the osteotomy.

Neck isthmus The neck isthmus is the narrowest portion of the femoral neck through which the blade of the implant passes. To ensure a successful outcome, the internal cortical border of the neck isthmus must not be perforated when the channel is gouged.

Wedge shape Some indications, such as SCFE or an aseptic necrosis of the femoral head, require a complex rotation of the proximal fragment which is difficult to visualize, since the shape of the wedge depends in a non-trivial way on the planning parameters. In this case, the conventional method can hardly account for the correct positioning of the cutting planes.

Biomechanical axis Relocating the proximal part of the femur affects the biomechanical load axis of the femur, which runs through the center of the femoral head [Pal02]. For patients in which the femur head center is displaced due to deformities, the correct biomechanics should be reconstructed. In all other cases, the biomechanical axis should be changed as little as possible through the intervention, so that secondary damage like knee arthrosis caused by a shift in the load distribution is avoided.

Implant positioning After the osteotomy, the fragments are held in place by a metal implant, which is screwed to the femur diaphysis. During the intervention, the implant and the femur diaphysis often do not align properly. In this case, they are either brought together by force, thus changing the position of the fragments, or they are not fixed together as firmly as possible.

This shows that an intertrochanteric femur osteotomy is a complex procedure with a long learning curve. It must be performed with high accuracy in order to achieve the desired therapeutic effect. Accurate execution also helps to promote the healing of the affected bone and helps to avoid complications such as pseudoarthritic bony non-unions.

1.1.3 The FEMOS system

In recent years, a new technique to performing operations demanding high precision has established itself: computer-navigated surgery, which enables the real-time tracking of surgical instruments during an operation. Such systems use specialized hardware, for example an infrared camera in combination with reflective markers which are attached to the instruments, to detect the position and orientation of surgical tools within a given reference frame. Together with image data of the patient acquired preoperatively or intraoperatively, this information is used to guide the surgeon during the intervention, for example by overlaying the images with a visualization of the instrument at its current position [Lan02].

This thesis proposes an integrated system for the planning and navigated execution of a corrective femur osteotomy. To our knowledge, no other approach exists which provides the surgeon with such a high degree of control over the expected result during the planning phase and allows for such a precise execution of this operation, using only intraoperative fluoroscopy as imaging source.

The system is called FEMOS (Femur Osteotomy), and was developed as a joint effort between the *Lehrstuhl für Informatik IX* of the *Technische Universität München* and the *Klinik für Orthopädie und Sportorthopädie* of the *Klinikum Rechts der Isar* in Munich.

1.2 Main Contributions of the Thesis

This thesis advances the state-of-the-art in computer-assisted surgery in the following ways:

1. **The FEMOS system allows osteotomies of the proximal femur to be planned based solely on fluoroscopic images.**

   Existing approaches usually require CT images to be acquired prior to the planning phase, which raises treatment costs and of course results in a higher radiation exposure for the patient. Also, the use of CT imaging demands an intraoperative registration step that is time-consuming and often involves the preoperative implantation of radio-opaque markers, thereby placing additional stress on the patient.

   With the FEMOS system, all information necessary for performing the intervention is obtained intraoperatively from two fluoroscopic images. As will be demonstrated, the model which is reconstructed from these two images is nevertheless sufficient for planning and executing a realignment of the proximal part of the femur with all six degrees of freedom, that is, for realizing any possible change in position or orientation.

2. **The FEMOS system enables optimal positioning of the implant**.

   A common problem with intertrochanteric osteotomy is that the shaft of the metal implant used to secure the fragments after the correction does not properly align with the femur shaft, to which it is screwed. This is mainly due to the fact that the final position of the implant depends to a large extent on the blade channel, which is gouged into the femoral neck *before* the osteotomy is performed. At this stage, it is not possible to accurately predict the fit of the implant as it will be *after* the osteotomy, which changes the relative orientation of the two fragments.

   The approach presented in this thesis solves this problem by letting the surgeon specify the desired postoperative position of the implant directly on the distal fragment during the planning phase, using a specially built instrument. The system uses this information to accurately calculate the optimal location of the blade channel on the proximal fragment before the operation.

3. **The system minimizes the amount of navigation required.**

   The portion of the procedure for which the navigation system is required could be reduced by using a specially designed alignment fixture, that allows the target pose to be ”stored” in a special template tool. The tracking system is used only during image acquisition and the planning phase. *During the actual execution of the intervention, the navigation system is no longer required.* This eliminates the need to use tracked instruments for the operation and hence avoids several common problems, such as references loosening through mechanical stress (vibrations) or visibility problems with the optical tracking system.

4. **The system gives the surgeon maximum control over the expected outcome of the operation.**

   During the planning phase, the surgeon can interactively optimize the parameters defining the osteotomy. The system can immediately calculate the biomechanical effects of the current parameter set (such as changes in leg length, shift of the biomechanical axis). The surgeon can interactively modify the values until he is satisfied with the result.

   This is also true for the parameters specifying the placement of the fixation plate, which are all determined in advance. The predicted location of the implant blade is displayed in the X-ray images, perspectively correct for both the proximal and distal fragments of the femur.

5. **The FEMOS system allows osteotomies to be performed with very high accuracy.**

   A large number of in-vitro tests were conducted to verify the accuracy of the FEMOS system. As these experiments show, the effective parameters of the performed osteotomies correspond very well with the planned parameters, and are superior to the results achievable with comparative methods with respect to accuracy and reproducibility.

1.3 Overview of the Thesis

The remainder of this thesis is organized as follows:

Chapter 2 describes the basics of the intervention and highlights the principal problems which can occur with the conventional approach. It also discusses related research conducted in this area.

Chapter 3 presents the basic FEMOS system devised to address the problems of the conventional practice. It describes in detail the algorithms used in the planning and navigation modules of the system.

Chapter 4 describes the shortcomings of the basic system and the measures taken to improve its usability and precision. The basic system exhibits difficulties with respect to the robustness of the navigated execution of the intervention as well as problems with the implant positioning. This chapter shows how both of these issues were solved.

Chapter 5 presents the results obtained by testing the system on plastic bones and anatomical specimens. The tests also include a comparison with the conventional operating method with respect to accuracy and reproducibility.

Chapter 6 concludes the work presented in this thesis and suggests some starting points for future research.

Chapter 2 Thesis Background

This chapter presents some information on the intervention and the concepts which are necessary to understand the main part of the thesis. It starts with a brief discussion of the general context of the thesis, including a short survey of related work in this area. This is followed by an overview of the method which has conventionally been used to perform a proximal femur osteotomy, pointing out the critical steps of this procedure. Then, the geometrical features of the femur are described, which are used to define a simplified model of the femur, on which all calculations in the subsequent chapters will be based. This is followed by a discussion of how this model is used by the surgeon to specify the desired outcome of the intervention, that is, how the input parameters for the planning algorithm are defined. Finally, this chapter contains a description of the metal implant, which is used for fixation after the operation.

2.1 General Context and Related Work

In a broader context, the system described in this thesis can be classified as a computer-aided surgery (CAS) system. CAS systems, which arose in the last decade of the past century, combine a number of technologies such as medical imaging in its various forms (CT, MR, fluoroscopy), position-sensing devices and advanced visualization techniques, in order to guide the surgeon in planning and performing surgical procedures [Lan02, Gun00]. The main purpose of CAS systems is to increase the accuracy and reproducibility of surgical interventions. Also, the use of CAS systems often makes it possible to use minimally invasive operation techniques, which reduce the physical stress that the patient is exposed to during the intervention.

Another positive effect is that through the use of a CAS system, it is often possible to minimize the surgical team's exposure to radiation [Eyk02]. With many conventional operating techniques it is often necessary to verify the position of surgical instruments inside the patients body by taking a large number of fluoroscopic images intraoperatively. With computer-aided

surgery, the position of the instrument is tracked by the 3D localizer, and hidden parts of the instrument can be visualized in previously acquired images, thereby making the repeated acquisition of images unnecessary.

As computer-aided surgery relies to a large extent on images, it must be ensured that the structures under treatment do not shift or change their shape between the taking of the images and the time of surgery (or the changes have to be compensated, which is difficult). Thus, orthopedics with its rigid bone structures is a field ideally suited for the use of CAS systems.

As proximal femur osteotomy, the intervention which is addressed by the FEMOS system, is itself an orthopedic intervention, this overview focuses on related work in the area of computer-aided orthopedic surgery (CAOS). In recent years, a lot of research has gone into making CAS systems available for a number of orthopedic interventions such as total hip replacement [Hub03, Zhe02, Han99], total knee replacement [Bat04, Spa03], fixation of various bone fractures [Jos98, Haz03, Via95], placement of pedicle screws in the spine [Ami00, Lai00, Mer98], and different kinds of osteotomies [Cro00, Tso98, Wan04, Kep04]. Common to all of them is that they are difficult to perform without the help of a CAS system.

Little research has been done regarding proximal femur osteotomy in connection with computer-aided surgery. However, similar approaches exist for different osteotomies at other locations, such as radius osteotomy, proximal tibia osteotomy or distal femur osteotomy. In the following sections, several existing approaches are briefly presented and discussed. Common to most of them is that they either allow planning only for a limited number of degrees of freedom (as opposed to the full 6 DOF required for proximal femur osteotomy), or are based on CT imaging, the use of which should be avoided if possible due to the harmful effects for the patient as well as for the high costs associated with it. Also, the use of preoperative imaging requires a registration between the coordinate systems of the image and patient to be performed intraoperatively. Using fluoroscopic imaging alone, this step may be avoided if the intervention is planned directly on the images taken intraoperatively, and the reference tracker stays in place the entire time between image acquisition and performance of the procedure.

With the exception of the technique described in section 2.1.1, all of the systems presented are limited to planning and performing the osteotomy alone, without taking into account the placement of the fixation plate.

2.1.1 Distal Radius Osteotomy [Cro00]

Croitoru *et al.* [Cro00] propose a system for performing a computer-aided distal radius osteotomy to correct wrist deformities. With this system, CT scans are preoperatively acquired from both wrists (the deformed and the healthy one). Surface models for both wrists are gen-

erated from the CT scans using isosurface segmentation. The model of the healthy side is mirrored to serve as a template for the deformed side.

In an interactive planning program, the deformed wrist is aligned with the healthy wrist, so that the proximal parts overlap. A cutting plane is selected, along which the model of the deformed radius is cut in two. The distal part of the cut model is then aligned with the healthy template, thereby defining the target pose of the intervention.

A virtual fixation plate is positioned on the model, which will *in vivo* fix the fragments relative to each other. The plate will be fixed with screws, the position of which is uniquely determined by the plate position. Then, the *inverse* transformation of the distal part of the model is applied to the location of the screws. This yields the position of the holes to be drilled on the intact bone, before the fragments are separated. The planning phase is now finished.

During the actual intervention, the preoperatively acquired CT scans are registered with the patient anatomy through a surface-based registration method [Ma 99]. An image-guided surgery system is used to drill the holes for the fixation plate on the intact femur. Afterwards, also with image guidance, the osteotomy is performed. Finally, the fixation plate is affixed to the fragments. The effective position of the fragments is determined by the pre-drilled holes.

According to [Cro00], significant increases in accuracy and reproducibility could be obtained through the system. The intervention described differs from proximal femur osteotomy in so far as the ”template” approach cannot be used for the latter, since it is not normally used to correct unilateral deformities. However, there are similarities with respect to the positioning of the implant. In the approach mentioned, the drill holes are positioned on the intact femur so that the implant is correctly positioned afterwards. In the case of femur osteotomy, this corresponds to the gouging of the blade channel, which must also be done *before* the osteotomy is performed, thereby anticipating the target pose. A drawback of the technique described is the need for preoperative CT scans required for planning, as opposed to the traditional approach for which two X-ray films suffice, and the registration step, which costs additional effort during the intervention.

2.1.2 High Tibial Osteotomy [Tso98]

Tso *et al.* [Tso98] propose a planning and guidance system for high tibial osteotomies. With their system, radio-opaque markers have to be inserted into the tibia prior to the actual intervention. These are needed later for registration purposes. A CT scan of the femoral condyles and the proximal tibia is acquired, from which a surface model is reconstructed via isosurface extraction. This model is used to plan the procedure preoperatively.

In the planning phase, the surgeon can interactively define the two cutting planes, which determine the wedge to be removed. The system is able to predict the result of the currently chosen resection planes by manipulating the surface models accordingly, so that the surgeon can inspect a 3D model of the expected result in advance. The cutting planes are adjusted until the surgeon is satisfied with the predicted result.

Intraoperatively, the implanted markers are located in the patient and registered with the preoperatively taken CT images. An image-guided surgery system is used to perform the operation. Kirschner wires are used as guides for the cutting of the two resection planes. The wires are placed with a tracked drill so that they are tangent to the planned planes.

The results reported in [Tso98] are very good, with a mean absolute error of only 1.2° in varus/valgus between the measured and intended angle[1]. However, only one rotational degree of freedom (varus/valgus) is quantitatively assessed, as opposed to a proximal femur osteotomy with three rotational DOFs. The use of CT imaging and the preoperative implantation of markers in this approach, which are both not needed with the conventional technique, additionally increase stress to the patient.

2.1.3 High Tibial Dome Osteotomy [Wan04]

Wang *et al.* [Wan04] propose a system for high tibial dome osteotomy. Their system is based on fluoroscopic images taken intraoperatively, so no additional CT images are required. Multiple images of the hip joint, the knee and the ankle of the affected limb must be acquired with a calibrated C-arm. Trackers attached to the femur and tibia of the affected limbs provide the coordinate reference frames. Before the osteotomy is performed, a third tracker must be attached so that the fragments can be tracked independently of each other.

From the fluoroscopic images, combined with additional data acquired through pivoting movements of the limbs, several anatomical landmarks are reconstructed which are used to define the coordinate system in which the parameters for the osteotomy are expressed.

Next, the intervention is planned using the fluoroscopic images. The surgeon can specify the axis about which the distal part of the tibia will be rotated, as well as the parameters defining the cylindrical osteotomy cut, which allows the two fragments to be rotated relative to each other.

The intervention is performed with image guidance. The cylindrical-shaped osteotomy surface is created using a tracked drill and chisel. Finally, the two fragments can be repositioned.

[1] In [Tso98], a mean error of 0.1° is reported. However, judging by the table with the detailed results, this number was obtained by averaging signed error values. Averaging the absolute error values yields a mean of 1.2°.

Since trackers were also attached to the fragments, the system can track their position in real-time and display the current state of the correction.

[Wan04] does not provide a numerical analysis of the results obtained with the system. Their approach appears well-thought out and feasible. It does not, however, address the problem of positioning the fixation plate. Furthermore, with three dynamic reference trackers attached at various parts of the leg, the approach presented relies heavily on the tracking system, which may cause problems during the intervention if any of them inadvertently becomes loose.

2.1.4 Upper Tibia Osteotomy [Has02]

An interesting approach is proposed in [Has02], which describes a way of performing an upper tibia osteotomy with a navigation system. The system, however, works without using any images at all *during* the procedure.

Preoperatively, the intervention is planned based on X-ray images. The planned parameters include the correction angle and some characteristics of the tibia plateau. The specified values are stored in the navigation system for later use during the surgery.

The procedure starts in the conventional way with a shortening osteotomy of the fibula. Then, two reference trackers are attached to the leg: one to the distal femur, the other to the tibia. Through passive movements of the hip joint and knee, the rotational centers of the joints are determined. Additionally, several exactly defined points are sampled at the lower leg, using a tracked pointer.

The features collected in this way are used to reconstruct a primitive model of the leg geometry. The osteotomy is then performed with specially constructed saw guides, which are aligned with the help of the tracking system, based on the preoperatively specified osteotomy parameters and the reconstructed model of the leg.

The big advantage of this approach is that it requires neither preoperatively acquired CT scans, nor intraoperatively acquired fluoroscopic images. A similar technique might be feasible for other mono- or birotational osteotomies. However, it is unlikely that the very reduced information gained from the tracking system alone is sufficient for complex 5 to 6 DOF osteotomies at the proximal femur, taking into account the more complex geometry of the femur (especially of the femoral neck) and more technically demanding fragment fixation, which have to be dealt with appropriately.

2.2 The Intervention

An intertrochanteric osteotomy is a procedure which is performed on the femur, the largest and strongest bone of the human body (see Figure 2.1). The femur is part of two joints: at its proximal end the hip joint, which is a multiaxial ball-and-socket joint, and at its distal end the knee joint, which is a hinge joint.

The intervention is performed on the proximal part of the femur, so the distal part with the knee joint is of no interest here. At its proximal end the femur features, most prominently, the near-spherical *femur head*, which together with the acetabulum forms the articulation of the hip joint. It is connected to the rest of the bone through the *femur neck*, the narrowest portion of which is called *neck isthmus*. The two trochanters, *trochanter major* and *trochanter minor*, are bony projections to which muscles are attached. The femur's mid section is called *femur shaft* or *diaphysis*.

The object of a proximal femur osteotomy is to realign the proximal part of the femur in relation to its distal part. This is achieved by cutting the bone in two parts along a plane slightly proximal of the trochanter minor (and distal of the trochanter major, hence *intertrochanteric*). Then, a bone wedge is removed from the proximal fragment, so that the latter can be tilted and repositioned. When the desired new position and orientation of the proximal fragment has been reached, the two parts are fixed in the new position using a metal implant. The implant remains in place until the bone has grown back together, and is then removed normally twelve months later in a second operation.

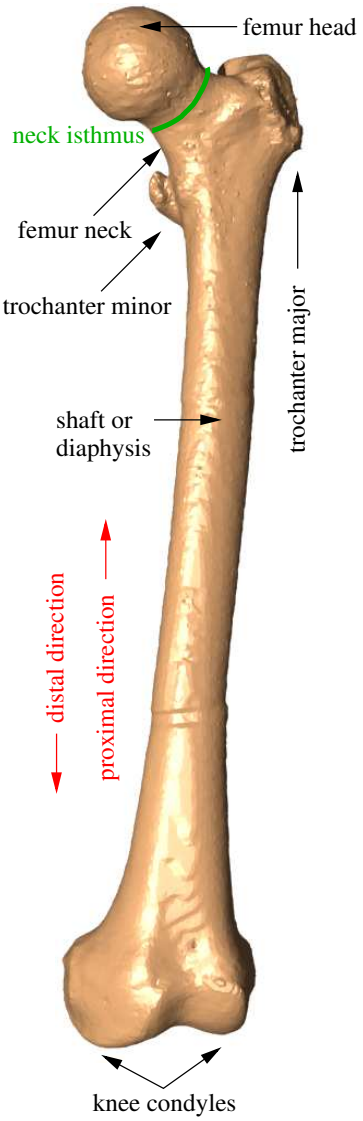

Figure 2.1. A full anterior view of a left femur

Traditionally, the intervention proceeds in the following stages:

1. A channel for the implant is gouged through the femoral neck with a bone chisel.
2. The femur is cut in two along the *osteotomy plane*, thereby creating a proximal and a distal fragment

3. A cut is made along a second plane through the proximal fragment. This plane, the *wedge plane*, intersects the osteotomy plane at an angle, thus forming a bone wedge, which is then removed.

4. The cutting surfaces of the two fragments are brought together. Through the excision of the wedge, their relative orientation has changed. The surgeon adjusts them until the final position has been reached.

5. The fragments are fixed with a metal implant, which is inserted into the gouged channel of the proximal part and then screwed to the distal part of the femur.

The critical stages in this procedure are:

- The gouging of the channel into which the implant will later be inserted. Due to lack of stability of the bone after the proximal fragment has been severed, the channel must be created before the separation. The problem consists in finding the correct position and orientation of the channel so that the implant perfectly aligns with the shaft of the femur *after* the wedge has been removed.

  Also, the femoral neck is quite narrow, so that there is a danger of damaging the bone surface (corticalis) with the chisel. For this reason, the gouging of the channel must be performed with utmost care. Since, during the intervention, the femoral neck is not directly visible to the surgeon, this usually requires multiple fluoroscopic images from different angles to be taken during the chiseling, so that the surgeon can assess the current position of the chisel inside the bone.

- Determining the shape of the wedge. Especially for complex osteotomies (that is, osteotomies involving angular modifications in more than one plane), the shape of the wedge is hard to visualize. However, for a successful outcome of the procedure, high precision in the shape of the wedge is required, as even small angular errors in the orientation of the wedge plane may lead to considerable deviations further away from that plane.

- Screwing the implant to the femur diaphysis. Once the two fragments are in correct position, the implant is screwed to the femur diaphysis. However, since the blade channel had to be gouged before the osteotomy was performed, the alignment of the plate shaft with the diaphysis is usually not optimal. Thus, the process of fixation induces shearing forces between the fragments, which may cause them to shift out of the optimal position.

Figure 2.2 shows some X-ray images of a patient treated with the conventional technique. An intertrochanteric osteotomy was performed to correct the significant valgus osteotomy, which caused the patient severe hip pain. Some problems with the conventional technique become obvious in the postoperative images: first, the position of the implant blade is suboptimal, as it does not pass centrally through the femur neck and hence comes close to perforating the interior corticalis of the neck. Secondly, the osteotomy plane along which the cut was made is situated too far distal, so that it runs into the trochanter minor. As muscles are attached to the trochanter minor, the cut should normally occur clearly proximal of it.

The FEMOS system was designed to address the critical issues of the conventional technique mentioned above, while at the same time deviating as little as possible from this procedure.

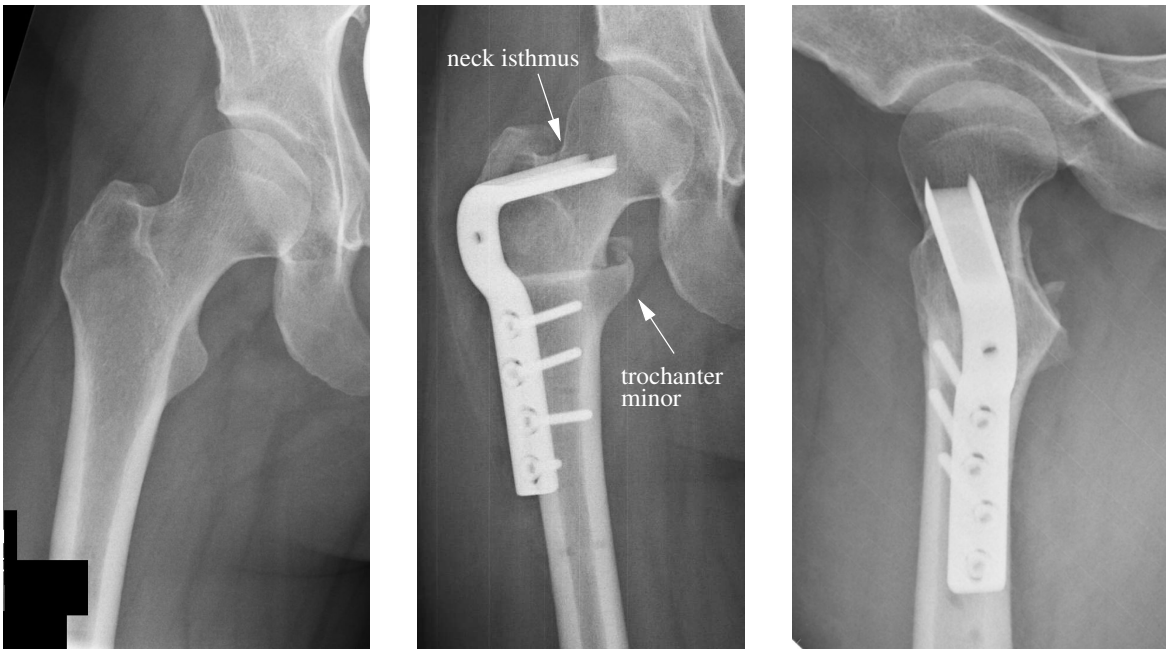

(a) Pre-OP, anterior/posterior (b) Post-OP, anterior/posterior (c) Post-OP, axial

Figure 2.2. X-ray images of a patient who was treated with the conventional technique

2.3 The Femur Geometry

The purpose of the FEMOS system is to modify the geometry of a given femur, according to a set of pre-specified parameters. During the planning phase of the intervention, no real 3D information about the surface of the femur is available due to lack of CT or MR images. Instead, a primitive 3D model of the proximal femur is constructed. This primitive model captures the

essential features of the femur well enough to enable accurate planning and execution of the procedure. The characteristics of the model used are described in the following.

2.3.1 The Abstract Femur Model

Since a bone is an biological object, it is difficult to exactly define geometric features on the femur. In most cases, there are no unambiguous points or straight lines to be found on an organic surface. This problem is dealt with by making the following simplifying assumptions:

- The femoral head is spherical in shape. Although this is only an approximation (for a better approximation see [Men97]), it has proven to be reliable in determining the center of the femoral head from the fluoroscopic images (see [Bur03b]).

- The proximal part of the femoral shaft is shaped like the frustum of an elliptical cone. The main part of the diaphysis, as a special case of this definition, is roughly cylindrical in shape, however it gradually gets wider in one dimension as it approaches the proximal part.

- The femoral neck isthmus has a roughly elliptical cross section. Even though this is only a crude approximation, it is sufficient for the FEMOS system to determine the center of the neck isthmus.

In detail, the abstract model describes the femur through the following features:

Femoral Head Center the center of the femoral head

Shaft Axis the central axis of the cylinder/cone approximating the proximal part of the femur shaft

Neck Isthmus Center the center of the isthmus of the femoral neck

Neck Axis the straight line connecting the femoral head center with the neck isthmus center

All of these features can be reproducibly determined with an accuracy which is sufficient for the intervention [Bur03b]. Figure 2.3 displays the primitive model defined by these features.

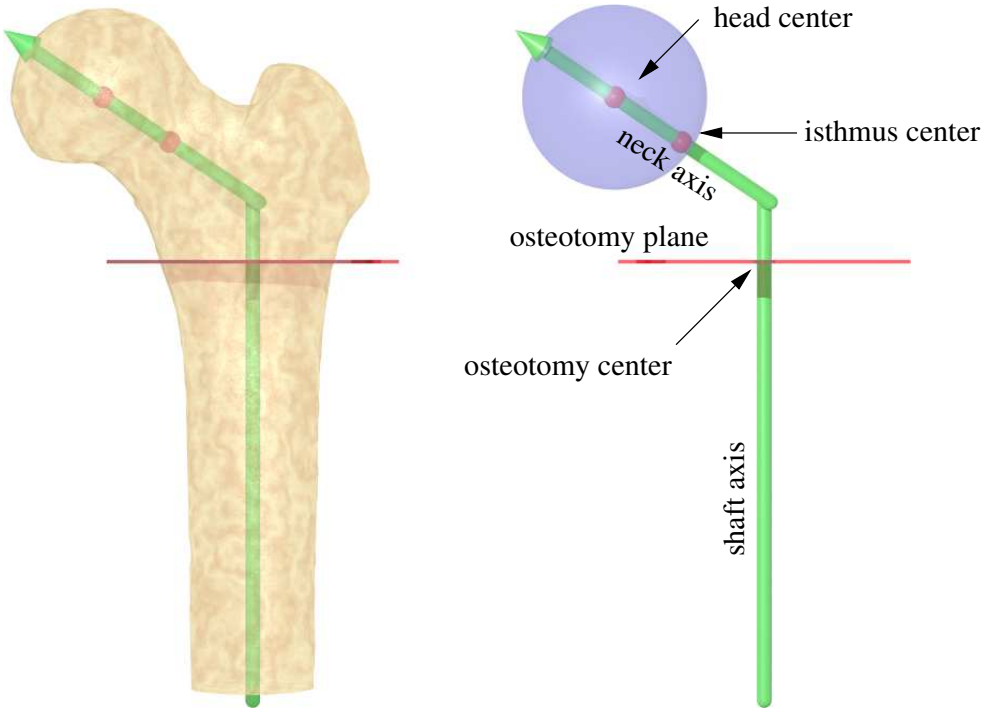

Figure 2.3. The femur model

Another feature needed during the planning phase is the location of the *osteotomy plane*, which is the plane along which the first cut through the femur is made. The location of this plane is not a feature of the femur, but is defined by the surgeon during the planning phase. However, as is obvious from the intervention being called *intertrochanteric* osteotomy, the osteotomy plane will always be chosen to lie in between the trochanters minor and major. Together with the femur shaft axis, the osteotomy plane also determines another important point, the *osteotomy center*, which is the point of intersection between the shaft axis and the osteotomy plane.

2.3.2 Anatomical Directions

The parameters specifying the osteotomy (see section 2.4) describe the effect of the osteotomy as seen from different viewing directions. These directions are defined as follows (all directions refer to a human standing upright):

anterior/posterior (AP) Front-to-back view, the view in which the femur appears when looked at frontally

lateral/medial (LM) From the side, the view in which the femur appears when looking at it from the side

superior/inferior (SI) Top-down view, the view in which the femur appears when looked at from above

These directions are illustrated in Figure 2.4.

2.3.3 The Osteotomy Coordinate System

To be able to specify the parameters of the desired osteotomy numerically, a coordinate system must be chosen. The osteotomy parameters are given in the *osteotomy coordinate system*, which is defined as follows (see Figure 2.4):

- The origin is the osteotomy center.
- The z axis points along the femoral shaft axis in proximal direction.
- The y axis points in anterior-posterior direction of the patient. This direction may not be exactly orthogonal to the femoral shaft axis, however for a normal femur the deviation amounts to only about 2 or 3 degrees. For use in the coordinate system, the y axis is chosen so that it is orthogonal to the z axis and at the same time minimizes the angular difference to the AP (anterior/posterior) vector.
- The x axis is chosen so that (x, y, z) form a right-handed coordinate system.

The rotational parameters describing the osteotomy (see 2.4.1) are defined in terms of projections onto the planes $\mathcal{E}_{xy}$, $\mathcal{E}_{xz}$ and $\mathcal{E}_{yz}$, which are the planes spanned by the base vectors of the coordinate systems.

2.4 Quantifying an Osteotomy

The goal of the intervention is a realignment of the proximal part of the femur in relation to the distal part. Since this change in orientation and position of the proximal fragment is a rigid transformation, it can be described by a 6D pose, the *target pose*, in a suitable coordinate system.

To completely specify the target pose of an osteotomy, three translational and three rotational parameters are required. Taken together, these six parameters uniquely define the target pose in 3D space. The following sections describe the way in which the target pose can be intuitively specified by the surgeon.

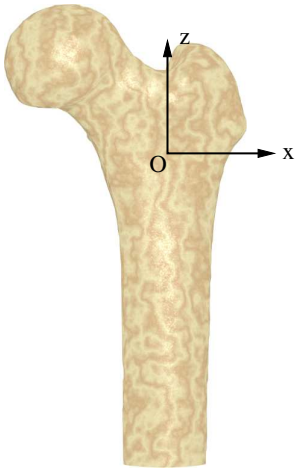

(a) anterior/posterior view with the axes and the origin of the osteotomy coordinate system

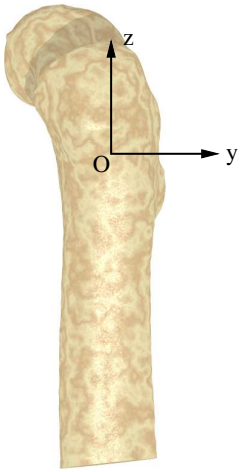

(b) lateral/medial view

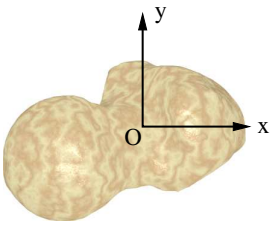

(c) superior/inferior view

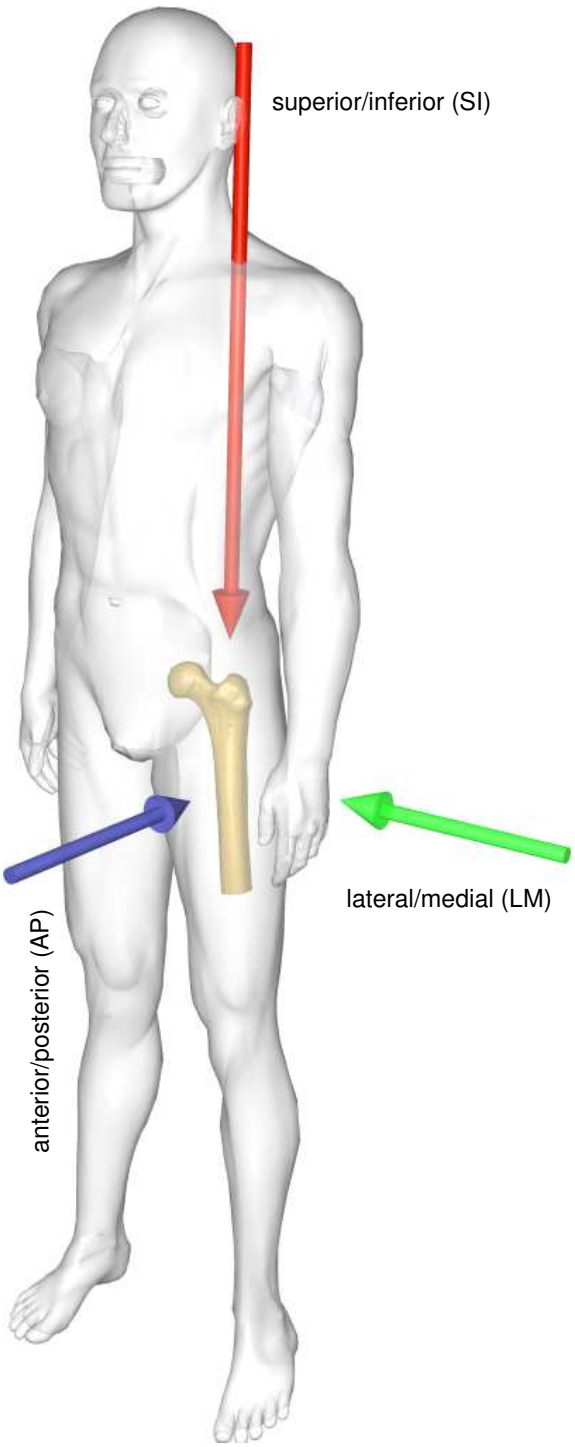

(d) The directions in relation to the human body

Figure 2.4. The anatomical view directions

2.4.1 Rotational Parameters

Traditionally, the rotational part of the desired result of a femur osteotomy has been described by three complementary value pairs, each representing an angular value:

- varus / valgus (ϕ_{varus})
- flexion / extension ($\phi_{flexion}$)
- rotation / derotation ($\phi_{rotation}$)

With each pair, the two values describe transformation in opposing directions, i.e. a valgization is the inverse of a varization and so on. Each value stands for a desired *change* of the femur under treatment, compared to the original femur. The value tuple $(0, 0, 0)$ represents a null osteotomy, that is, no change of the orientation of the proximal part at all.

Taken together, these values completely describe the desired change in orientation of the proximal femur fragment (one could, for example, aim for 15° valgization, 10° flexion and 5° rotation). The following sections discuss these parameters in detail.

2.4.1.1 Varus/Valgus

In case of the *varus/valgus* angle, the femoral neck axis is projected onto the plane $\mathcal{E}_{xz}$ of the osteotomy coordinate system. The varus/valgus angle appears as the angle between the projections of the original neck axis and the transformed neck axis, (see Figure 2.5a, b). If the transformation increases the angle between the neck axis and the shaft axis of the transformed femur compared to the original one, it is called ”valgization”, otherwise ”varization”

For computational purposes, the varus/valgus angle ϕ_{varus} is regarded as a signed angular value. Values of $\phi_{varus} > 0$ denote a varization by ϕ_{varus} degrees, values of $\phi_{varus} < 0$ a valgization by $-\phi_{varus}$ degrees.

2.4.1.2 Flexion/Extension

For the *flexion/extension* angle, the femoral shaft axis (as opposed to the neck axis like in varus/valgus and rotation/derotation) is projected onto the yz plane. The flexion/extension angle appears as the angle between the projection of the original and transformed axis (see Figure 2.5c, d). If the transformation results in proximal fragment being tilted towards the anterior of the patient, it is called *flexion*, otherwise *extension*.

Again, the flexion/extension angle is represented by the signed value $\phi_{flexion}$ with positive values denoting a flexion and negative values denoting an extension.

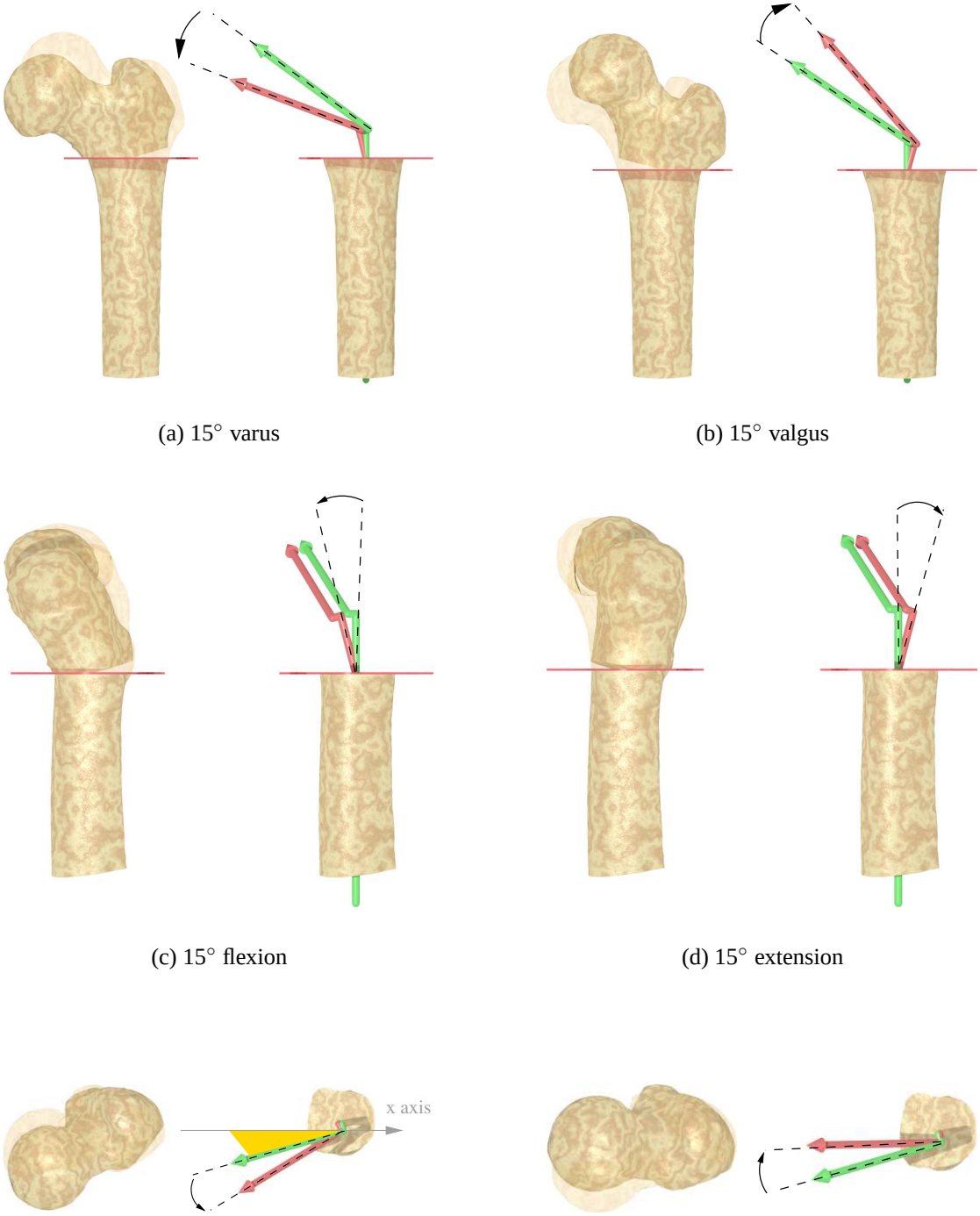

(a) 15° varus

(b) 15° valgus

(c) 15° flexion

(d) 15° extension

(e) 15° rotation. The antetorsion angle is marked yellow.

(f) 15° derotation

Figure 2.5. Overview of the effects of the rotational parameters.

> **Note:** Please observe the difference in the definition of the flexion/extension angle, as opposed to the varus/valgus and rotation/derotation angle: whereas the two latter are defined with respect to the projections of the femoral *neck* axis, the definition of the flexion/extension is based on the projection of the femur *shaft* axis.

2.4.1.3 Rotation/Derotation

With *rotation/derotation*, the angle appears between the projections of the original and transformed neck axis onto the xy plane (see Figure 2.5e, f). Depending on the sense of rotation, it is called rotation or derotation.

The rotation/derotation angle is defined based on the *antetorsion angle*, which is the angle between the projection of the femoral neck axis onto $\mathcal{E}_{xy}$ and the x axis of the reference frame. The antetorsion of a normal femur amounts to between 7° and 12° (see Figure 2.5e). If the transformation increases this angle, it is referred to as rotation, otherwise derotation.

The rotation/derotation angle is represented by the signed angular value $\phi_{rotation}$, which denotes a rotation for positive values of $\phi_{rotation}$ and a derotation for negative values.

2.4.2 Differences to the Conventional Technique

There is an important difference in the way the parameters determining the intervention are handled by the FEMOS system as opposed to the conventional technique[2].

As described in the previous sections, with the FEMOS system, the rotational part of the desired result is determined by the three values varus/valgus, flexion/extension and rotation/derotation in such a way that, after the operation, the changes appear between the preoperative and postoperative femur as projections under different view directions. Each of these three angles can directly be measured in the corresponding projection so that, for example, by taking X-ray images in AP direction before and after the intervention, the angle between the two neck axes would exactly match the originally specified varus/valgus angle (assuming the intervention was accurately performed, of course).

This would not be the case, however, with the conventional operation method. The reason for this is the way in which the cutting planes and the amount of the final rotation are derived from the input values in this case. As can be seen in the description of the operating technique in section 2.2, the orientation of the chisel (and hence of the wedge cutting plane) is based

[2]For reasons of comparison, both kinds were actually implemented in FEMOS , so technically the system works with both ways.

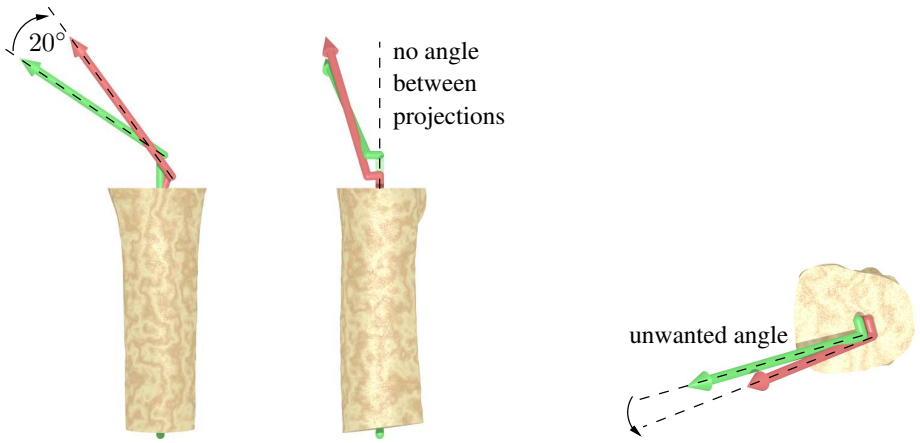

(a) varus/valgus (anterior view) (b) flexion/extension (lateral view) (c) rotation/derotation (superior view)

Figure 2.6. The result of an uncompensated valgization (seq) of 20°. Both flexion (seq) and rotation (seq) were 0°. While the flexion angle (proj) of the result remains unaffected (angle between shaft axes), an unwanted change to the rotation (proj) is introduced (angle between neck axes).

on the values for varus/valgus and flexion/extension by first tilting the chisel in varus/valgus direction and then *subsequently* in flexion/extension direction, both times with the respective angles. Later, after the wedge has been removed, the proximal fragment is rotated relative to the distal fragment by the rotation/derotation angle specified.

With respect to the rotational realignment of the resulting femur — ignoring the translations — this procedure is equivalent to performing consecutive rotations by the specified amounts about the y-axis (varus/valgus), the x-axis (flexion/extension) and z-axis (rotation/derotation) of the osteotomy coordinate system *in this order*. The problem with this approach, however, is that these three transformations are not mutually independent: a rotation of the proximal fragment about the z-axis (corresponding to rotation/derotation) also influences the projection of the femur neck axis in AP direction (corresponding to varus/valgus).

As a consequence, by performing the three transformations in consecutive order, as done with the conventional approach, the angles between the projections of the pre- and postoperative femur do not exactly correspond to the input values. These effects are empirically known, of course, and have so far been clinically compensated for in the planning phase. However, this is usually done without quantitatively assessing the error associated with these circumstances. Either way, it should be noted that the angular values used during the intervention do not exactly correspond to the values measured in the result. To avoid ambiguity, in the rest of

this chapter the angles used in the conventional technique will be marked by *(seq)*, whereas the angles measured between the projections of the neck or shaft axes will be denoted by *(proj)*.

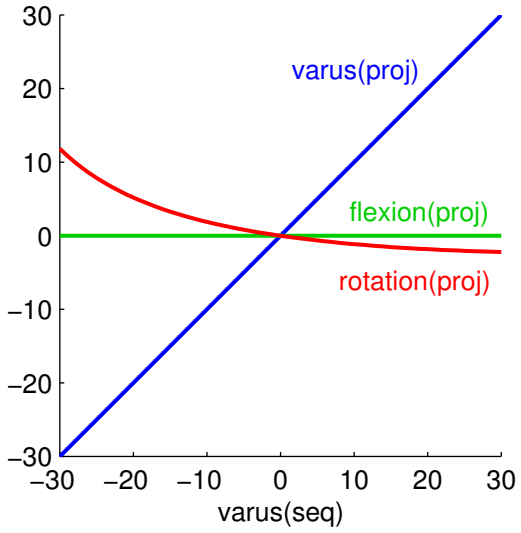

(a) Varying varus/valgus (seq), unwanted effects on flexion (proj) and rotation (proj)

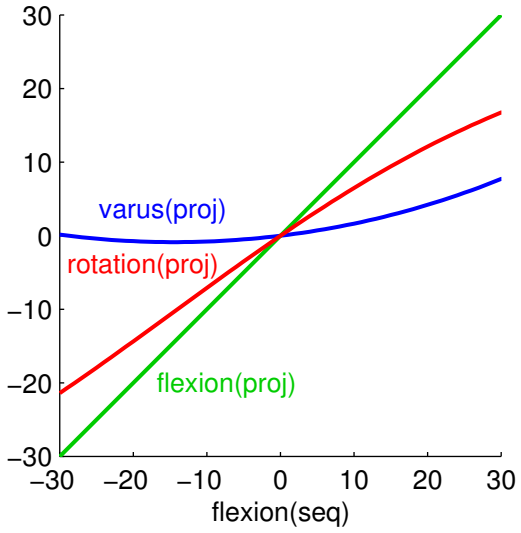

(b) Varying flexion/extension (seq), unwanted effects on varus (proj) and flexion (proj)

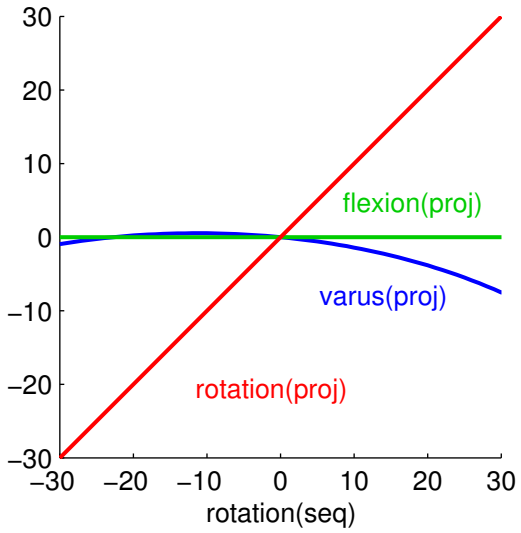

(c) Varying rotation/derotation (seq), unwanted effects on varus (proj) and flexion (proj)

Figure 2.7. Mutual influence of the different parameters in projection. The units on all axes are degrees.

The magnitude of this effect is displayed in Figure 2.7. For each of the three values in ”sequential” mode, the diagrams show how the remaining values are affected if no compensation is applied. The three curves in each graph correspond to the angular amounts (proj) by which the pre- and postoperative femurs differed in the respective projections.

As can be seen in Figure 2.7a, an uncompensated varization/valgization (seq) influences the measured rotation (proj). However, it does not influence the projected flexion/extension angle (proj), owing to the fact that the femoral shaft axis is the z-axis of the osteotomy coordinate system and hence does not change its projected direction when rotated about the y-axis. Similarly, as can be seen in Figure 2.7c, flexion (proj) is not affected by a rotation (seq), as the shaft axis itself is the axis of rotation and therefore remains unchanged. As Figure 2.7b shows, however, an uncompensated flexion (seq) heavily affects both of the other parameters under projection.

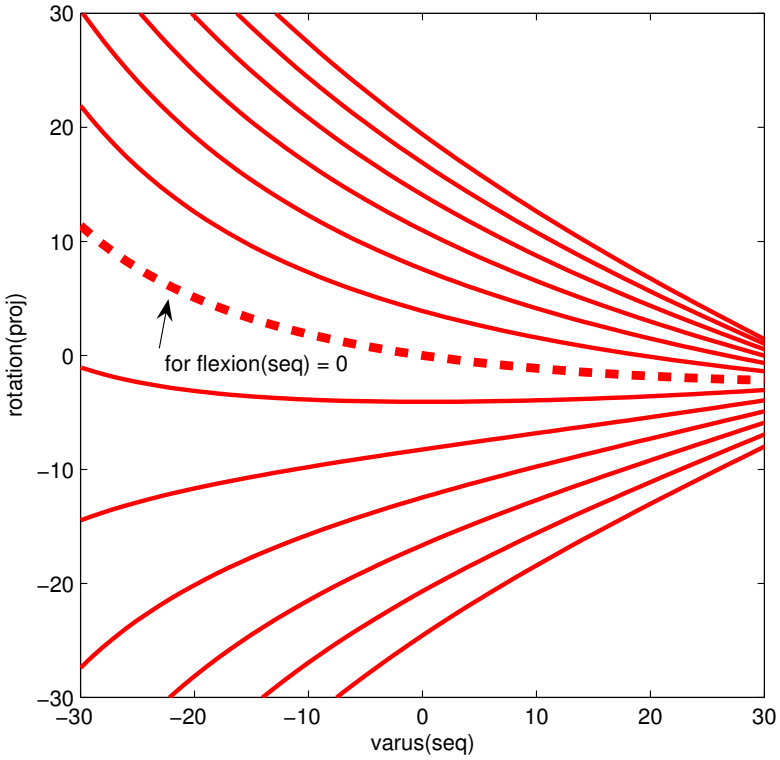

Figure 2.8. Combined influence of varus/valgus (seq) and flexion/extension (seq) on the measured rotation (proj). A single curve depicts the measured rotation for a fixed flexion, and a varus/valgus angle ranging from -30° to 30°. The flexion angle varies in steps of 5° between the curves, ranging from -30° in the topmost curve to 30° in the bottommost. The dashed curve corresponds to a flexion of 0°.

Figure 2.8 displays the influence of a correction with *combined* varus/valgus (seq) and flexion/extension (seq) parameters on the rotation/derotation (proj). As can be seen, the effect is substantial.

We believe the way in which the FEMOS system handles the parameters to be superior to the conventional method, because thus the input parameters actually correspond to the values measured in the result, and therefore the outcome becomes more predictable. For means of comparison, however, the sequential mode of interpreting the planning parameters was also implemented in the FEMOS system. The corresponding calculations are described in section 3.5.3.4.

2.4.3 Translational Parameters

In addition to the rotational parameters specifying the varus/valgus, flexion/extension and rotation/derotation angles, the following translational parameters further specify the desired location of the proximal fragment after the operation (see also Figure 2.9):

- translation in anterior/posterior direction (t_{AP})
- translation in lateral/medial direction (t_{LM})
- translation in superior/inferior direction (t_{SI})

These parameters define the amount by which the proximal part of the femur is to be translated after all of the rotations, defined through the rotational parameters, have been performed.

The entire procedure of determining the target pose of the proximal fragment can be imagined as happening in two stages:

1. A preliminary pose, based on ϕ_{varus}, $\phi_{flexion}$ and $\phi_{rotation}$ ***alone*** is calculated. This preliminary pose is well-defined, in the sense that for any set of values, an unambiguous pose can be determined, following the algorithm which is described in the next chapter.
2. The translation, as defined through t_{AP}, t_{LM} and t_{SI}, is applied.

Both steps combined yield the final target pose.

The values for t_{AP}, t_{LM} and t_{SI} are to be given so that positive values stand for translations in anterior, lateral and superior directions, while negative values represent translations in posterior, medial and inferior direction, respectively.

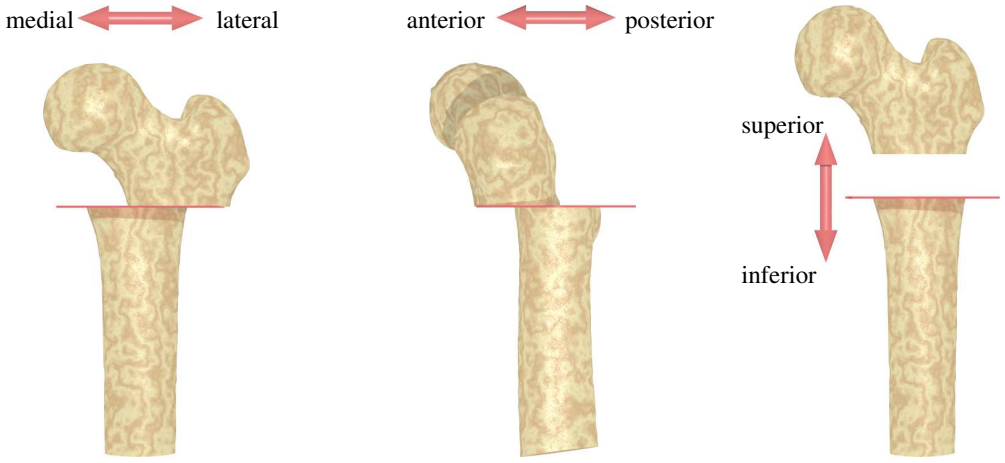

(a) anterior/posterior (b) lateral/medial (c) superior/inferior

Figure 2.9. Translations in the various directions

2.4.4 The Wedge Size

Apart from the values that specify the rotation and translation of the desired result, there is one more parameter governing the shape of the wedge to be cut out: the wedge size w with $0 \leq w \leq 1$ (in some cases, values greater than 1 are possible, see below). The wedge size defines how far the wedge extends into the femoral shaft. The value 0 indicates that no wedge will be excised. A value of 1 means that the wedge extends through the entire width of the femur.

The wedge is formed by two intersecting planes: the wedge plane and the osteotomy plane. While the osteotomy plane remains fixed, different wedge sizes can be created by translating the wedge plane in proximal or distal direction.

As can be seen in Figure 2.10, the wedge size mainly affects the superior/inferior translation of the (already tilted) proximal fragment. The orientation of the fragment remains constant. Traditionally, it has been used to control the shortening/lengthening occurring after the intervention, for example in order to lessen the tension of M. iliopsoas with its distal insertion at the trochanter minor. While the wedge size usually not exceeds $w = 1$, greater values, which result in a larger portion of bone being removed, are sometimes used to achieve extreme shortening. In these cases, the two planes forming the wedge intersect outside the femur, rather than inside as for $0 \leq w \leq 1$.

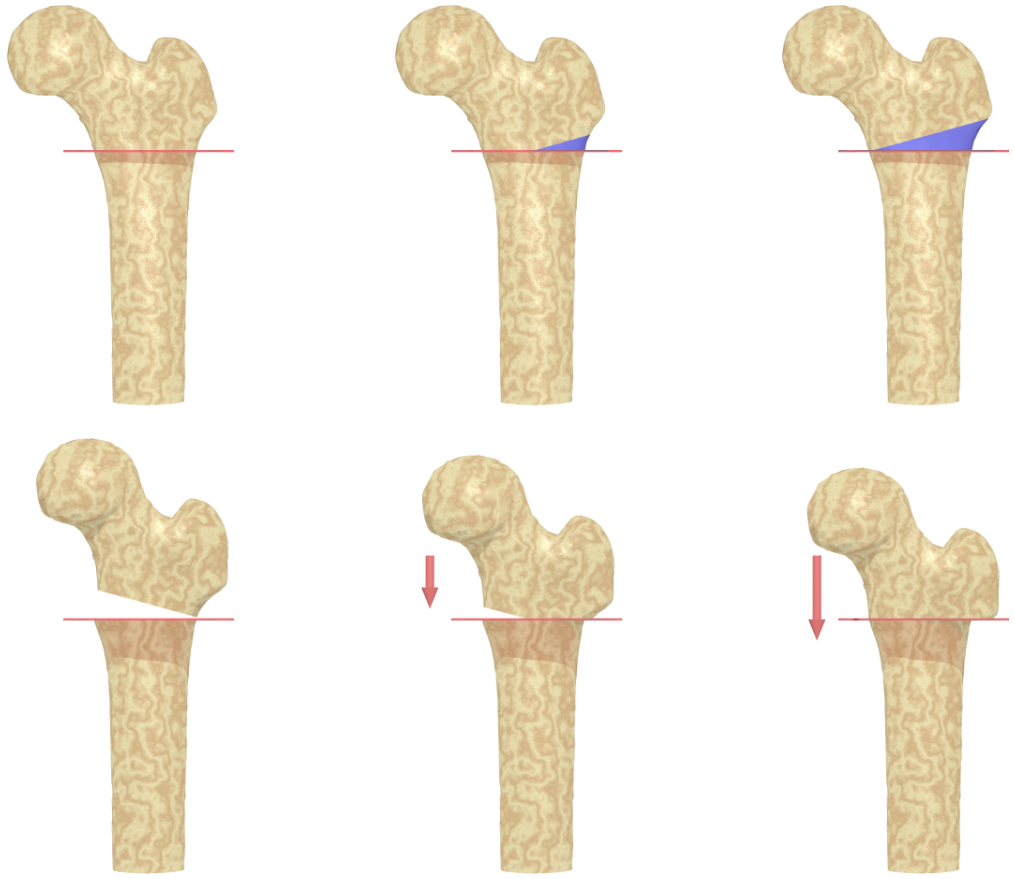

(a) $w = 0$ (no wedge = limiting case, shown for illustrative purpose only)

(b) $w = 0.5$ (half wedge)

(c) $w = 1$ (full wedge)

Figure 2.10. Different wedge sizes. The wedge which is removed is marked in blue. The bottom row displays the femora after the removal of the wedge and realignment of the proximal fragment.

2.5 The Implant

After the osteotomy has been performed, the fragments need to be fixed in their new position. This is done using specially manufactured osteotomy plates, which are L-shaped metal implants (see Figure 2.11). The osteotomy is fixed by inserting the blade of the implant into the femoral neck and then screwing the shaft of the plate to the femur diaphysis. Before the plate can be inserted into the femoral neck, the blade channel must be gouged with a bone chisel. After insertion, the implant sits tight in the channel and the bone fragments are pressed

together and are thus fixed.

Figure 2.11. An assortment of implants as typically used to fix the bone fragments after an osteotomy

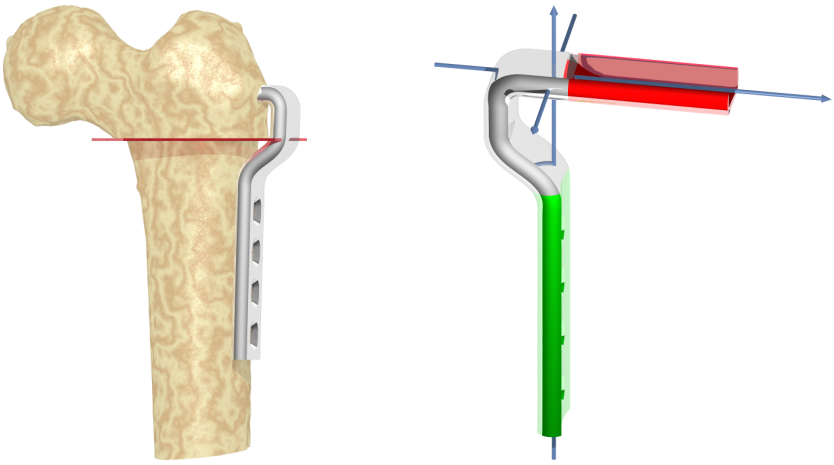

(a) after 15° varization

(b) 3D view, with the implant shaft (green) and the blade (red)

Figure 2.12. The implant, which must be positioned so that its blade goes through the neck and its shaft aligns with the femur diaphysis.

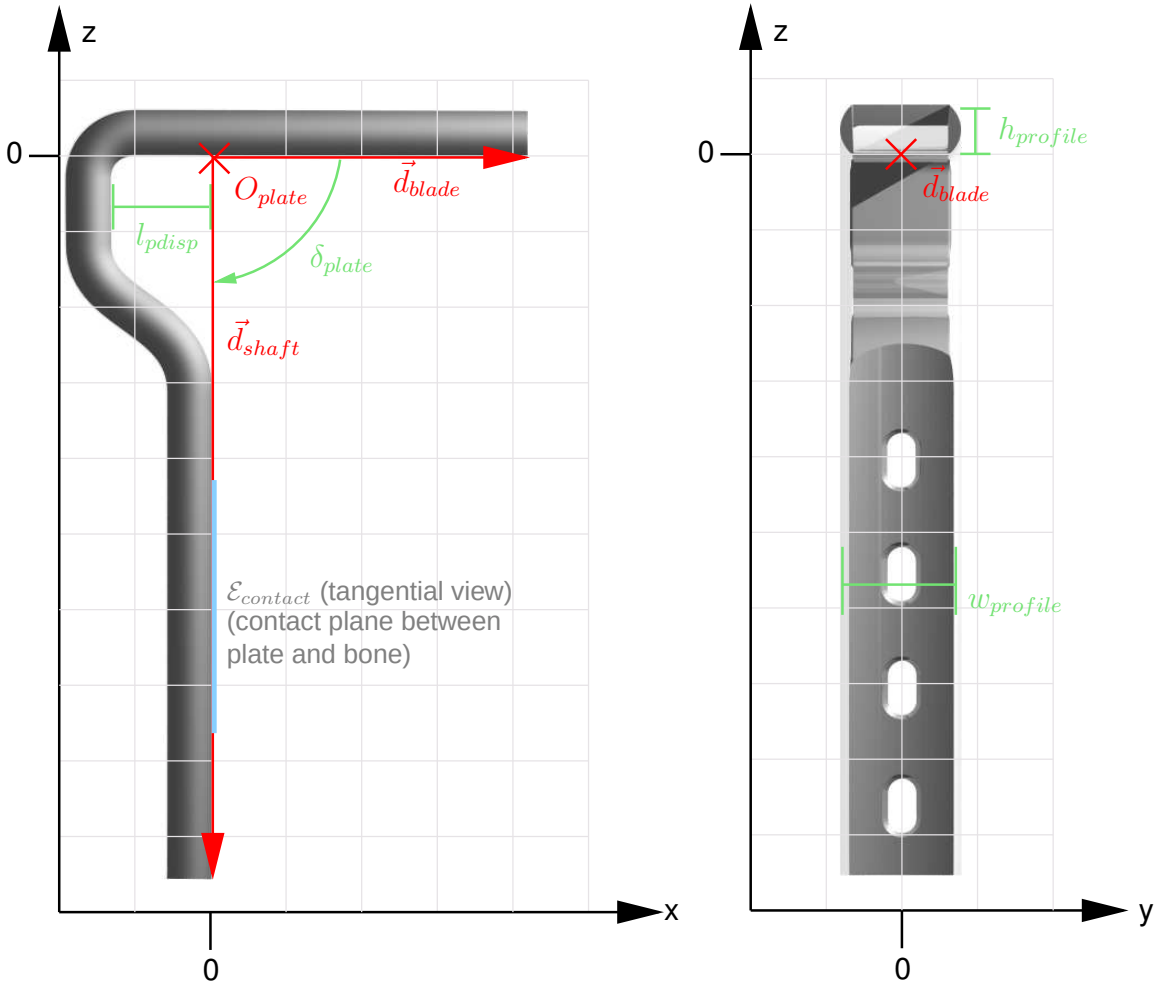

Figure 2.13. The implant geometry in side view (left, view direction = y) and front view (right, view direction = $-x$). The image shows a standard 4-hole osteotomy implant, drawn to scale.

The most important parts of the plate are the *plate shaft*, which is screwed to the femur diaphysis for fixation, and the *plate blade*, which is hammered into the proximal part of the femur (see Figure 2.12). A variety of osteotomy plates exists, which differ with respect to the following properties [Moc95]:

Blade Length Length of the blade. It defines how far the blade protrudes over the plate's shaft plane, which is the plane at which the implant touches the femur shaft. This value may vary to accommodate different lengths of the femur neck.

Total Height Height of the implant, measured from the underside of the blade to the end of the shaft. Longer plates are needed for specific procedures, for example in fracture treatment.

Plate Angle The angle between the implant's blade and shaft. This angle is usually 90° (the effective angle of the implant may be a few degrees less, so that the plate is spread open when it is screwed to the femur diaphysis and thus a greater force is applied to the fragments, which are locked together under tension). Specific indications may also require a plate angle of 95° or 130°.

Displacement The offset of the bent part of the plate in relation to its shaft. The amount of displacement is chosen depending on how far the proximal fragment (trochanter major) protrudes over the distal fragment after the osteotomy.

Profile The width and height of the implant's cross section

Table 2.1 lists the parameters, by which a plate is represented in the FEMOS system. The parameters must always be given in the *plate coordinate system*, which is displayed in Figure 2.13. The plate model defined by these parameters is needed by the system for calculations involving the implant, for example during the implant positioning step.

Parameter	Description
O_{plate}	The plate origin, which corresponds to the origin of the implant coordinate system *PlateCS*. It is situated where the shaft plane meets the underside of the blade.
δ_{blade}	The angle between the blade and the shaft.
$\vec{d}_{blade}$	The vector pointing in the direction of the plate's blade. Anchored at the origin, the vector's tip coincides with the tip of the blade.
$\vec{d}_{shaft}$	The vector pointing in direction of the plate's shaft. When anchored at the plate origin, the vector's tip coincides with the distal end of the plate shaft.
d_{pdisp}	Displacement amount of the plate.
$w_{profile}$	Width of the plate profile
$h_{profile}$	Height of the plate profile
$\mathcal{E}_{contact}$	Tangent plane to the plate shaft. This is the contact plane between the plate and the femur diaphysis. It contains the origin.

Table 2.1. Overview of the features obtained in the 3D reconstruction

Chapter 3 The Basic System

This chapter describes the details of the basic variant of the FEMOS system. The system assists the surgeon in the planning and performance of an intertrochanteric osteotomy, which comprise the acquisition of fluoroscopic images, the interactive planning phase, the actual execution of the operation with the aid of a tracking system and the final assessment of the achieved result. This chapter presents the original implementation of the system, which, however, turned out to have some shortcomings that became obvious during testing. How these weaknesses were eliminated will be discussed in the next chapter.

3.1 System Setup

The FEMOS system is a modular system, which combines several components to achieve its purpose. Its main constituents are:

Tracking System The tracking system obtains the position and orientation of specially prepared medical tools in 3D space. This is done by attaching to the tools specially prepared reflective markers, the position of which can be detected by an infrared camera. The tracking system serves as the link between the real world, in which the intervention is physically performed, and the virtual world of the computer, in which the intervention is planned.

C-arm fluoroscope Fluoroscopy is an imaging modality based on X-ray technology, which makes images visible on a fluorescent screen. Fluoroscopy devices are standard equipment in operating rooms, and are used to intraoperatively acquire images of the patient. The image data is made externally available via a video interface. Using a specially prepared C-arm and its positioning data obtained through the tracking system, it becomes possible to determine the internal and external camera parameters so that the images can be used in image-guided surgery.

Computer System The FEMOS system runs on a PC-based computer. The computer is connected to both the tracking system and the fluoroscopy device, so that it has access to the position data of the surgical instruments and the fluoroscopic images acquired with the C-arm. The computer is used intraoperatively to plan the intervention, and later guides the surgeon during its execution.

The tracking system and the fluoroscopy device are described in detail in the remainder of this section. The main constituents of the system can be seen in Figure 3.1, which displays an overview of the general setup.

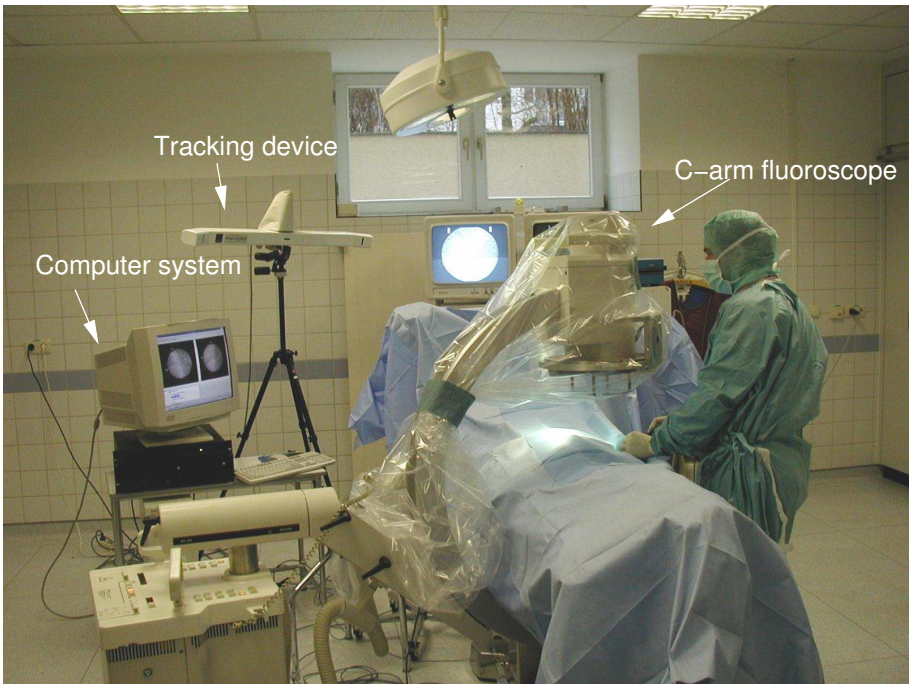

Figure 3.1. System setup (the image shows a different camera, which was used in an earlier iteration of the system)

A prototype of the system was implemented using the Polaris^{TM}(Northern Digital, Waterloo, Canada) tracking system, a BV-21 (Philips, Germany) fluoroscopy device and an Intel Pentium 2GHz computer. The software was entirely written in C++ and runs under the Linux operating system.

3.1.1 The Tracking System

In order to guide the surgeon during the intervention, a medical navigation system must be able to detect the position and orientation of the surgical tools in relation to the patient at any

given time. This is achieved through the use of a real-time 3D localizer. A variety of such systems exist, utilizing different physical effects for localization [Sim97], including ultrasound or magnetism [Lan02, Gun00]. Most commercially available systems, however, use optical tracking.

With optical tracking, specially prepared markers have to be attached to the object to be tracked. These markers are detected by a camera, and the system can compute their 3D position in the camera coordinate system. Optical tracking systems reach a precision of up to 0.1mm [Kha00]. Various factors affect the global performance of such a system, such as the intrinsic accuracy of the camera system, the arrangement of the markers on the tool, and the size and geometry of the instrument itself[Sch01].

A distinction is made between *active* and *passive* optical tracking. Active tracking uses LEDs as markers, whereas passive tracking utilizes retro-reflective spheres reflecting incoming light back to its source. Both kinds of systems operate with infrared light to keep interferences from surrounding visible light at a minimum.

To be able to detect the orientation, rather than the mere position, of the medical instruments to which the markers are attached, it is necessary to combine a number of markers to a *tracker*, which is a rigid compound of markers with a known geometry (see Figure 3.2). At least three markers, arranged to an asymmetrical triangle to avoid ambiguity, are necessary to uniquely determine the full 6D pose (three translational and three rotational degrees of freedom) of a tracker. More markers may be added to yield more stable tracking results [Wes04].

The FEMOS system was implemented and tested using the Polaris^{TM}(Northern Digital, Waterloo, Canada) passive optical tracking system, which is able to detect the position of reflective markers at an update rate of 60 Hz and an accuracy error of 0.35 mm RMS[1]. The instruments were tracked with custom built trackers.

Before it can be used, such a tracker must be made known to the tracking system. This is done by uploading its geometry (the layout of its spheres in the tracker coordinate system) to the camera controller. Once this has been done, the camera can detect the location of the tracker's spheres in 3D space, match their positions with the predefined layout of the trackers and thus report a 6D pose $\mathbf{M}_{TrackerCS \rightarrow CamCS}$, describing the location and orientation of the tracker in the camera coordinate system. Effectively, the pose $\mathbf{M}_{TrackerCS \rightarrow CamCS}$ is a coordinate transformation from the tracker coordinate system *TrackerCS* to the camera coordinate system *CamCS*.

Observing certain uniqueness constraints in the layout of the markers, the tracking system can handle several trackers simultaneously, thus enabling the use of multiple tools. The con-

[1]Root mean square

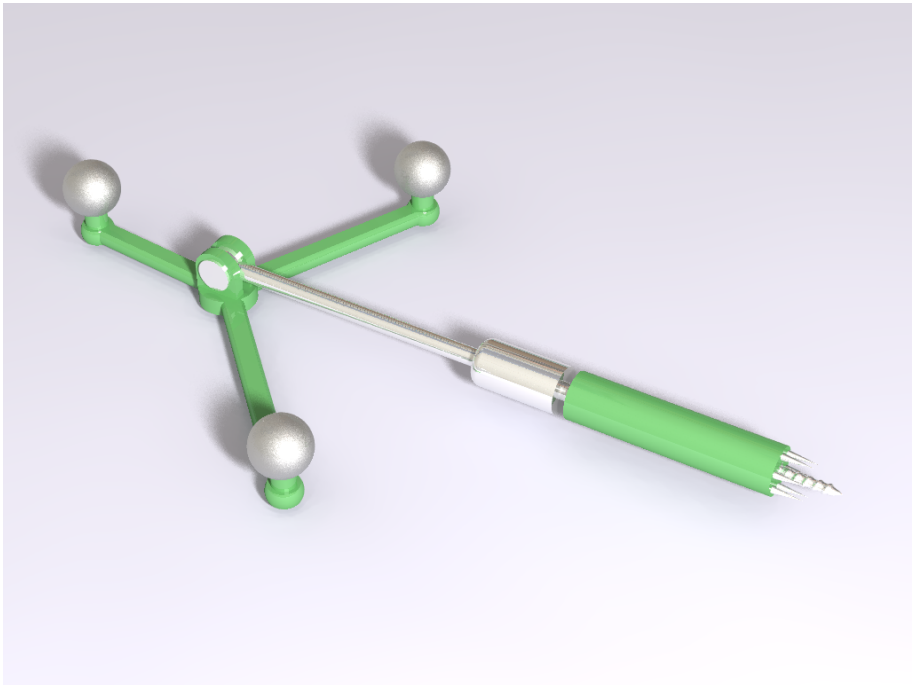

Figure 3.2. The model of a tracker, attached to a bone clamp. The surface of the spheres is covered with a reflective coating.

straints mentioned are needed to avoid ambiguity when matching the set of detected spheres to the tracker layouts.

3.1.1.1 Tool Calibration

Normally, the objects to be tracked are medical instruments, such as a bone chisel, a drill, a saw or just a pointer. To enable these to be tracked, trackers are attached to them. Before these tools can be used for navigation, they must be calibrated. Calibration is the process of determining the coordinate transformation which relates the tool geometry to the current pose of the tracker reported by the camera system.

The tool geometry $\mathcal{G}_{tool}$ specifies the tool shape (for example the location of the tool tip $T_{[ToolCS]}$, the direction of the tool's main axis or similar features) in the tool coordinate system *ToolCS*. The choice of the tool coordinate system is arbitrary, but reasonable choices would usually derive from the physical shape of the instrument. For example for a drill, it might be useful to define a coordinate system so that the origin corresponds to the tip of the drill and the z axis to its main direction.

Tool calibration is usually performed using a specially designed calibration device with rigidly attached markers, for which the marker/geometry relation is known (by design, for

example). During calibration, the tool which is to be calibrated is brought into a predefined position on the calibration device (for example, a pre-drilled hole in the case of a drill calibration).

The following coordinate systems are involved in the calibration procedure:

- The camera coordinate system *CamCS*
- The coordinate system of the calibration device *CalibCS*. This is the coordinate system in which the marker layout of the calibration device is defined. Furthermore, the geometry of the calibration device itself is defined in this coordinate system, for example, the position at which the tip of the drill would be located when it is held in a predefined position.
- The coordinate system of the tool *ToolCS*, in which the tool geometry is defined — for example the position of the tip of the drill.
- The tracker coordinate system *TrackerCS*, in which the marker layout of the tracker attached to the tool is defined.

The goal of the calibration is to find the transformation $\mathbf{M}_{ToolCS \rightarrow TrackerCS}$, the *calibration pose*, which represents the relation between the tool coordinate system and the coordinate system of the tracker, as it is currently attached.

Once the tool and the calibration device have been brought together in their predefined positions, the following poses can be obtained from the tracking device:

- The pose $\mathbf{M}_{CalibCS \rightarrow CamCS}$, which represents the transformation between the coordinate system of the calibration device and the camera coordinate system
- The pose $\mathbf{M}_{TrackerCS \rightarrow CamCS}$, which is the transformation between the coordinate system of the tracker attached to the tool, and the camera coordinate system

Also, the pose $\mathbf{M}_{ToolCS \rightarrow CalibCS}$ is known *from the construction of the calibration device*, since the tool's position on the calibration device is established, given that the two are held in the predefined position.

Now, the calibration pose $\mathbf{M}_{ToolCS \rightarrow TrackerCS}$ can be determined:

$$\mathbf{M}_{ToolCS \rightarrow TrackerCS} = \mathbf{M}^{-1}_{TrackerCS \rightarrow CamCS} \cdot \mathbf{M}_{CalibCS \rightarrow CamCS} \mathbf{M}_{ToolCS \rightarrow CalibCS}$$

Using the obtained calibration pose, it is now possible to find the current position of any feature of the tool geometry in the camera coordinate system. For example, assuming that the

position of the tip of a drill is given in tool coordinates as $T_{[ToolCS]}$, its current position in the camera coordinate system is

$$T_{[CamCS]} = \mathbf{M}_{TrackerCS \to CamCS} \cdot \mathbf{M}_{ToolCS \to TrackerCS} \cdot T_{[ToolCS]}$$

3.1.1.2 Reference Frame

The position sensor reports the poses of the trackers in the coordinate system *CamCS*, which is fixed to the camera. However, during a medical intervention, the frame of reference and hence the localization of the tracked tools must be relative to the part of the patient's body which is to be treated. This ensures that the localization remains valid, even if the patient or the camera system is moved.

To enable a localization independent of the relative position of the patient, a reference tracker, called *dynamic reference frame (DRF)*, must be rigidly attached to the region to be referenced. For the reference tracker, the camera reports a pose $\mathbf{M}_{DRF \to CamCS}$, whose inverse, namely $\mathbf{M}^{-1}_{DRF \to CamCS} = \mathbf{M}_{CamCS \to DRF}$, can be interpreted as a coordinate transformation from the camera coordinate system to the desired reference frame. Care must be taken to ensure that the reference tracker is positioned as close to the target area as possible, because small errors in the rotational part of the measured pose will have a leverage effect on the translational error of all other trackers in this reference frame, which increases linearly with the distance to the reference tracker.

With the reference tracker in place, it is possible to answer the basic question in medical navigation:

> "With respect to the reference frame, where is feature X of the tool geometry currently located?"

Given a feature $X_{[ToolCS]}$, for example a point or a line, of the tool geometry in the tool coordinate system, the current location $X_{[DRF]}$ of this feature in the reference frame is

$$X_{[DRF]} = \mathbf{M}_{CamCS \to DRF} \cdot \mathbf{M}_{TrackerCS \to CamCS} \cdot \mathbf{M}_{ToolCS \to TrackerCS} \cdot X_{[ToolCS]}$$

In the case of a proximal femur osteotomy, the reference coordinate system must be relative to the femur bone, as it is the target of the treatment. Since the bone is cut in two during the intervention, *two* references are required — one for each fragment, proximal and distal. The references are usually fixed to the femur by drilling a threaded Kirschner wire[2] into the bone, to which the tracker is mounted.

[2] Also called K-wire: thin, rigid wires commonly used in orthopedics to stabilize bones fragments.

The distal reference tracker must be attached at the beginning of the intervention, before any of the images are taken, and must remain in place through the entire navigated portion of the operation. The proximal reference is attached just before the femur is osteotomized. Geometric objects whose coordinates are given relative to the distal or proximal references, receive the suffixes [*DistCS*] and [*ProxCS*], respectively, for example $P_{[DistCS]}$ or $Q_{[ProxCS]}$.

3.1.2 Fluoroscopic Imaging

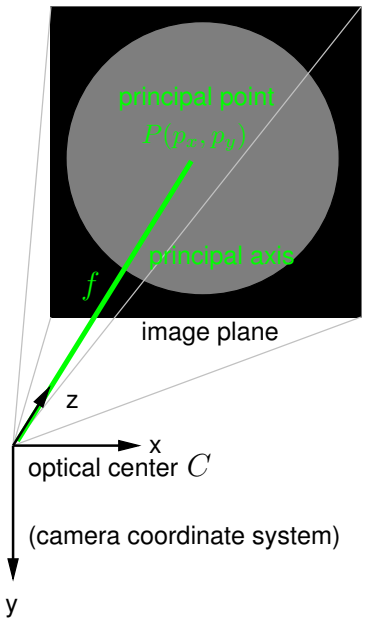

Figure 3.3. The pinhole camera model

Fluoroscopy is an imaging technique based on X-ray technology. As opposed to traditional X-ray imaging, in which X-rays impinge on a photographic plate which is blackened according to the intensity of the rays, fluoroscopic imaging uses a special detector connected to a video screen, so that the images can be displayed instantly. Due to the immediate availability of the images and the capability to display real-time image sequences, fluoroscopic imaging is often used intraoperatively, and C-shaped fluoroscopes (C-arms) have long been standard equipment in operating rooms. A drawback of using intraoperative fluoroscopy is the ensuing radiation exposure of the patient and especially of the surgical team, who are affected repeatedly with every operation.

Because of its widespread availability in operating rooms, fluoroscopic imaging has become an essential part of many image-guided surgery systems [Jos98, Suh, Hof99]. For use in such systems, the fluoroscopic device is treated as a pinhole camera [Har00], which models an ideal perspective camera. The model specifies the following parameters (see Figure 3.3):

- The position (optical center) C and orientation of the camera in the reference coordinate system. These are the *extrinsic* parameters of the camera, which can be expressed as a 6D pose transforming the camera coordinate system into the reference coordinate system. These parameters also determine the *principal axis* of the camera, which is traditionally defined as the z axis of the camera coordinate system.

- The focal length f of the camera, which is the distance of the image plane from the optical center. The image plane is orthogonal to the principal axis.

- A 2D point P, the *principal point*, which specifies the pixel coordinates of the point in

the image at which the principal axis intersects the image plane. The principal point and the focal length are called the *intrinsic* camera parameters.

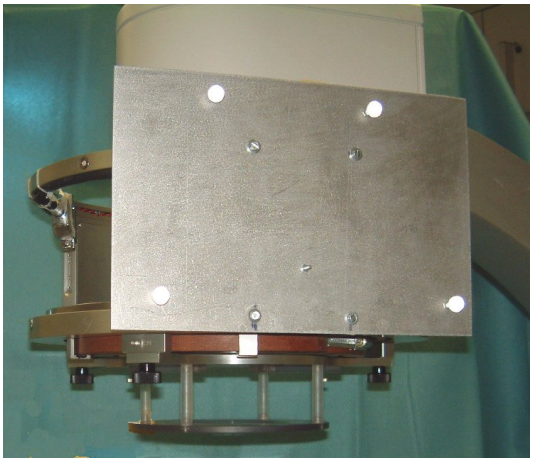

(a) The calibration device on the C-arm

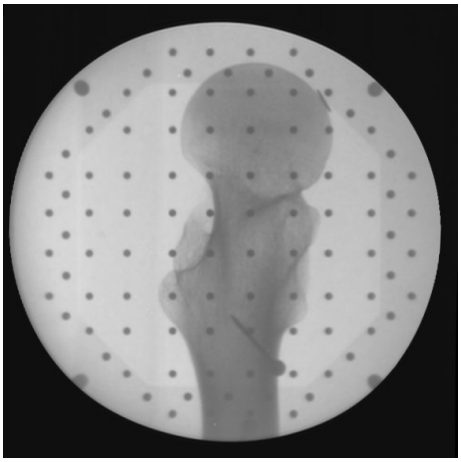

(b) A fluoroscopic image with projected markers of the calibration device

Figure 3.4. The acquisition of calibrated fluoroscopic images

To be able to obtain these parameters with the images, the C-arm must be specially prepared by mounting a calibration device with an attached tracker to its detector (see Figure 3.4a). The calibration device consists of two parallel plastic plates several centimeters apart, into which radio-opaque metal spheres arranged to an irregular grid were implanted. The device is mounted on the detector in such a way that these plates are aligned parallel to the image plane, and the projections of the metal markers are visible in the acquired image (see Figure 3.4b).

The calibration device serves the following purposes:

- A problem with the use of fluoroscopic images for image-guided surgery is that these images exhibit significant geometric distortions. Causes include interference of the earth's magnetic field with the trajectory of electrons inside the device, or torsional deformation of the C-arm frame due to its own weight [Nol00]. For conventional use, this is unproblematic, as the surgeon needs to assess the image information only qualitatively. However, this is a problem for image-guided surgery, which requires quantitative information. Thus, before the images can be used, they have to be undistorted, based on the location of the projected markers in the image [Bra99].

- Since the geometries of the two parallel marker grids in the calibration device are known, it is possible to derive the intrinsic parameters of the camera by analyzing the marker's projections in the final image.

- Also since the calibration device has a tracker attached, whose relation to the marker geometries is known, it is possible to determine the extrinsic camera parameters (position and orientation).

The calibrated images can now be used quantitatively for the navigation system, for example by overlaying to the images a perspectively-correct visualization of a surgical instrument. For the FEMOS system, another fundamental aspect is most relevant: with the camera parameters known, it is possible to determine a 3D projection line for any given point (x, y) in the 2D image. This line is the set of all 3D points, which are projected to (x, y) under the given camera parameters. Calculations of this sort are used by the system to reconstruct a 3D model of the femur based on two fluoroscopic images alone.

3.2 Overview of the Intervention with the Basic System

This section gives an overview of the operation as it is performed with the FEMOS system. The following sections will discuss the individual steps in detail. Generally, the intervention proceeds in the following stages:

1. **Image Acquisition** Two fluoroscopic images from different directions are acquired of the femur under treatment. They serve as basis for the reconstruction of the femur model in the next step, and are also used later to guide the surgeon during the operation.

2. **Model Reconstruction** A primitive 3D femur model is reconstructed from the images. The model describes the essential features of the femur, such as the location of its head, its shaft and several more.

3. **Interactive Planning** The surgeon selects the planning parameters for the intervention. He receives immediate feedback about the effects of the current parameters (varus/valgus, flexion/extension etc.), which he can optimize until he is satisfied with the predicted results.

4. Computer-assisted Execution After the planning has been completed, the intervention is performed with the help of the tracking system. This step involves the gouging of the blade channel, the excision of the bone wedge, and finally the tracking of the two separate fragments until the specified target pose has been reached.

As mentioned before, the critical phases of the osteotomy are the gouging of the blade channel and the removal of the bone wedge. Thus, the important parameters to be determined during the planning phase are:

- The location of the osteotomy plane, which is one of the bounding planes of the wedge.
- The location of the wedge plane, which, together with the osteotomy plane, forms the wedge to be removed.
- The location of the blade channel.

The FEMOS system assists the orthopedic surgeon in determining the correct values for these parameters so that the intervention can then be performed with help of the tracking system. Once the blade channel has been gouged and the bone wedge removed, the critical phase of the intervention (in terms of accuracy of the achieved result) is essentially over. What remains to be done is positioning the separated fragments and fixing them to each other, using the metal implant.

3.3 Image Acquisition

In the image acquisition step, two fluoroscopic images of the proximal femur are acquired. Based on these images, a primitive 3D model of the femur will be reconstructed later. Later the images will also be used during the navigation phase of the intervention to guide the surgeon.

The images are taken intraoperatively with a calibrated C-arm [Bra99], which means the following things (see also section 3.1.2):

- The images are unwarped, which means that unwanted distortions are detected and removed
- The external and internal camera parameters of the images are determined.

The reference coordinate system in which the camera parameters are given must be relative to the femur bone under treatment, which requires a reference tracker to be placed on the distal fragment prior to the image acquisition. This tracker stays in place for the entire duration of the navigated part of the intervention. Special care must be taken to fix the tracker securely, so it will not come loose due to mechanical impact caused by the gouging and sawing following later.

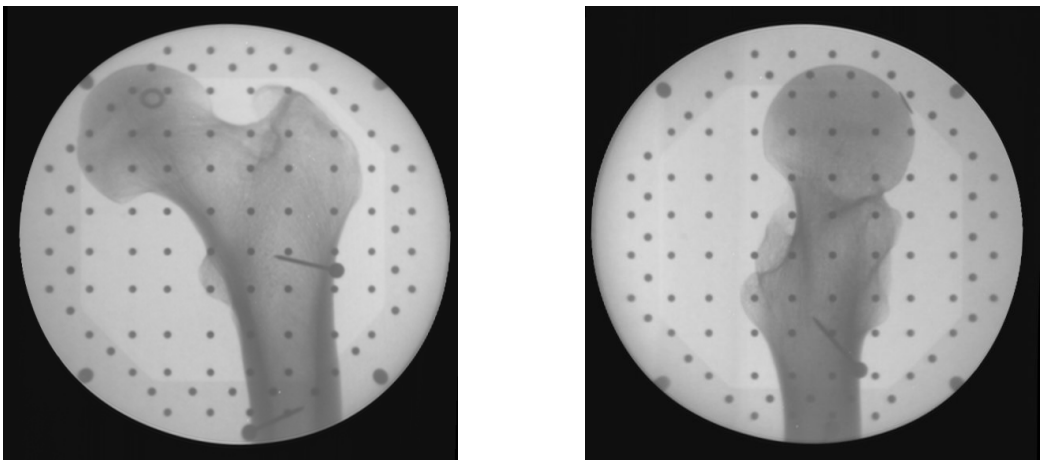

(a) AP view (b) axial view

Figure 3.5. The two calibrated images to be acquired.

For the model reconstruction to be possible, the images must be taken from two different directions:

anterior/posterior One of the images must be taken in AP direction. Special care must be taken to ensure that the direction in which this image is taken coincides with the anatomical AP direction, since some parts of the calculation depend upon this direction.

axial The second image must be taken in axial direction, showing the femur in a view direction which ensues from the AP direction by a rotation about the femur neck axis of about 70°. Intraoperatively, this image is taken by angling the patient's leg at the hip and moving the detector of the C-arm inwardly around the thigh. The exact angle at which this image is taken is not significant. To enable a robust model reconstruction in the next stage, however, it is important that the femur neck is well visible and that there is a sufficiently large angle ($> 60°$) relative to the AP image.

Parameter	Description
H	the position of the femoral head
r_H	the radius of the femoral head
N	the location of the femoral neck shaft isthmus
$\ell_{shaft} = (A, \vec{a})$	the femoral shaft axis, described by its base point A and direction vector $\vec{a}$. The direction vector $\vec{a}$ is chosen so that it points in proximal direction and has unit length.
r_S	the radius of the femoral shaft in the vicinity of the osteotomy plane
$\mathcal{E}_{lateral}$	a plane which is tangent to the lateral femur shaft
$\vec{d}_{AP}$	anatomical AP direction
γ	CCD (caput-collum-diaphysis) angle, which is the angle between the shaft axis and the neck axis of the femur
$\mathcal{E}_{osteo}$	the osteotomy plane, the plane along which the first cut of the osteotomy is made

Table 3.1. Overview of the features obtained in the 3D reconstruction. All of these features are specified in the coordinate system *DistCS* of the distal reference tracker.

3.4 Model Reconstruction

After the images have been acquired, a primitive 3D model of the femur can be reconstructed [Got05]. This reconstruction requires the interaction of the surgeon. The features of the femur which are reconstructed in this step are listed in Table 3.1.

> **Note:** Since the camera parameters associated with the images were determined in the coordinate system of the distal reference, *DistCS*, all of the features listed in Table 3.1 will also be calculated in this coordinate system. This means that, after the model reconstruction, the location of all of these features will be given relative to the distal reference.

Since the pinhole camera models corresponding to the two images are known, the features mentioned can be obtained through geometrical calculations. The main idea here is that every point P on the image plane of a pinhole camera is the representative of an entire line, namely the line connecting P to the camera's optical center. Through perspective projection all points on this line are projected onto P. If the internal and external camera parameters are known, as

is the case here, it is possible to specify the 3D line represented by P in the given coordinate system.

If, in two images taken from different directions, the projections of a 3D point appear as $P1$ and $P2$, respectively, the position of the original 3D point can be calculated by intersecting the projection rays corresponding to $P1$ and $P2$. In other words, this method allows the actual 3D coordinates of any point on the femur to bet determined, if its projections on at least two different images are known.

Similarly, a line in a single 2D image represents a plane in 3D space. If the 2D projection line of the same 3D line appears in two different 2D images, the original 3D line can be obtained from the projections by intersecting the corresponding planes (see Figure 3.6).

The following sections describe in detail how the features listed in Table 3.1 can be obtained.

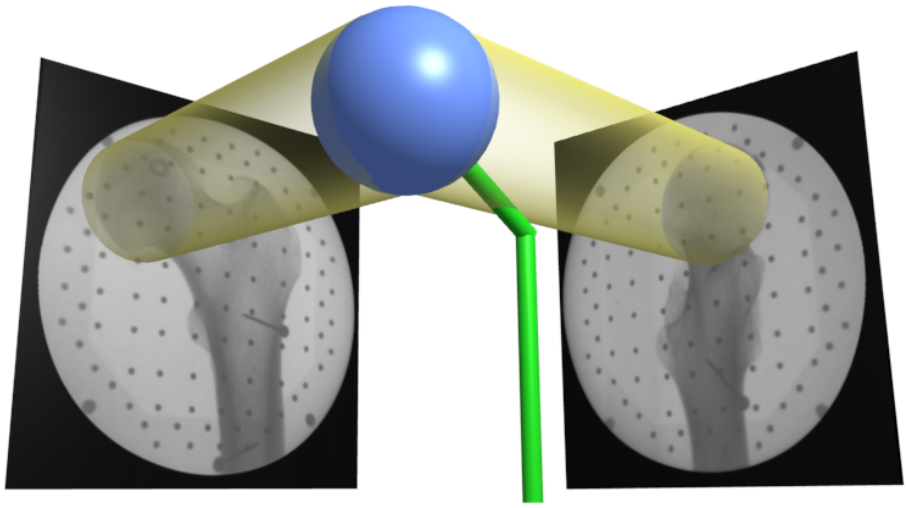

Figure 3.6. Construction of the primitive model from the fluoroscopic images, taken at different angles. The features are reconstructed from their projections which are visible in the two images.

3.4.1 The AP Direction

The vector $\vec{d}_{AP}$, which points in the anatomical AP direction, can immediately be determined from one of the images: it is the view direction of the camera with which the AP image was taken. All the surgeon has to do is tell the system which of the two images was taken in this direction.

This direction vector is used several times in the calculations of the FEMOS system, so it is important that the view direction of this camera does coincide with the actual anatomical AP direction.

3.4.2 The Femur Head

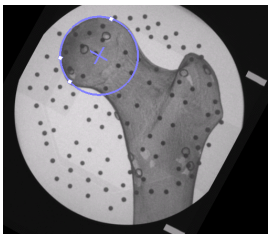
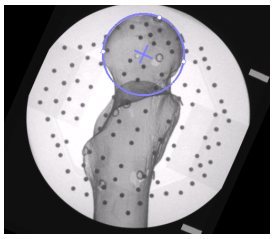

The femoral head is approximately spherical in shape, since the hip is a ball-and-socket joint and the femoral head can rotate freely in the acetabulum. As demonstrated in [Men97], a better approximation is a rotational conchoid, but for the purpose at hand it suffices to assume a spherical shape.

Under orthogonal projection, a sphere is projected to a circle on the image plane. With perspective projection as in the case of a pinhole camera, however, the projection rays hitting the sphere form a cone, which is intersected by the image plane and thus yields a conic section as projection. Since the femoral head always appears close to the principal point of the fluoroscopic images, however, the projection can be regarded as a circle for all practical purposes.

During the intervention, the surgeon manually marks the projection of the femoral head in each image by selecting three points on its outline. Since three points on a 2D plane uniquely define a circle, the system can now easily calculate the circle which approximates the projection. Once these circles have been marked in both images, the system proceeds to determine the following features:

- The location of the femur head center H, which is calculated by intersecting the projection rays of the two centers of the circles which were marked in the two images.
- The radius of the femoral head, which can be calculated from the radius of the 2D circles once the 3D position of their center is known

The radius of the femoral head is not used in any calculations of the planning system, however it is useful for the visualization of the femur model.

3.4.3 The Shaft Axis

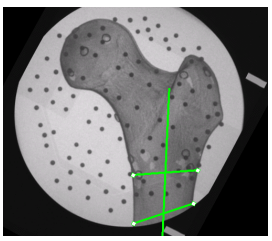
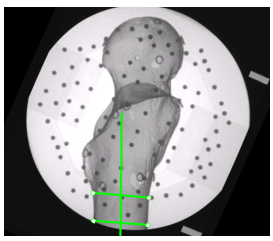

The femoral shaft axis is an anatomically described, yet not sharply defined feature. It is the line running along the center of the femoral shaft. Since the femoral shaft is not an ideal cylinder, there is no unique straight line representing the shaft axis. However, the proximal part of the femoral shaft is sufficiently cylindrical to allow for a reasonable approximation by a straight line.

To determine the 3D line representing the shaft axis, the surgeon needs to mark the projections of the shaft axis in the 2D images. This happens by selecting two pairs of points on the outline of the femoral shaft in the projection. The two points of each pair must lie on different sides of the shaft, defining a line segment which crosses the shaft. In each image, the projection of the shaft axis is obtained by connecting the centers of the two line segments. Together with the pinhole camera parameters, the actual 3D shaft axis can then be calculated by intersecting the 3D planes corresponding to the 2D lines marked in the images.

3.4.4 The Neck Isthmus

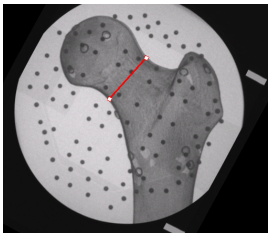

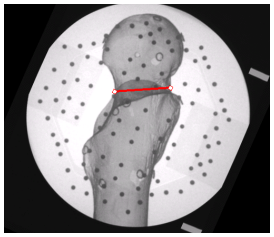

The isthmus of the femoral neck is the narrowest part of the femoral neck. It is important because the blade of the implant which is inserted after the osteotomy has been performed must pass through the isthmus without perforating the bone surface. Most importantly, the center of the neck isthmus N, together with the femoral head center H, defines the femoral neck axis used in the specification of the osteotomy input parameters.

The isthmus of the femoral neck is specified by the surgeon by marking a pair of points in both 2D images: one point on each side of the isthmus, which define a line segment running across the isthmus. The isthmus center can now easily be calculated by intersecting the projection rays corresponding to the centers of the line segments.

Once the femoral shaft axis and the neck axis have been determined, it is possible to calculate the CCD (caput-collum-diaphysis) angle γ, which appears between the neck axis and the shaft axis.

3.4.5 The Corticalis Tangent Plane

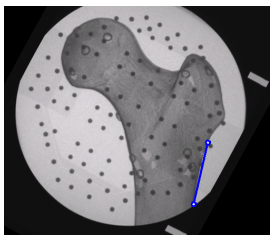

For the positioning of the implant, it is important to know the location of the lateral corticalis. The corticalis is the strong exterior structure of the bone, to which the implant will be screwed. Since there is no real 3D information about the surface of the bone available, the system suggests a default for the position of the implant, in which the implant's shaft aligns with the plane tangent to the corticalis.

To obtain the plane, the surgeon needs to mark two points on the projection of the lateral corticalis in the AP image. The tangent plane $\mathcal{E}_{lateral}$ to the corticalis is calculated as follows:

- An auxiliary plane $\mathcal{E}_{aux}$ is defined, which contains both the femur head center and the femoral shaft axis. This definition is unique, since the head center does not lie on this axis. Let the normal vector of $\mathcal{E}_{aux}$ be called $\vec{n}_{aux}$.
- The two points marked by the surgeon on the projection of the corticalis correspond to two projection rays, which intersect $\mathcal{E}_{aux}$ in two points, P_1 and P_2. Let the vector $\vec{v}_{diff} := P_1 - P_2$ be their difference vector.
- Now, $\mathcal{E}_{lateral}$ can be defined:

$$\mathcal{E}_{lateral} := \mathcal{E}(P_1, \vec{v}_{diff}, \vec{n}_{aux})$$

The plane thus found has the following properties:

- It contains both P_1 and P_2, which lie on the lateral corticalis (or close to it, due to perspective error)
- It is perpendicular to $\mathcal{E}_{aux}$, which, as it contains the shaft axis, in turn intersects the corticalis orthogonally.
- From these two conditions, it follows that $\mathcal{E}_{lateral}$ is tangent to the lateral corticalis.

The plane $\mathcal{E}_{lateral}$ is used in the plate positioning algorithm described in section 3.5.4 as a starting point in the calculation of the default implant pose.

3.4.6 The Trochanter Minor

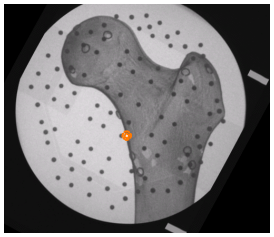

Finally, the surgeon must mark a point in the AP image which indicates a location slightly proximal of the trochanter minor in the AP image. This point serves two purposes: first, it enables the system to set the location of the osteotomy plane $\mathcal{E}_{osteo}$ in the femur model. Secondly, it allows the system to determine the radius r_S of the femur diaphysis in the vicinity of the osteotomy plane.

To permit a stable fixation of the bone fragments after the osteotomy, the osteotomy plane must be orthogonal to the femoral shaft. Also, the plane should usually be located slightly proximal of the trochanter minor. Thus, the plane $\mathcal{E}_{osteo}$ is defined as follows:

- It is orthogonal to the femoral shaft axis ℓ_{shaft}

- The projection ray of the point marked by the surgeon intersects the plane $\mathcal{E}_{aux}$, defined so that it contains the femur head center and the femoral shaft axis, in a point which is located proximal of the trochanter minor. $\mathcal{E}_{osteo}$ is chosen so that it contains this point.

The radius r_S of the femoral diaphysis, which will later be used for the wedge calculations, is obtained by measuring the distance between the projection line of the marked point and the femoral shaft axis.

3.4.7 Left Femur, Right Femur?

Several parts of the calculation depend on whether the femur under treatment is left or right side. For example, a vector pointing in 'medial' (towards the middle of the body) direction on the left femur would be anti-parallel to its right-side counterpart.

From the femur features described above, it is possible to deduce which case, left or right, is at hand: given the values for the proximal shaft axis vector $\vec{a}$, the AP direction $\vec{d}_{AP}$ and the direction of the femur neck $H - N$ (which is the vector pointing from the neck isthmus to the neck center), the following value is calculated:

$$D := \det(\vec{d}_{AP}, \vec{a}, H - N)$$

For $D > 0$, the vectors $\vec{d}_{AP}$, $\vec{a}$ and $(H - N)$ form a right-hand system, which means the femur is right-side. Otherwise, for $D < 0$, the femur is left-side.

3.5 Interactive Planning

During this phase of the system, the surgeon specifies the planning parameters and assesses the predicted effects of the current parameter set. This is an iterative process in which the user continually refines the parameters, until a satisfactory configuration has been found. The following requirements must be fulfilled for a valid solution:

- The desired therapeutic effect should be reached. For example, in case of an osteonecrosis of the femoral head, the affected part of the head should be rotated out of the load area.

- It must be ensured that the blade of the metal implant does not perforate the femoral neck. In particular, the blade should pass through the isthmus of the femoral neck as centrally as possible.

- Effects on the biomechanical leg axis should be kept at a minimum to avoid secondary damage after the operation (unless, of course, the purpose of the operation is a shifting of this axis).

- The shaft of the implant must align with the femur diaphysis, so that the implant can be screwed tightly to the bone.

Normally, not all of these requirements can be fully satisfied so that a tradeoff has to be found. However, the FEMOS system can make a prediction of all of the effects mentioned above, so that the surgeon can vary the input parameters until a good compromise has been reached. All of this happens during the planning phase, that is, before the actual procedure is begun. Figure 3.7 displays the user interface of the FEMOS system during the planning phase.

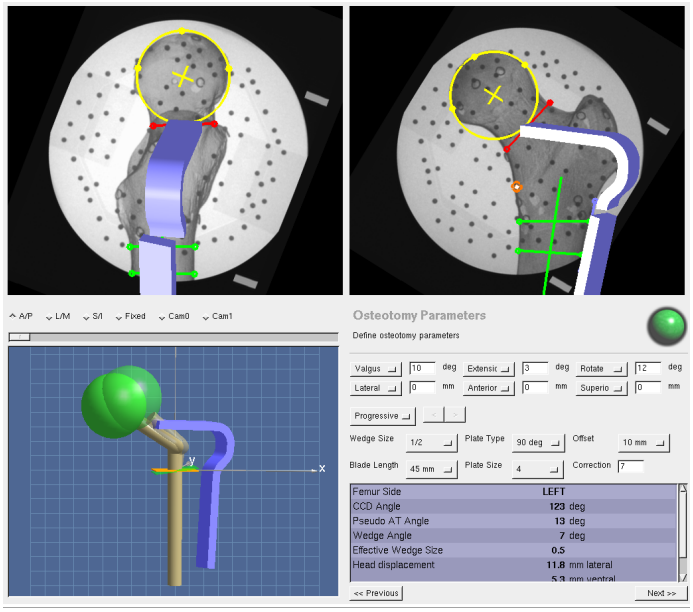

Figure 3.7. A screenshot of the planning module of the FEMOS system. On the right side, the user can enter the osteotomy parameters. The left side shows the effect of the parameters on the primitive femur model.

The main goal of the planning phase is the calculation of the two essential parameters determining the intervention:

- The target pose $\mathbf{M}_{target}$, which represents the change of alignment of the proximal femur fragment. This pose is determined automatically from the input parameters specified by the user. Together with a given osteotomy plane, it also implicitly defines the shape of the wedge to be cut out of the femur.

- The plate pose $\mathbf{M}_{PlateCS \rightarrow DistCS}$, which specifies the position of the implant on the femur. This pose is found via two steps: first, the system calculates a default pose, based on the input parameters and certain reasonable constraints for the placement of the implant. Secondly, the user can interactively refine this default position.

How these two parameters are obtained is discussed in detail in the following sections.

3.5.1 The Input Parameters for the Planning Algorithm

Table 3.8 lists the input parameters for the planning algorithm, which must be known before the target parameters can be determined. They are either taken from the reconstructed model or are specified by the user during the planning phase (a detailed description of these parameters was given in 2.4).

Parameter	Description	Source
H	the position of the femoral head	femur model
r_H	the radius of the femoral head	femur model
N	the location of the femoral neck shaft isthmus	femur model
O	the osteotomy center $(0, 0, 0)$	femur model
$\vec{a}$	the normalized shaft axis vector, pointing in proximal direction	femur model
$\vec{b}$	the unit vector pointing from N to H so that $\vec{b} :=$ normalize$(H - N)$	femur model
r_S	the radius of the femoral shaft	femur model
γ	CCD angle	femur model
$\mathcal{E}_{osteo}$	the osteotomy plane	femur model
ϕ_{varus}	varus/valgus angle	user input
$\phi_{flexion}$	flexion/extension angle	user input
$\phi_{rotation}$	rotation/derotation angle between	user input
t_{AP}	translation in anterior/posterior direction	user input
t_{LM}	translation in lateral/medial direction	user input
t_{SI}	translation in superior/inferior direction	user input
w	wedge size	user input

Figure 3.8. The input parameters used by the planning algorithm

3.5.2 The Target Parameters

Table 3.3 shows the parameters, which need to be determined based on the input parameters described in the previous section.

Parameter	Description
M_{target}	The target pose of the osteotomy. This pose transforms the proximal fragment from its original, preoperative position to the desired, postoperative position
κ	The effective wedge angle. This is the angle of the wedge which is cut out of the bone
$\mathcal{E}_{wedge}$	The wedge plane. This is the plane which forms the wedge together with the osteotomy plane
ρ	The final rotation angle (see below)
$\vec{w}_{dir}$	The wedge direction, which is a vector perpendicular to both the wedge edge and the shaft axis $\vec{a}$, pointing away from the wedge body

Table 3.3. The target parameters to be determined

In terms of these parameters, the intervention proceeds in the following steps (see also Figure 3.9):

1. The bone is cut through along the osteotomy plane $\mathcal{E}_{osteo}$
2. A second cut along the wedge plane $\mathcal{E}_{wedge}$ creates a wedge together with $\mathcal{E}_{osteo}$, which is then removed
3. The two femur fragments are now tilted about the hinge of the (removed) wedge, until the cutting surfaces of the two fragments are in contact.
4. The *proximal* fragment is rotated ρ degrees about the femoral shaft axis of the *distal* fragment.
5. The translation specified by the input parameters t_{AP}, t_{LM} and t_{SI} is applied

As can be seen, the target pose of the proximal fragment is reached by consecutively performing three transformations, once the wedge has been removed: tilting the fragment along the wedge edge, rotating it on the osteotomy plane about the shaft axis, and applying the user-defined translation.

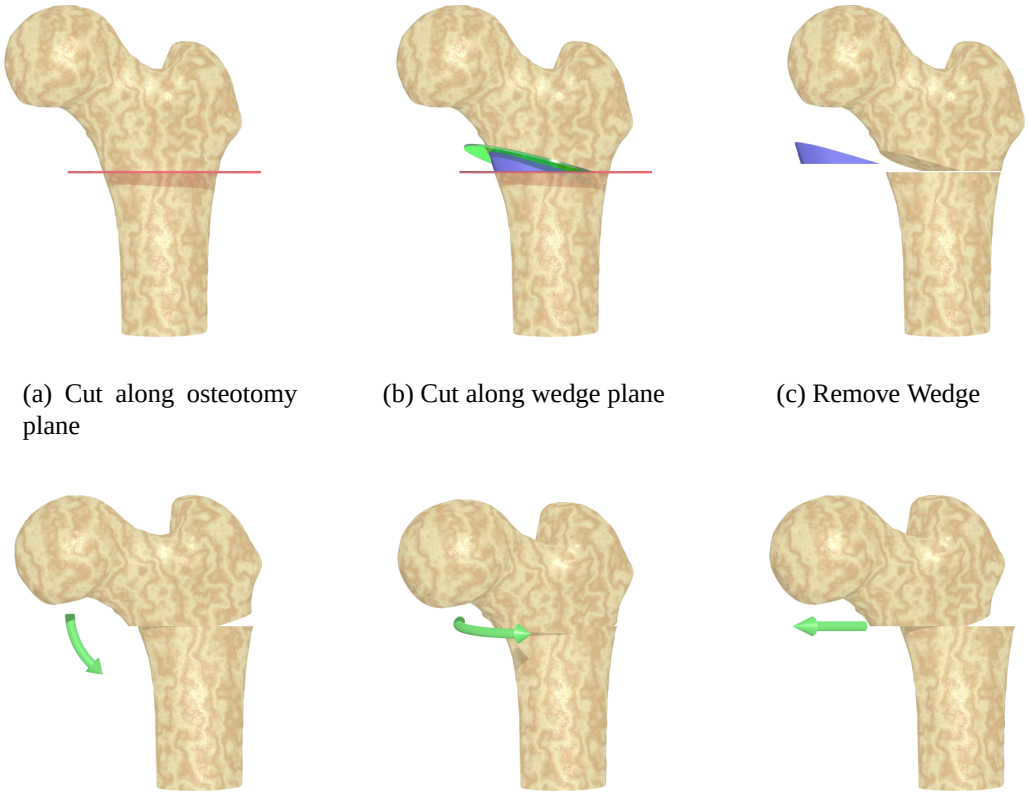

(a) Cut along osteotomy plane

(b) Cut along wedge plane

(c) Remove Wedge

(d) Tilt about wedge edge by angle κ

(e) Rotate about shaft axis by angle ρ

(f) Translate by (t_{AP}, t_{LM}, t_{SI})

Figure 3.9. Schematic overview of the intervention. Steps (d) to (f) illustrate how the fragment is transformed to its target position.

An important fact which will later be used in the calculations is that the target pose $\mathbf{M}_{target}$ is a pure rotation if $w = 0.5$ (a half wedge!) and $t_{AP} = t_{LM} = t_{SI} = 0$. This is the case since, for $w = 0.5$, the wedge edge intersects the femur shaft axis, which means that it contains the origin of the osteotomy coordinate system. This, in turn, makes the origin a fixed point in both the steps (d) and (e), as well as in (f) in which no translation occurs for $t_{AP} = t_{LM} = t_{SI} = 0$. Thus, the origin is a fixed point of the target pose, which means that the translational part $\mathbf{T}_{target}$ vanishes and the target pose is a pure rotation, so that $\mathbf{M}_{target} = \mathbf{R}_{target}$.

Figure 3.10 displays a schematic diagram of the primitive femur model with the geometrical features used in the planning algorithm.

The goal of the intervention is to implement the target pose $\mathbf{M}_{target}$ as accurately as possible. The target pose can be represented as a tuple consisting of a rotation and a translation vector $\mathbf{M}_{target} = (\mathbf{R}_{target}, \mathbf{T}_{target})$. Every part X of the original femur geometry can be

transformed into the new geometry by applying the target pose: $X' = \mathbf{M}_{target} \cdot X$.

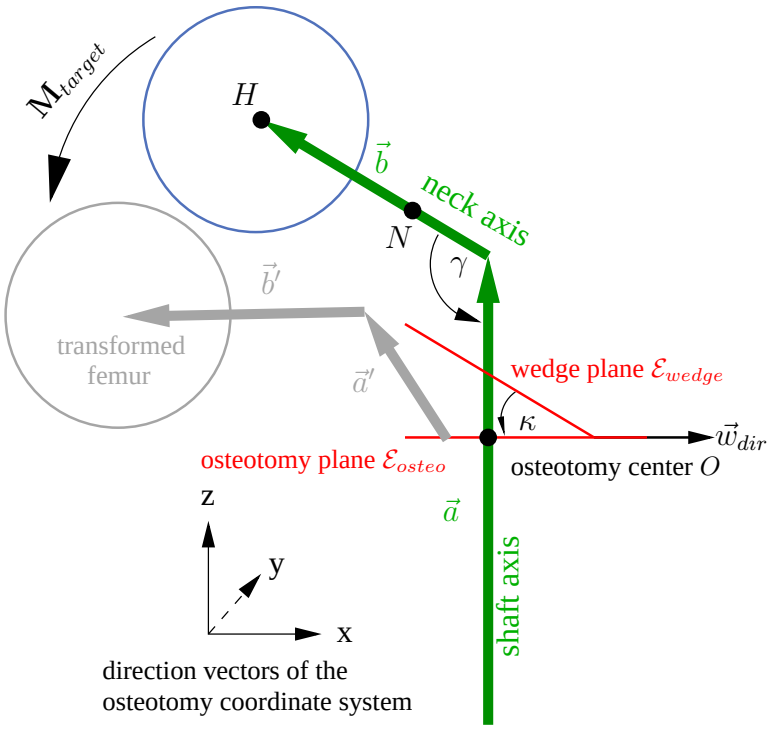

Figure 3.10. The primitive femur model with the parameters used in the planning algorithm. For the calculations, all vectors are assumed to be unit vectors.

3.5.3 The Planning Algorithm

This section describes the algorithm which calculates the target parameters from the input parameters. The algorithm, as presented here, operates in the osteotomy coordinate system *OsteoCS* (for a definition, see section 2.3.3). Therefore, all input parameters have to be converted accordingly before the algorithm can be performed. This mainly affects the input parameters taken from the model reconstruction, such as the femur head center, the shaft axis etc., which were originally determined in the coordinate system of the distal reference, *DistCS*.

The transformation between the osteotomy coordinate system *OsteoCS* and the distal reference coordinate system *DistCS* is defined as follows:

- The origin O_{osteo} of the osteotomy coordinate system *OsteoCS* is the intersection of the

shaft axis ℓ_{shaft} and the osteotomy plane $\mathcal{E}_{osteo}$, thus

$$\begin{aligned} O_{osteo[DistCS]} &= \text{intersect}(\mathcal{E}_{osteo[DistCS]}, \ell_{shaft[DistCS]}) \\ O_{osteo[OsteoCS]} &= (0,0,0) \end{aligned}$$

- The z axis of the *OsteoCS* is the shaft axis $\vec{a}$ of the femur:

$$\begin{aligned} \vec{z}_{osteo[DCS]} &= \vec{a}_{[DCS]} \\ \vec{z}_{osteo[OCS]} &= (0,0,1)^{\mathrm{T}} \end{aligned}$$

- The y axis of the *OsteoCS* points in AP direction, given by $\vec{d}_{AP}$. Because, according to the construction described in section 3.4, $\vec{a}$ and $\vec{d}_{AP}$ are not necessarily orthogonal, $\vec{y}_{osteo[DCS]}$ cannot immediately be set to the value of $\vec{d}_{AP}$. Rather, it must be reorthogonalized with respect to the shaft axis a by applying the vector cross product twice[3]:

$$\begin{aligned} \vec{y}_{osteo[DCS]} &= \vec{a} \times \vec{d}_{AP[DCS]} \times \vec{a} \\ \vec{y}_{osteo[OCS]} &= (0,1,0)^{\mathrm{T}} \end{aligned}$$

Through these correspondences (one point and two vectors), the coordinate transformation $\mathbf{M}_{DistCS \rightarrow OsteoCS}$ is uniquely determined and can be used to convert the parameters accordingly.

3.5.3.1 The Target Rotation

The target pose $\mathbf{M}_{target} = (\mathbf{R}_{target}, \mathbf{T}_{target})$ consists of a rotational part $\mathbf{R}_{target}$ and a translational part $\mathbf{T}_{target}$. The rotational part $\mathbf{R}_{target}$ is implicitly given through the angular values ϕ_{varus}, $\phi_{flexion}$ and $\phi_{rotation}$, because only a single rotation exists which will yield these specific angular differences in the projections.

The translational part $\mathbf{T}_{target}$ depends on the wedge size w as well as the user-defined translation (t_{AP}, t_{LM}, t_{SI}).

The wedge size w does not affect the rotational part of the target pose – it only influences the extent to which the femur will eventually be shortened or lengthened (see Figure 2.10).

[3] For two non-orthogonal vectors $\vec{u}$ and $\vec{v}$, the double cross product $\vec{u}' := \vec{v} \times \vec{u} \times \vec{v}$ yields the vector $\vec{u}'$, which is orthogonal to $\vec{v}$, with the minimum possible deviation from the original vector $\vec{u}$.

Since $\vec{a}$ (direction of the shaft axis) and $\vec{b}$ (direction of the neck axis) are vectors, they are not affected by the translational part of the target pose. Hence, their transformed counterparts $\vec{a}'$ and $\vec{b}'$ depend alone on the target rotation:

$$\vec{a}' = \mathbf{M}_{target} \cdot \vec{a} = \mathbf{R}_{target} \cdot \vec{a}$$

$$\vec{b}' = \mathbf{M}_{target} \cdot \vec{a} = \mathbf{R}_{target} \cdot \vec{a}$$

> **Note:** In the following, for any feature X of the original femur geometry, the expression X' denotes the same feature in the target geometry so that $X' = \mathbf{M}_{target} \cdot X$.

This chapter describes how the target rotation $\mathbf{R}_{target}$ is obtained by first determining $\vec{a}'$ and $\vec{b}'$ from the input parameters, through which they are implicitly given. Since two pairs of corresponding vectors, in this case $\vec{a} \rightarrow \vec{a}'$ and $\vec{b} \rightarrow \vec{b}'$, uniquely define a rotation, it will then be possible to construct the sought-after target rotation $\mathbf{R}_{target}$.

Like any rotation, the rotation $\mathbf{R}_{target}$ can be decomposed into three consecutive rotations about the z, y and x axes:

$$\mathbf{R}_{target} = \mathbf{R}_x \cdot \mathbf{R}_y \cdot \mathbf{R}_z \tag{3.1}$$

The partial rotations are defined as follows:

$\mathbf{R}_x$ A rotation about the x axis, which corresponds to a flexion/extension due to the definition of the osteotomy coordinate system. This rotation alone is responsible for the flexion part of the target pose (see below).

$\mathbf{R}_y$ A rotation about the y axis

$\mathbf{R}_z$ A rotation about the z axis, which, again due to the definition of the osteotomy coordinate system, is identical with the femoral shaft axis $\vec{a}$.

As usual, the rotations are performed in right-to-left order: first $\mathbf{R}_z$, then $\mathbf{R}_y$ and finally $\mathbf{R}_x$. The axes given in the description of the rotations are the axes of the static coordinate system, not those of any rotated system.

The flexion angle $\phi_{flexion}$ is defined as the angle between the projections of $\vec{a}$ and $\vec{a}'$ onto the plane $\mathcal{E}_{yz}$ (see section 2.4). Since $\vec{a}$ is the rotation axis of $\mathbf{R}_z$, the latter does not change $\vec{a}$ at all. The subsequent rotation $\mathbf{R}_y$, which is a rotation about the y axis, *does* change $\vec{a}$, however

it *does not* change[4] its projection onto $\mathcal{E}_{yz}$! Thus, the flexion/extension part of the target pose is completely determined by $\mathbf{R}_x$ alone, since the direction of the projected vector is invariant under the other two rotations. Hence, the only possible way to introduce the required flexion angle in equation 3.1 is to define $\mathbf{R}_x$ as a rotation about the x axis by the flexion angle:

$$\mathbf{R}_x = \mathbf{R}(\vec{e}_x, \phi_{flexion})$$

Determining $\mathbf{R}_z$ and $\mathbf{R}_y$ in a similar way is not possible, because all three rotations (including $\mathbf{R}_x$) contribute to varus/valgus and rotation/derotation to varying degrees.

Instead, consider the following auxiliary definitions:

$$\vec{a}^* := \mathbf{R}_x^{-1} \cdot \vec{a}' = \mathbf{R}_y \cdot \mathbf{R}_z \cdot \vec{a} \tag{3.2}$$

$$\vec{b}^* := \mathbf{R}_x^{-1} \cdot \vec{b}' = \mathbf{R}_y \cdot \mathbf{R}_z \cdot \vec{b} \tag{3.3}$$

Here, the two vectors $\vec{a}^*$ and $\vec{b}^*$ are defined, which are the "unflected" versions of $\vec{a}$ and $\vec{b}$.

The remainder of the calculation proceeds as follows:

1. The vector $\vec{b}'$ is determined from the osteotomy input parameters
2. Equation 3.3 yields the vector $\vec{b}^*$
3. From $\vec{b}^*$, the vector $\vec{a}^*$ is inferred through geometrical considerations
4. Given $\vec{a}^*$, rearranging equation 3.2 yields the vector $\vec{a}$

Now, the vector $\vec{b}'$, which is the transformed version of the femur neck axis, can easily be determined from $\vec{b}$, ϕ_{varus} and $\phi_{rotation}$ (while $\phi_{flexion}$ is not involved here, as per definition it does not depend on $\vec{b}$ or $\vec{b}'$). By definition, the values ϕ_{varus} and $\phi_{rotation}$ represent the angles between the projections of $\vec{b}$ and $\vec{b}'$ onto the planes $\mathcal{E}_{xz}$ and $\mathcal{E}_{xy}$. Let these four projections be called $\vec{b}_{xz}$, $\vec{b}'_{xz}$, $\vec{b}_{xy}$ and $\vec{b}'_{xy}$.

The vectors $\vec{b}_{xz}$ and $\vec{b}_{xy}$ can immediately obtained from $\vec{b}$ by setting its y or z component to 0:

$$\vec{b}_{xz} := \begin{pmatrix} b_1 \\ 0 \\ b_3 \end{pmatrix}, \vec{b}_{xy} := \begin{pmatrix} b_1 \\ b_2 \\ 0 \end{pmatrix}$$

[4] In fact, it changes the length of the projected vector, but not its direction which alone is relevant.

Given the projections of the original neck axis vector $\vec{b}$, it is possible to determine the projections of the transformed axis vector $\vec{b}'$, which was precisely defined in terms of these projections (see Figure 3.11)! Now, by its very definition, the projection $\vec{b}'_{xz}$ of $\vec{b}'$ onto $\mathcal{E}_{xz}$ is simply $\vec{b}_{xz}$ rotated by the varus angle:

$$\vec{b}'_{xz} = \begin{pmatrix} b'_{xz1} \\ 0 \\ b'_{xz3} \end{pmatrix} := \mathbf{R}(\vec{e}_y, \phi_{varus}) \cdot \vec{b}_{xz}$$

Analogously, the vector $\vec{b}'_{xy}$ can be determined from $\vec{b}_{xy}$:

$$\vec{b}'_{xy} = \begin{pmatrix} b'_{xy1} \\ b'_{xy2} \\ 0 \end{pmatrix} := \mathbf{R}(\vec{e}_z, \phi_{rotation}) \cdot \vec{b}_{xy}$$

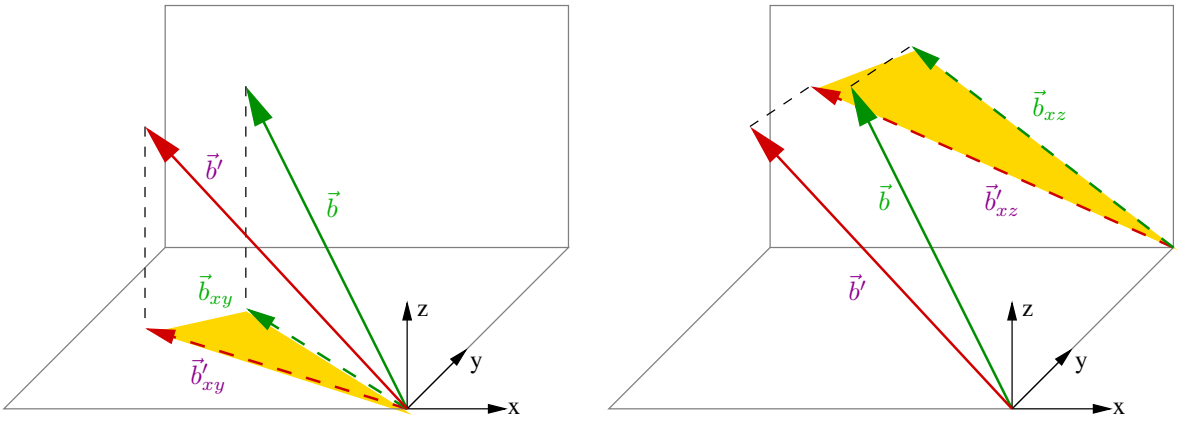

Figure 3.11. The projections of the two neck axis onto the xy and xz planes. The angles between the projected vectors are displayed yellow.

$\vec{b}'_{xz}$ and $\vec{b}'_{xy}$ are the projections of $\vec{b}'$ onto the xz and xy planes. From these two projections, it is possible to determine $\vec{b}'$ itself:

$$\vec{b}' = \text{normalize}(\begin{pmatrix} b'_{xy1} \\ b'_{xy2} \\ \frac{b'_{xy1}}{b'_{xz1}} b'_{xz3} \end{pmatrix})$$

With $\vec{b}'$ known, equation 3.3 can now be used to calculate $\vec{b}^*$.

The next step is the calculation of $\vec{a}^*$, which is characterized as follows:

(A1) Since, according to equation 3.2, $\vec{a}^* = \mathbf{R}_y \cdot \mathbf{R}_z \cdot \vec{a} = \mathbf{R}_y \cdot \vec{a}$, the vector $\vec{a}^*$ is parallel to the xz plane and thus orthogonal to $\vec{e}_y$.

(A2) The vectors $-\vec{a}$ and $\vec{b}$ enclose the CCD angle γ between them (see Figure 3.10), because $\vec{a}$ represents the original femur axis, and $\vec{b}$ represents the original neck axis. It follows that $-\vec{a}^*$ and $\vec{b}^*$ enclose the same angle, since the angle between two vectors remains unchanged under rotation. Eliminating the sign of $-\vec{a}^*$, this can be expressed as

$$\text{angle}(\vec{a}^*, \vec{b}^*) = \pi - \text{angle}(-\vec{a}^*, \vec{b}^*) = \pi - \gamma$$

(A3) $\vec{a}^*$ is a unit vector, thus $|\vec{a}^*| = 1$

Now, imagine $\vec{a}^*$ and $\vec{b}^*$ both being anchored at the origin. In this configuration, the tip of the sought-after vector $\vec{a}^*$ lies inside the xz plane, as follows from (A1). Furthermore, (A2) and (A3) alone characterize the set of unit vectors enclosing the angle $\pi - \gamma$ with the vector $\vec{b}^*$, calculated before, which is exactly the set of vectors whose tips lie on the circle $\mathcal{C}$, defined as follows (see figure 3.12):

- all points on $\mathcal{C}$ have a distance of 1 to the origin, since $\vec{a}^*$ is a unit vector
- The plane $\mathcal{E}_\mathcal{C}$ containing the circle $\mathcal{C}$ has the normal vector $\vec{n}_\mathcal{C} := \vec{b}^*$ (which, when anchored on $\mathcal{C}$, points into the halfspace not containing the origin)

Thus, the conditions (A1) to (A3) are fulfilled exactly by those vectors whose tips lie in the xz plane *and* on the circle $\mathcal{C}$, when anchored at the origin. To find those candidates for $\vec{a}^*$, it is therefore necessary to calculate the intersection between the xz plane and the circle $\mathcal{C}$.

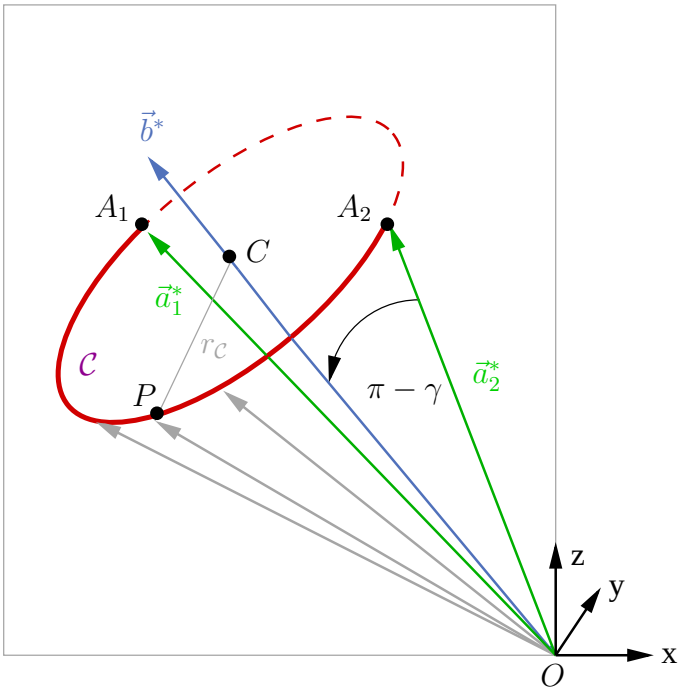

Figure 3.12. The circle $\mathcal{C}$, formed by the tips of the unit vectors (gray) with the angle $\pi - \gamma$ between them and $\vec{b}^*$. Intersecting $\mathcal{C}$ with the xz plane yields the points A_1 and A_2.

In 3D space, a circle intersects a plane in 0, 1 or 2 points[5]. In the case of no intersection points, an osteotomy with the chosen parameters is not feasible, which, however, never happens within a reasonable parameter range. With one point, the solution is unique. In the general case of two intersection points, one solution has to be discarded (see below).

To find the two intersection points A_1 and A_2 of the general case, first the center C of the circle $\mathcal{C}$ needs to be calculated. Any point P on the circle forms a right-angled triangle together with C and the origin O. The angle at the triangle vertex O is the angle between $\vec{a}^*$ and $\vec{b}^*$, namely $\pi - \gamma$. Thus, the distance c of C from O can be calculated:

$$c = \overline{OC} = \overline{OP} \cdot \sin(\pi - \gamma) = |\vec{a}^*| \cdot \cos\gamma = \cos\gamma$$

As OC has the same direction as the unit vector $\vec{b}^*$, it is possible to calculate the circle center C:

$$C = O + c \cdot \vec{b}^*$$

Similarly, the radius r_C of the circle can be obtained, which is the other side of the triangle:

[5] or ∞ if the circle lies in the plane, which cannot happen here

$$r_{\mathcal{C}} = \overline{CP} = \cos(\pi - \gamma)$$

Now, with $\mathcal{C}$ uniquely defined through $(C, r_{\mathcal{C}}, \vec{n}_{\mathcal{C}} = \vec{b}^*)$, it is possible to calculate the two points A_1 and A_2, at which $\mathcal{C}$ intersects the xz plane:

$$\{A_1, A_2\} := \text{intersect}(\mathcal{C}, \mathcal{E}_{xz})$$

As mentioned before, this operation always yields two solutions for a reasonable parameter range. The location vectors of A_1 and A_2, are the two candidate solutions $\vec{a}_1^*$ and $\vec{a}_2^*$. One of these is normally invalid, since, although fulfilling the constraints (1) to (3) as mentioned above, the resulting vector $\vec{a}'$ would point in distal direction. For some extreme angle values, two technically valid solutions exist (see Figure 3.13 for a 45° valgus). However, this does not happen for parameters in the normal range (0° to 20°). The correct solution is always found by choosing the vector from $\{\vec{a}_1^*, \vec{a}_2^*\}$ which encloses the smaller angle with the original shaft axis $\vec{a}$.

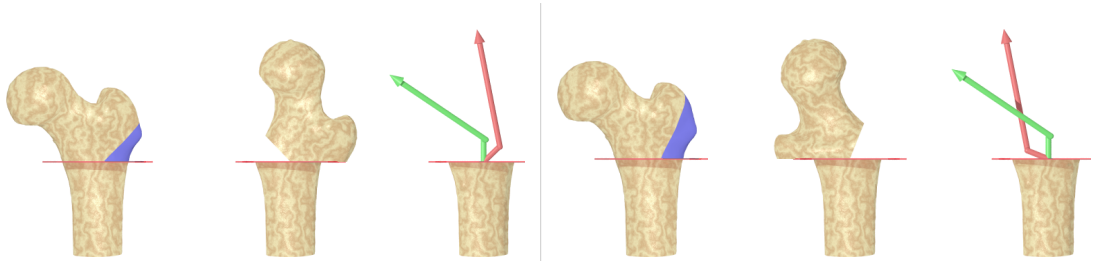

(a) First solution (b) Second solution

Figure 3.13. The two solutions for a 45° valgus osteotomy. In both cases, there is a 45° angle between the original (green) neck axis vector $\vec{b}$ and the transformed target vector $\vec{b}'$ (red). The values for flexion/extension and rotation/derotation match, too. However, solution (b) would be discarded, as the angle between the original and transformed shaft axes is lower in (a).

Now, from equation 3.2, it is finally possible to determine $\vec{a}'$. Thus, two pairs of vectors $(\vec{a}, \vec{b})$ and $(\vec{a}', \vec{b}')$ are known, which are mapped onto each other through $\mathbf{R}_{target}$. They therefore uniquely define a rotation in $\mathbb{R}^3$. Let $(\vec{u}_1, \vec{u}_2, \vec{u}_3)$ be the normalized versions of $(\vec{a}, \vec{a} \times \vec{b}, \vec{a} \times \vec{b} \times \vec{a})$, so that they form an orthonormal base. Let $(\vec{u}'_1, \vec{u}'_2, \vec{u}'_3)$ be the same for $(\vec{a}', \vec{a}' \times \vec{b}', \vec{a}' \times \vec{b}' \times \vec{a}')$. The rotation $\mathbf{R}_{target}$ can now be determined as follows:

$$\mathbf{R}_{target} := \mathbf{R}(\vec{u}_1, \vec{u}_2, \vec{u}_3) \cdot \mathbf{R}(\vec{u}'_1, \vec{u}'_2, \vec{u}'_3)^{-1}$$

3.5.3.2 The Wedge Parameters

Based on the target rotation $\mathbf{R}_{target}$, it is now possible to calculate the parameters defining the wedge. These are

- the wedge plane $\mathcal{E}_{wedge}$, which forms the wedge together with the given osteotomy plane $\mathcal{E}_{osteo}$
- the effective wedge angle κ, the angle between $\mathcal{E}_{wedge}$ and $\mathcal{E}_{osteo}$
- the wedge direction vector $\vec{w}_{dir}$, which describes the orientation of the wedge on the osteotomy plane

The location of the wedge plane $\mathcal{E}_{wedge}$ essentially depends on two things: the target rotation $\mathbf{R}_{target}$ and the wedge size w.

The key to determining these parameters are the following observations:

(B1) For a wedge size $w = 0.5$ and a $t_{AP} = t_{LM} = t_{SI} = 0$, the target pose $\mathbf{M}_{target}$ is identical to the target rotation $\mathbf{R}_{target}$. The reasons for this were explained in section 3.5.2.

(B2) The target pose brings the osteotomy plane and the wedge plane together, which means that after the osteotomy, the two planes coincide:

$$\mathcal{E}_{osteo} = \mathbf{M}_{target} \cdot \mathcal{E}_{wedge} \tag{3.4}$$

This is displayed as the tilting step in Figure 3.9.

(B3) The values (t_{AP}, t_{LM}, t_{SI}) have no effect on the wedge plane, as they determine only how the proximal fragment has to be moved *after* the wedge excision[6].

(B4) With all other parameters being equal, the wedge planes for different values of w differ only in translation (see Figure 2.10).

This leads to the following algorithm for determining $\mathcal{E}_{wedge}$, the details of which are explained below:

[6] Technically, this is true only for t_{AP} and t_{LM}. Any movement of the proximal fragment in inferior direction, as with $t_{SI} < 0$, requires an adjustment of $\mathcal{E}_{wedge}$ to avoid self-collision of the fragments. This special case is covered in a broader scope in section 4.1.2

1. Calculate $\mathcal{E}^*_{wedge}$ for the wedge size $w^* = 0.5$, which is identical to $\mathcal{E}_{wedge}$ except for a translation caused by the different wedge size

2. Calculate the amount by which $\mathcal{E}^*_{wedge}$ has to be translated to yield the actual wedge size w

According to (B1), for the wedge size $w^* = 0.5$, the target pose is equal to its rotational part $\mathbf{R}_{target}$ if $t_{AP} = t_{LM} = t_{SI} = 0$, which can be assumed here due to (B3). Thus, $\mathbf{M}_{target}$ can be substituted by $\mathbf{R}_{target}$ in equation 3.4, given in (B2). Rearranging yields

$$\mathcal{E}^*_{wedge} = \mathbf{R}^{-1}_{target} \cdot \mathcal{E}_{osteo}$$

which can be directly calculated, since both $\mathbf{R}_{target}$ and $\mathcal{E}_{osteo}$ are known.

According to (B4), $\mathcal{E}^*_{wedge}$ and $\mathcal{E}_{wedge}$ differ only in translation, which means that both form the same angle with $\mathcal{E}_{osteo}$, namely the effective wedge angle κ. This angle can be calculated from the plane normals:

$$\kappa = \text{angle}(\vec{n}_{wedge}, \vec{n}_{osteo})$$

> **Note:** The normal vector of a plane is not unique (even if a unit vector is assumed), since if $\vec{n}$ is a plane normal, the vector $-\vec{n}$ is, too. In the case at hand, the two vectors $\vec{n}_{osteo}$ and $\vec{n}_{wedge}$ must be chosen so that both of them point in proximal direction.

$\mathcal{E}_{wedge}$ can be obtained from $\mathcal{E}^*_{wedge}$ through a translation on the osteotomy plane by the amount $(2w - 1) \cdot r_{shaft}$, which depends on the wedge size w and the shaft radius r_{shaft}. This translation, which acts orthogonally to the line of intersection between $\mathcal{E}^*_{wedge}$ and $\mathcal{E}_{osteo}$, can be replaced by a translation in the direction of the normal vector $\vec{n}_{wedge}$ of $\mathcal{E}^*_{wedge}$ by the amount $\sin\kappa \cdot (2w - 1) \cdot r_{shaft}$, which yields the wedge plane $\mathcal{E}_{wedge}$:

$$\mathcal{E}_{wedge} = \mathbf{T}(\sin\kappa \cdot (2w - 1) \cdot r_{shaft} \cdot \vec{n}_{wedge}) \cdot \mathcal{E}^*_{wedge}$$

The last remaining wedge parameter, $\vec{w}_{dir}$, can be calculated as the normalized projection of the wedge plane normal $\vec{n}_{wedge}$ onto the osteotomy plane, which is the xy plane in the osteotomy coordinate system:

$$\vec{w}_{dir} := \text{normalize}(\text{proj}_{\text{xy}}(\vec{n}_{wedge}))$$

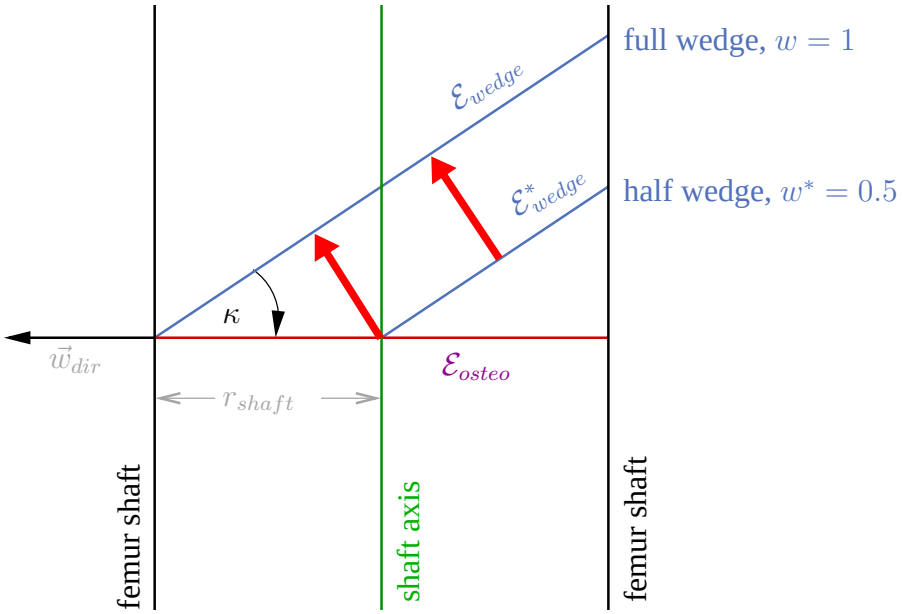

Figure 3.14. The wedge plane $\mathcal{E}_{wedge}$ for the real wedge size w can be obtained from $\mathcal{E}^*_{wedge}$ through a translation in direction of the plane normal (red arrows) by the amount $sin\kappa \cdot (2w-1) \cdot r_{shaft}$.

3.5.3.3 The Target Pose

Finally, it is possible to determine the target pose $\mathbf{M}_{target}$ itself. This pose can be interpreted as the concatenation of three transformations (in right-to-left order), which correspond exactly to the steps (d) to (f) in Figure 3.9:

$$\mathbf{M}_{target} = \mathbf{T}_{trans} \cdot \mathbf{R}_{axis} \cdot \mathbf{M}_{tilt} \tag{3.5}$$

with the following properties:

- $\mathbf{M}_{tilt} = (\mathbf{R}_{tilt}, \mathbf{T}_{tilt})$ rotates the proximal fragment about the edge of the excised wedge. It is composed of a rotational part $\mathbf{R}_{tilt}$ and a translational part $\mathbf{T}_{tilt}$.
- $\mathbf{R}_{axis}$ is a rotation about the shaft axis. This is a pure rotation, since its axis of rotation passes through the origin of the osteotomy coordinate system
- $\mathbf{T}_{trans}$ is the final translation defined by (t_{AP}, t_{LM}, t_{SI})

This section describes how these three transformations are obtained. First, to be able to calculate $\mathbf{M}_{tilt}$, it is necessary to know its axis of rotation, the wedge edge ℓ_{wedge}. This axis does not normally contain the origin of the coordinate system, hence $\mathbf{M}_{tilt}$ is not a pure rotation.

The exception is a half-wedge, for which the wedge edge intersects the femoral shaft axis in the origin, so that the translational part $\mathbf{T}_{tilt}$ vanishes.

The wedge edge ℓ_{wedge} is identical to the line of intersection between $\mathcal{E}_{osteo}$ and $\mathcal{E}_{wedge}$:

$$\ell_{wedge} := \text{intersect}(\mathcal{E}_{osteo}, \mathcal{E}_{wedge})$$

The tilting pose $\mathbf{M}_{tilt}$ is simply a rotation about this axis by the angle κ:

$$\mathbf{M}_{tilt} = (\mathbf{R}_{tilt}, \mathbf{T}_{tilt}) := \text{axisrotate}(\ell_{wedge}, \kappa)$$

Now it is possible to determine $\mathbf{R}_{axis}$. As the translations in equation 3.5 have no influence on the rotational part of the target pose and can be ignored, the following relation holds between the rotations:

$$\mathbf{R}_{target} = \mathbf{R}_{axis} \cdot \mathbf{R}_{tilt}$$

or, since $\mathbf{R}_{target}$ and $\mathbf{R}_{tilt}$ are known:

$$\mathbf{R}_{axis} = \mathbf{R}_{target} \cdot \mathbf{R}_{tilt}^{-1}$$

This leaves $\mathbf{T}_{trans} = \vec{t}_{trans}$ to be determined, which is very easy: since the osteotomy coordinate system was chosen so that its axes correspond exactly to the anatomical directions anterior/posterior, lateral/medial and superior/inferior, the translation can immediately be given:

$$\vec{t}_{trans} = \begin{pmatrix} t_{LM} \\ -t_{AP} \\ t_{SI} \end{pmatrix} \text{ for a left femur and } \vec{t}_{trans} = \begin{pmatrix} -t_{LM} \\ -t_{AP} \\ t_{SI} \end{pmatrix} \text{ for a right femur}$$

The reversal of the sign of t_{LM} depending on the femur side stems from the fact that, for a left femur, the x axis points in lateral direction, while for a right femur it points in medial direction.

With $\mathbf{T}_{trans}$, all components necessary for the calculation of the target pose as given in equation 3.5 have been determined, and $\mathbf{M}_{target}$ can finally be obtained.

3.5.3.4 The Sequential Planning Mode

As mentioned in section 2.4.2, in the case of the conventional operation method, the target pose is not defined by angular projections (”projection mode”), but rather by a sequence of rotations about different axes (”sequential mode”). The two ways of determining the target pose only differ in the calculation of the rotational part $\mathbf{R}_{target}$ of the target pose and are otherwise identical. The FEMOS system implements both modes of interpreting the input parameters. The ”projection mode” was described above; this section shortly presents the far simpler algorithm for the ”sequential mode”.

The rotational part of the target pose $\mathbf{R}_{target}$ is defined through a concatenation of the following transformations (given in the osteotomy coordinate system):

1. Rotate about the y-axis by ϕ_{varus}
2. Rotate about the x-axis by $\phi_{flexion}$
3. Rotate about the z-axis by $\phi_{rotation}$

This immediately makes clear how $\mathbf{R}_{target}$ has to be calculated for the sequential (traditional) planning mode:

$$\mathbf{R}_{target} := \mathbf{R}(\vec{e}_z, \phi_{rotation}) \cdot \mathbf{R}(\vec{e}_x, \phi_{flexion}) \cdot \mathbf{R}(\vec{e}_z, \phi_{varus})$$

After the $\mathbf{R}_{target}$ has been determined, the calculation proceeds as described in the previous section.

3.5.4 Implant Position

After the target parameters have been determined, the system calculates the default pose $\mathbf{M}_{PlateCS \rightarrow DistCS}$ for the implant, which is the pose transforming the plate geometry from the plate coordinate system into the reference frame of the distal fragment. The definitions of the plate geometry and the implant coordinate system *PlateCS* were given in section 2.5.

Because of anatomical considerations, it is clear that the plate pose must be chosen so that

- the central axis of the blade passes through the femoral neck isthmus, so that the danger of it perforating the corticalis is minimized
- the shaft aligns with the femur diaphysis

(a) The implant shaft aligns with the femur diaphysis, and the extension of the blade goes straight through the neck isthmus center (red point).

(b) Abstract model of the positioned plate

Figure 3.15. A perfectly positioned implant.

With regard to the reconstructed femur model, these constraints can be formulated as follows (see Figure 3.15):

(C1) The plate shaft vector $\vec{d}_{shaft}$ must be parallel to the projection of the femur axis onto the lateral corticalis tangent plane $\mathcal{E}_{lateral}$. This condition ensures that the plate shaft will align with the lateral corticalis, as seen in the AP image.

(C2) The blade must pass through the isthmus center N. This condition ensures that the blade pierces the narrowest part of the neck centrally.

(C3) The blade of the implant must be parallel to the plane spanned by the femoral shaft axis vector $\vec{a}$ and the line connecting the femoral head H with the neck isthmus N. This ensures that the blade passes through the neck following the direction of the neck axis.

(C4) The plate origin must lie on the corticalis tangent plane $\mathcal{E}_{lateral}$. This ensures that the implant is in contact with the femur diaphysis.

> **Note:** Unless stated otherwise, all geometrical features mentioned in this section, such as $\mathcal{E}_{lateral}$ or $\vec{a}$, are given in the coordinate system of the distal reference frame *DistCS*.

This formulation of the constraints allows to straightforwardly deduce an algorithm which calculates the desired plate pose $\mathbf{M}_{PlateCS \to DistCS}$. Given the femur geometry and the original

plate parameters $O_{plate[PlateCS]}$, $\vec{d}_{shaft[PlateCS]}$ and $\vec{d}_{blade[PlateCS]}$, specifying the plate origin, the direction of the plate shaft and the direction of the plate blade in the plate coordinate system, the parameters O_{plate}, $\vec{d}_{shaft}$ and $\vec{d}_{blade}$ can be determined. These parameters describe the plate in its default pose in the distal reference frame[7].

It follows from (C1) that the shaft direction $\vec{d}_{shaft}$ can be calculated like this ($\vec{a}$ is the *proximal* direction of the femur shaft axis, but the plate shaft must point in distal direction, hence $-\vec{a}$ is projected):

$$\vec{d}_{shaft} := \text{normalize}(\text{proj}(-\vec{a}, \mathcal{E}_{lateral}))$$

(C3) means that the blade vector $\vec{d}_{blade}$ must be parallel to the plane spanned by $(H-N)$ and $\vec{a}$ of the *transformed* femur, since the implant is inserted after the osteotomy was performed. Let n_{plate} be the normal vector of this plane. n_{plate} can be calculated as follows:

$$n_{plate} := \text{normalize}(\mathbf{M}_{target} \cdot (\vec{a} \times (H - N)))$$

The blade vector $\vec{d}_{blade}$ must satisfy the following conditions:

- The angle between $\vec{d}_{blade}$ and $\vec{d}_{shaft}$ must be the original plate angle δ_{plate}
- $\vec{n}_{plate}$ must be orthogonal to $\vec{d}_{blade}$.

These conditions yield the following equations:

$$|\vec{d}_{shaft}| = 1 \tag{3.6}$$
$$< \vec{d}_{shaft}, \vec{d}_{blade} > = \cos \delta_{plate} \tag{3.7}$$
$$< \vec{n}_{plate}, \vec{d}_{blade} > = 0 \tag{3.8}$$

Equation 3.6 was added, since 3.7 and 3.8 uniquely specify the direction of the vector but not its length, which can be chosen freely and is set to unit length in equation 3.6. This also permits the simplification made in equation 3.7, since both $\vec{d}_{shaft}$ and $\vec{d}_{blade}$ have now unit length.

With $\vec{d}_{blade} = (x_1, x_2, x_3)$, $\vec{d}_{shaft} = (s_1, s_2, s_3)$, $\vec{n}_{plate} = (n_1, n_2, n_3)$ and $q := cos(\delta_{plate})$, the equations can be rewritten as:

[7] As mentioned, objects are here assumed to be given in the distal coordinate system *DistCS* unless otherwise stated, hence $O_{plate} = O_{plate[DistCS]}$ and so on

$$\sqrt{x_1^2 + x_2^2 + x_3^2} = x_1^2 + x_2^2 + x_3^2 = 1 \tag{3.6*}$$

$$s_1 x_1 + s_2 x_2 + s_3 x_3 = q \tag{3.7*}$$

$$n_1 x_1 + n_2 x_2 + n_3 x_3 = 0 \tag{3.8*}$$

Using elementary algebra, these three equations can be solved[8] for $\vec{d}_{blade} = (x_1, x_2, x_3)$:

$$u_1 = \frac{s_2 n_3 - s_3 n_2}{s_1 n_2 - s_2 n_1} \qquad u_2 = \frac{s_1 n_3 - s_3 n_1}{s_2 n_1 - s_1 n_2}$$

$$v_1 = \frac{q n_2}{s_1 n_2 - s_2 n_1} \qquad v_2 = \frac{q n_1}{s_2 n_1 - s_1 n_2}$$

$$a = u_1^2 + u_2^2 + 1 \qquad b = 2u_1 v_1 + 2u_2 v_2 \qquad c = v_1^2 + v_2^2 - 1$$

$$l_{1,2} = \frac{-b \pm \sqrt{b^2 - 4ac}}{2a}$$

$$\vec{d}_{blade,1} = \begin{pmatrix} u_1 l_1 + v_1 \\ u_2 l_1 + v_2 \\ l_1 \end{pmatrix}, \; \vec{d}_{blade,2} = \begin{pmatrix} u_1 l_2 + v_1 \\ u_2 l_2 + v_2 \\ l_2 \end{pmatrix}$$

There are two solutions, $\vec{d}_{blade,1}$ and $\vec{d}_{blade,2}$. One of them is the sought-after vector, the other one is the same vector rotated by 180° about $\vec{d}_{shaft}$. By inspecting the constraints given, it becomes obvious that two such solutions exist. Of these solutions, the one pointing in medial direction must be chosen. The vector $\vec{d}_{medial}$, pointing in medial direction, can be obtained from the AP direction $\vec{d}_{AP}$ and the direction of the femur shaft axis $\vec{a}$, pointing in proximal direction. Further, the medial direction depends on whether the treated femur is a left or a right femur:

[8] The solution given does not work for $(s_1 n_2 - s_2 n_1) = 0$ (division by zero). However, since the three equations are symmetrical with respect to the variable's indexes, a permutation of these (e.g. $1 \rightarrow 2 \rightarrow 3 \rightarrow 1$) is bound to yield a valid solution, because (s_1, s_2, s_3) and (n_1, n_2, n_3) are guaranteed not to be collinear.

$$\vec{d}_{medial,left} = \vec{a} \times \vec{d}_{AP}, \qquad \vec{d}_{medial,right} = \vec{d}_{AP} \times \vec{a}$$

Of $\vec{d}_{blade,1}$ and $\vec{d}_{blade,2}$, the one enclosing the smaller angle with $\vec{d}_{medial}$ must be chosen.

At this point of the calculation, the shaft vector $\vec{d}_{shaft}$ and the blade vector $\vec{d}_{blade}$ of the plate are known, and hence the plate's orientation. What remains to be determined is the location of the plate, which is given by the position of the plate origin O_{plate}. From (C4), it is known that O_{plate} lies on $\mathcal{E}_{lateral}$. Further, the blade must pass through the neck isthmus center *after* the transformation, according to (C2). Let ℓ_{blade} be the central line of the blade, which has the following properties:

- It contains the point $\mathbf{M}_{target} \cdot N$, the transformed neck isthmus center.
- It has the direction vector $\vec{d}_{blade}$.
- It contains the plate origin O_{plate}, which needs to be determined.

Thus, ℓ_{blade} can be given as

$$\ell_{blade} = (\mathbf{M}_{target} \cdot N) + \lambda \cdot \vec{d}_{blade} \qquad \lambda \in \mathbb{R}$$

Since O_{plate} is known to lie on $\mathcal{E}_{lateral}$ and ℓ_{blade}, it can be found by intersecting these two:

$$O_{plate} = \text{intersect}(\mathcal{E}_{lateral}, \ell_{blade})$$

The default pose for the implant is now fixed, since O_{plate}, $\vec{d}_{shaft}$ and $\vec{d}_{blade}$ are all known.

3.5.5 System Feedback

Once the target parameters were calculated, the system can give the surgeon feedback about the predicted effects of the current parameters. The calculations can be performed on a standard PC without noticeable delay, thus allowing the surgeon to iteratively modify the parameters until a satisfactory result has been reached.

3.5.5.1 Optimization of the Implant Position

As described in section 3.5.4, the system determines a default position for the implant. However, the algorithm used to obtain the default position operates on the primitive femur model only, and hence it may prove necessary for the surgeon to manually adjust the plate position thus determined.

To enable the surgeon the best possible assessment of the current position of the implant, a visualization of the plate is overlaid on the fluoroscopic images acquired earlier during the intervention. Seeing the projected plate model in the images, the surgeon can adjust the positioning parameters. The system yields immediate feedback on the current parameters, which can be iteratively be refined until the surgeon is satisfied.

In assessing the current implant position, the surgeon is especially interested in determining

- how the blade of the implant is situated within the proximal part of the femur (femur neck), and
- how the shaft of the implant aligns with the femur diaphysis

Since the images show the *preoperative* femur, and the plate will be implanted to the *transformed* femur, it is not possible to simply overlay a visualization of the plate model on top of the images. Such a visualization would fit either at the femur neck or at the femur shaft, but never both. Also, modifying the preoperative images in a way as to display the postoperative femur is impracticable, for an osteotomy changes the 3D geometry of the bone, the result of which cannot simply be anticipated through 2D image manipulation.

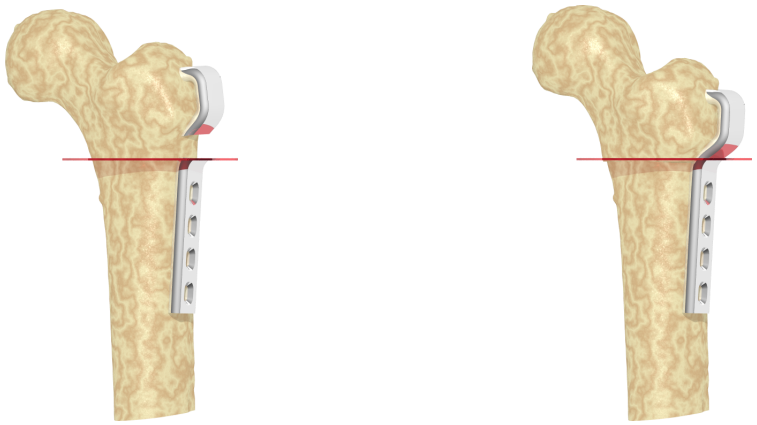

(a) Split plate, pre-OP. The pose between the two parts is the inverse target pose.

(b) post-OP

Figure 3.16. The plate model, separated into two fragments which will align after the osteotomy.

Instead of trying to modify the proximal and distal parts of femur in the images to reflect the transformation, the FEMOS system overcomes this problem by splitting the plate into a distal

and a proximal part. Thus, the *inverse target pose* can be applied to the proximal part of the implant, so that this part of the plate is displayed in correct relation to the proximal fragment of the (intact) femur, just as it will appear in the transformed femur (see Figure 3.16).

Thus, the surgeon can assess the position of the two parts of the implant separately — the distal part (which is not going to be changed by the osteotomy) at the femur diaphysis, and the proximal part, as it will appear after the osteotomy, at the femur neck.

Since the internal and external camera parameters of the two images are known, it is possible to set up a 3D display window, which emulates the properties of the camera and renders in correct perspective a view consisting of the fluoro images and 3D objects such as a model of the implant. The FEMOS system uses the OPENGL[Woo97] library to display this view.

The cut between the proximal and distal parts of the implant should occur along the osteotomy plane, because this is the plane at which the two fragments will later meet. The poses $\mathbf{M}_{plate,distal}$ and $\mathbf{M}_{plate,proximal}$ at which the plates need to be rendered can be given as follows:

$$\mathbf{M}_{plate,distal} = \mathbf{M}_{PlateCS \rightarrow DistCS}$$

$$\mathbf{M}_{plate,proximal} = \mathbf{M}_{target}^{-1} \cdot \mathbf{M}_{PlateCS \rightarrow DistCS}$$

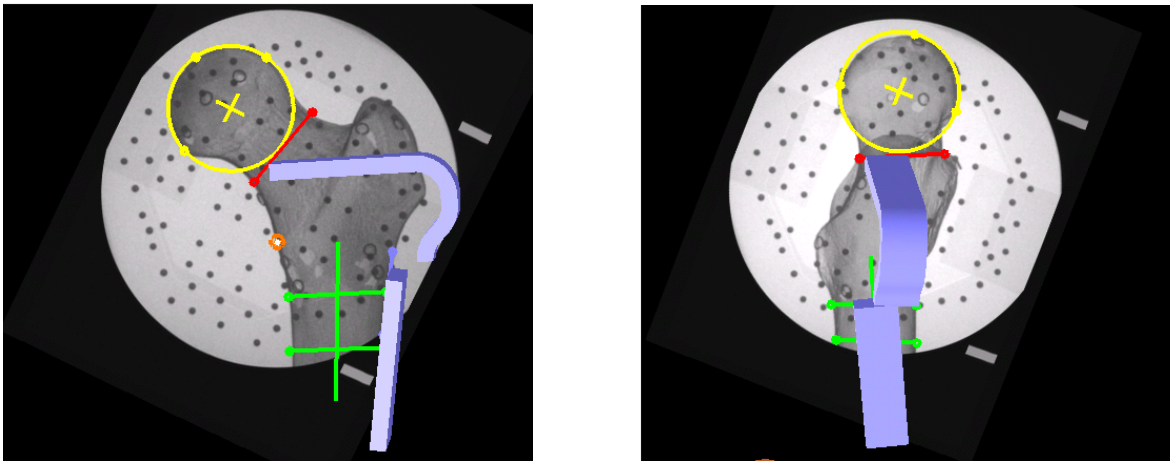

(a) AP view (b) Axial view

Figure 3.17. The planning view with overlaid plate model. Through the split visualization, both parts are displayed on the intact femur in the position they will later have on the corrected femur.

Figure 3.17 shows the view which is presented to the user. The user interface further provides buttons and sliders with which the surgeon can modify the plate position in any of the

available six degrees of freedom (three translations, three rotations) until an optimal location has been obtained.

3.5.5.2 Biomechanical Effects

Another point to be considered when performing a femur osteotomy is the effect of the correction on the biomechanical leg axis. Physiologically, the mechanical leg axis is an imaginary line which connects the centers of the hip joint, the knee joint and the upper ankle joint [Pal02]. Since this axis transmits the entire body weight (or at least half of it, considering the opposite leg), undue shifting of it will impose considerable biomechanical stress on the involved parts. Besides shifting the leg axis, the osteotomy also has a direct impact on the length of the leg. Depending on the wedge angle and wedge size, the leg may be considerably shortened or lengthened.

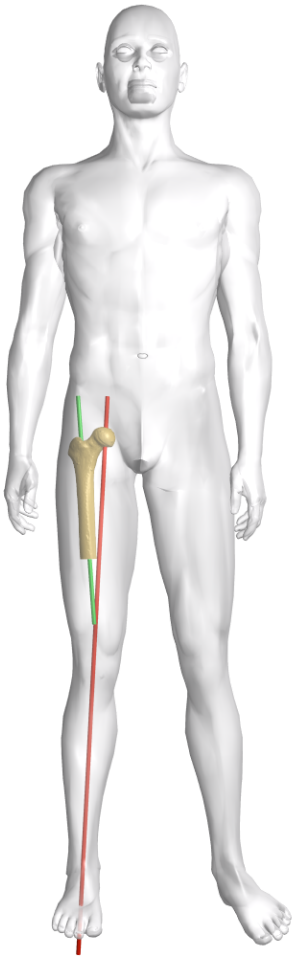

Figure 3.18. The biomechanical axis (red) forms a 7° angle with the anatomical shaft axis (green)

Both of these implications should be kept in mind while optimizing the osteotomy parameters. The FEMOS system supports the surgeon in assessing these effects by calculating the displacement of the femur head, which would ensue from the currently specified parameters. The displacement can be expressed as a 3D vector

$$\vec{t}_{disp} = \begin{pmatrix} t_{lateral} \\ t_{ventral} \\ t_{superior} \end{pmatrix}$$

giving the extent of the displacement of the femoral head in lateral/medial, ventral/dorsal and superior/inferior directions. The first two signify a shift of the mechanical leg axis in the particular directions, the last one represents a lengthening/shortening of the leg. The vector $\vec{t}_{disp}$ must be given in a coordinate system relative to the biomechanical leg axis, which is related to but not identical with the osteotomy coordinate system, being defined relative to the anatomical femur shaft axis.

In the physiological case, the angle β between the femoral shaft axis and the mechanical leg axis amounts to 7° when seen in AP direction. The angle which appears in the sagittal plane is negligible. Thus, the mechanical leg axis can be obtained by rotating the shaft axis by β about the y-axis of the osteotomy coordinate system (which does point in AP direction).

Since the FEMOS system does not have enough data to reconstruct the actual mechanical leg axis (which would, by definition, require additional knowledge about the location of the center of the knee joint), the physiological normal value for β can be used to obtain a reasonable approximation for the location of the leg axis. Alternatively, the actual value of β could be determined externally (for example from a full-length X-ray of the femur) and entered manually. Thus, $\vec{t}_{disp}$ can be found as follows:

$$\vec{t}_{disp} = \underbrace{\mathbf{R}(\vec{e}_y, \beta)}_{\text{rotation about the y-axis by } \beta} \cdot \underbrace{(\mathbf{M}_{target} \cdot H - H)}_{\text{head center displacement}}$$

The component values of $\vec{t}_{disp}$ are immediately calculated on every parameter change made by the user. They are permanently displayed in the planning mode of the system, so that the user can compensate undue shifting of the axis by adjusting the input values accordingly.

3.6 Computer-assisted Execution

After the planning phase has been finished, the surgeon proceeds to performing the actual intervention. In chronological order, the necessary steps are:

1. Gouging of the blade channel
2. Sawing the femur through along the osteotomy plane
3. Cutting a wedge out of the proximal fragment by sawing along the cutting plane
4. Repositioning of the fragments until the target pose is reached and fixing them with an implant

All of these steps are performed with the help of a custom navigation module. The global reference frame for the navigation is provided by the tracker which was attached to the *distal* part of the femur prior to the image acquisition. In order to use the position tracking for the steps mentioned above, trackers must be attached to the chisel, the saw and the *proximal* part of the femur.

For each of the steps mentioned above, the guiding system provides the surgeon with several views of the abstract model and the fluoroscopic images which were used in the planning

phase. All of these views additionally show a perspectively correct visualization of the currently used tool (saw, chisel).

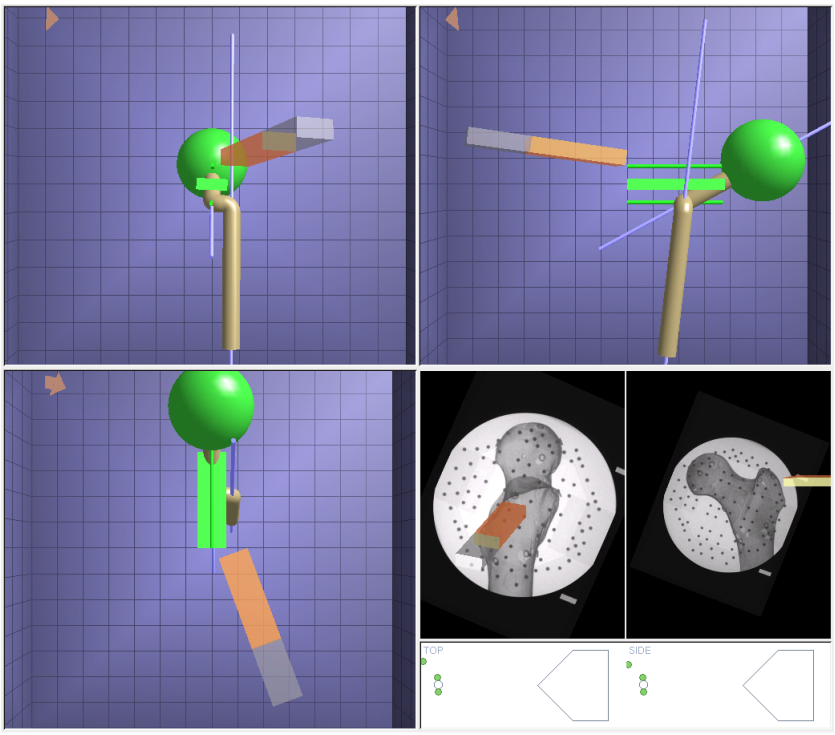

Figure 3.19. A screenshot of the navigation module of the FEMOS system. The orange/gray shape represents the tracked chisel. The gray part of the chisel shape corresponds to the actual tip of the instrument, the orange part is a virtual extension along its main direction. The surgeon must position the chisel so that it aligns with the green cuboid, which represents the blade channel.

3.6.1 Gouging of the Blade Channel

The gouging of the blade channel has to be performed prior to any of the other steps, since after the proximal part of the femur has been severed from the distal part, it lacks the stability necessary for the chisel to penetrate the bone. Like the implant, which will later be inserted into the channel, the chisel has a U-shaped profile, which guarantees a tight fit of the implant in the bone.

In order to be used with the navigation system, the geometry of the chisel must be known. For the purposes at hand, a very simple model of the chisel's geometry is sufficient: it can be represented by a tuple $\mathcal{G}_{chisel} = (O, \vec{d}_{long}, \vec{d}_{up}, w_{profile}, h_{profile})$, giving the position of the chisel's tip O, the vector of the chisel's main direction $\vec{d}_{long}$,the vector pointing upwards, $\vec{d}_{up}$ and the width/height of the chisel profile. The geometry is specific to a given chisel and never

changes.

Before it can be used, the chisel needs to be calibrated as described in section 3.1.1.1. After this has been done, the chisel can be displayed in the navigation module of the FEMOS system (see Figure 3.19). In various views which are continuously updated, the surgeon can see the current position of the chisel in relation to the reconstructed femur model as well as in the fluoroscopic images which were acquired earlier.

In the implant positioning step of the planning phase, the plate pose $\mathbf{M}_{PlateCS \rightarrow DistCS}$ was determined. The location of the blade channel corresponds to the location of the implant blade, relative to the proximal fragment. Thus, the blade channel can be modeled as a cuboid object, which encases the blade of the implant. Let $\mathcal{G}_{channel}$ be a geometric description of the blade channel in the plate coordinate system. The pose $\mathbf{M}_{channel}$, by which this geometry is transformed into that of the actual target channel of the reference frame is given as

$$\mathbf{M}_{channel} := \mathbf{M}_{target}^{-1} \cdot \mathbf{M}_{PlateCS \rightarrow DistCS}$$

The inverse target pose $\mathbf{M}_{target}^{-1}$ must be premultiplied, since $\mathbf{M}_{PlateCS \rightarrow DistCS}$ specifies the pose of the plate *after* the osteotomy, and hence presupposes the osteotomy target pose. However, the blade channel must be gouged *before* the osteotomy is performed, and hence this implicit target pose must be reversed.

3.6.2 The Fragment Reference Pose

Before the cuts are made, a reference tracker must be attached to the proximal part of the femur, in addition to the already present tracker of the distal fragment. This tracker serves two purposes:

- It provides a reference for the cutting of the wedge plane of the proximal fragment. Since the fragments are already separated at this stage, the tracker on the distal fragment cannot be used for this purpose.
- It is required for the fragment tracking step, in which both femur parts are tracked independently of each other until the target pose has been reached.

> **Note:** The proximal reference tracker should be attached only *after* the blade channel was gouged, since the repetitive hammering of the chisel may cause the tracker to loosen itself.

Once the tracker has been attached, and *before* the fragments are separated, the pose $\mathbf{M}_{fragref}$ of this new tracker in reference to the already existing tracker of the distal fragment has to be acquired. This pose stores the original relation of the distal and proximal fragment and will later be used to convert the geometrical features of the femur (which are all given in the distal reference frame) to the proximal reference frame. Let $\mathbf{M}_{DistCS \rightarrow CamCS}$ and $\mathbf{M}_{ProxCS \rightarrow CamCS}$ denote the tracker poses of the two fragment trackers as reported by the tracking system. The fragment reference pose $\mathbf{M}_{fragref}$ is defined as

$$\mathbf{M}_{fragref} := \mathbf{M}^{-1}_{ProxCS \rightarrow CamCS} \cdot \mathbf{M}_{DistCS \rightarrow CamCS}$$

This pose is taken before the cutting starts and is then stored for later use.

3.6.3 Removal of the Wedge

The removal of the wedge happens in two steps: first, the entire femur is cut through along the osteotomy plane, thereby dividing it into a distal and a proximal fragment. Then, a second cut must be made along the wedge plane of the proximal fragment.

The cuts are performed using a calibrated saw. As with the chisel, the system must know the basic geometry of the saw to be able to display it in the navigation view. In the FEMOS system, the saw geometry is represented as a tuple $(\vec{d}_{long}, \vec{d}_{up}, r_{blade}, \alpha_{blade})$, specifying the longitudinal direction of the saw, its ”upwards” direction, the radius of the saw blade and its fanning angle.

The navigation system guides the surgeon by displaying the target plane and the current position of the saw. For the osteotomy plane $\mathcal{E}_{osteo}$, the distal tracker is used as reference, and for the wedge plane $\mathcal{E}_{wedge}$, the proximal tracker is used.

3.6.4 Fragment Positioning

After the wedge has been removed, the surgeon moves the fragments in relation to each other, until the target pose has been reached. Since both fragments have trackers attached to them, the system can track them independently of each other, inversely determine the osteotomy parameters of their current location, and display these to the user. The surgeon now modifies the position of the fragments, until the parameters inversely calculated from the current position match the planned values. If the removal of the wedge was performed with sufficient accuracy, this is a moderately difficult task, since just bringing the fragments together at their respective cutting planes eliminates three degrees of freedom altogether, leaving only one rotational (ro-

tation of the proximal fragment about the shaft axis) and two translational (movement parallel to the cutting plane) degrees of freedom to be matched.

3.6.4.1 Inverse Calculation of the Parameters

This section describes the algorithm used to inversely calculate the osteotomy parameters of a given pose. More specifically, the algorithm solves the following problem:

> Given a pose $\mathbf{M}_{current}$, representing a relocation of the proximal fragment relative to the intact femur, determine the parameters $(\phi_{varus}, \phi_{flexion}, \phi_{rotation}, t_{LM}, t_{AP}, t_{SI})$, specifying the osteotomy whose target pose would be $\mathbf{M}_{current}$.

In the case at hand, $\mathbf{M}_{current}$ is the osteotomy pose between the distal and proximal fragment during the fragment tracking. This pose is not immediately known, but can be calculated as follows ($\mathbf{M}_{DistCS \to CamCS}$ and $\mathbf{M}_{ProxCS \to CamCS}$ are the current poses of the distal and proximal tracker, respectively):

$$\mathbf{M}_{current[DistCS]} = \mathbf{M}^{-1}_{DistCS \to CamCS} \cdot \mathbf{M}_{ProxCS \to CamCS} \cdot \mathbf{M}_{fragref}$$

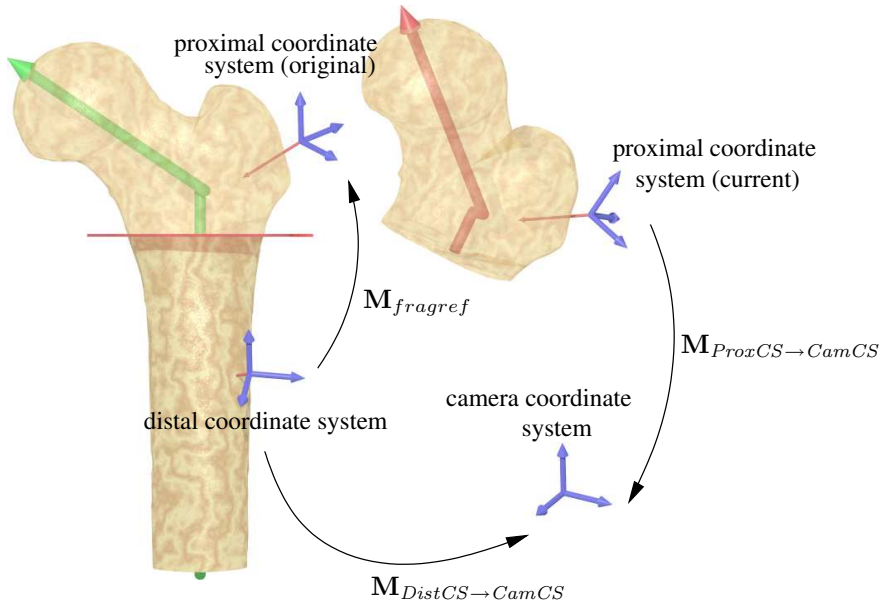

Figure 3.20. The poses involved in determining $\mathbf{M}^{*}_{current}$

For any feature X of the proximal part of the original femur geometry (for example, the femur head center), this pose yields the transformed feature $X' = \mathbf{M}_{current[DistCS]} \cdot X$ according

to the current location of the tracked fragments. Both X and X' are given in the coordinate system of the distal fragment *DistCS*. However, for the subsequent calculations, the target pose must be given in the osteotomy coordinate system, since the osteotomy parameters are specified relative to this coordinate system (see Figure 3.20):

$$\mathbf{M}_{current[OsteoCS]} = \mathbf{M}_{DistCS \rightarrow OsteoCS} \cdot \mathbf{M}_{current[DistCS]} \cdot \mathbf{M}_{OsteoCS \rightarrow DistCS}$$

> **Note:** All further calculations described in this chapter will be performed in the osteotomy coordinate system *OsteoCS*. All geometrical parameters are understood to be given in this coordinate system, including $\mathbf{M}_{current} := \mathbf{M}_{current[OsteoCS]}$.

Now, the osteotomy parameters can be obtained from $\mathbf{M}_{current}$. To do this, first the *angular* parameters are determined. Since these parameters are defined in terms of angles between projections of vectors (see 2.4.1), they can easily be calculated from the given target pose. Let $\vec{a}$ be the direction of the femur shaft axis and $\vec{b}$ the direction of the femur neck axis, both given in the osteotomy coordinate system. It is now possible to calculate the transformed vectors $\vec{a}'$ and $\vec{b}'$:

$$\vec{a}' := \mathbf{M}_{current} \cdot \vec{a}$$

$$\vec{b}' := \mathbf{M}_{current} \cdot \vec{b}$$

The angular parameters $(\phi_{varus}, \phi_{flexion}, \phi_{rotation})$ can now be determined as follows:

- the varus angle ϕ_{varus} is the angle between the projections of $\vec{a}$ and $\vec{a}'$ onto the xz plane
- the flexion angle $\phi_{flexion}$ is the angle between the projections of $\vec{b}$ and $\vec{b}'$ onto the yz plane
- the rotation angle $\phi_{rotation}$ is the angle between the projections of $\vec{a}$ and $\vec{a}'$ onto the xy plane

All of these values are *signed* angles, that is, they are given with respect to a certain rotation axis (see section 2.4.1 for details).

After these values have been determined, a *forward calculation* is performed with the parameters $(\phi_{varus}, \phi_{flexion}, \phi_{rotation}, 0, 0, 0)$. This means, a target pose is calculated for the given angular parameters, with all translational input parameters set to 0. Let this pose be called $\mathbf{M}^*_{current}$.

> **Note:** Only for a wedge size $w = 0.5$, the transformation $\mathbf{M}^*_{current}$ will be a genuine rotation from $\mathbb{R}^3$, because only then does the center of rotation coincide with the origin (osteotomy center). In all other cases, $\mathbf{M}^*_{current}$ will also contain a translational part, however not including any additional translations after the tilting and rotation of the proximal fragment (see Figure 3.9).

Both $\mathbf{M}^*_{current}$ and $\mathbf{M}_{current}$ will orient the proximal fragment in the same way, but they still differ in translation. However, this difference is equal to the sought-for translation vector $\vec{t} = (t_{LM}, t_{SI}, t_{AP})^T$, which can be calculated as follows:

$$\vec{t} := \mathbf{M}_{current} \cdot O - \mathbf{M}^*_{current} \cdot O$$

Now, all elements of the parameter vector $(\phi_{varus}, \phi_{flexion}, \phi_{rotation}, t_{LM}, t_{AP}, t_{SI})$ are known and can displayed in the user interface to represent the current configuration of the realigned fragments.

Chapter 4 System Improvements

During the development of the basic system as described in the preceding chapter, some shortcomings of the system design became obvious:

- The positioning of the distal part of the plate is not satisfactory. It was rarely possible to achieve a good alignment of the implant shaft with the femur diaphysis. The problem is that the system does not have enough information about the structure of the femur surface to predict the fitting of the plate in a particular position. The two images acquired at the start of the intervention are sufficient for reconstructing some essential features of the femur, but do not provide enough information to infer the actual 3D surface needed for adequate plate alignment. However, a tight fit of the implant is crucial for a successful outcome.

- The tool navigation proved error-prone for two reasons. First, it turned out to be very difficult for the surgeon to realize the intervention as planned. Although the correct position and orientation for the saw and the chisel are displayed on the screen, the surgeon still has to operate the instruments freehandedly. While it is comparatively easy to *position* the tool correctly (that is, find a given point on the bone with the navigated tool), it is a much more difficult task to arrive at the correct *orientation*. Both with the chisel and the saw, it was nearly impossible to obtain results with a satisfying accuracy (that is, perform the intervention exactly as planned) due to lack of guidance. Errors in the orientation of the cutting planes and the chisel channel were hard to correct, once the tools had started to drift off.

  Secondly, the mechanical vibrations induced by the saw and the gouging of the channel in several cases caused the trackers to loosen themselves during testing the system. Especially during the sawing phase, which involves three trackers in different locations (distal fragment, proximal fragment and the saw itself), high-frequent oscillations occurred which made it very difficult to ensure that all of the trackers stayed in place.

While this problem may be alleviated by using improved fixation devices to attach the trackers to the bone and the instruments, we nevertheless believe this to be a genuine problem which occurs during real operations. Even if the risk of the trackers loosening themselves may be greatly reduced, the problem remains that if it happens anyway, the success of the entire intervention may be at stake, for example if the reference tracker is affected. Since there is no easy way to readjust a loose reference tracker (which would require the original position of the tracker to be reproduced *exactly*), the navigation system would be useless for the rest of the intervention.

- The osteotomy plane was chosen to be perpendicular to the femoral shaft axis. This, however, is not the optimal choice for the osteosynthesis: the bone fragments are pressed together by the implant with a force which acts orthogonal to the implant's blade and thus parallel to the shaft of the plate. Since the latter is not parallel to the shaft axis, the force is not transmitted orthogonally to the osteotomy plane, as should be the optimal case.

In this chapter, two improvements to the basic system are presented, which resolve all of the issues mentioned above. These two enhancements both involve specially constructed pieces of hardware, which together with the software of the FEMOS system solve the problems at hand. The two enhancements are

Tracked Plate Dummy The problem of the implant positioning is solved by using a tracked implant template, which is a hardware model of the shaft of the osteotomy plate. The surgeon uses the template, whose shape matches that of the actual implant, to find a position on the femur shaft at which the template fits well. The template is provided with a tracker, so that it's position can be tracked by the localizer. With this information, it becomes possible to calculate and display on the screen the position of the entire implant, as it would appear when fixed at the current location of the template. Thus, the surgeon can intraoperatively specify the position of the implant directly on the femur.

In addition to that, the plate dummy can be used to create a guide for the sawing of the osteotomy plane. This was achieved by letting the plate dummy not only determine the position of the implant, but also the location of the osteotomy plane so that it is always parallel to the blade of the implant. For details, see the discussion below.

Osteotomy Target Pose Guide To solve the problem of inaccurate execution of the planned intervention, a set of hardware tools and corresponding software modules was devised, which allowed the actual intervention to be performed *without the need for a navigation*

system, while at the same time providing high-precision guidance to the tools of the surgeon. All of the three critical steps of the intervention — the gouging of the blade channel as well as the sawing along the osteotomy plane and the cutting plane — and the final positioning of the fragments are supported in this way. The main idea is to use Kirschner wires (also called K-wires) as guides for all of these steps. K-wires, which are normally used to stabilize bone fragments, are rigid, thin wires with a sharp tip that can be drilled into the bone. The correct placement of the wires is achieved using our specially constructed hardware.

The two enhancements mentioned greatly increase the accuracy and robustness of the FEMOS system. The mechanical guides even allow the surgeon to perform the intervention unnavigated, because the navigation system is no longer needed after the planning phase has been completed (of course, *during* the planning phase it is required for the positioning of the plate dummy). Besides the benefit of eliminating the difficulties related to the loosening trackers, this also solves the ever-present problem of accidental marker occlusion during an operation in which an optical tracking system is used.

> **Note:** The improvements of the system were only implemented for a standard osteotomy plate, because for each individual plate type specialized tools with matching geometries have to be built. The further discussion is based on the standard plate displayed in Figure 2.13. However, the concepts described can easily be modified to include other plates of different angles and shaft lengths.

4.1 The Tracked Plate Dummy

The plate dummy is a piece of hardware manufactured so that its shape corresponds to that of the osteotomy plate shaft which is later screwed to the femur diaphysis (see Figures 4.1 and 4.2). The underside of the template is rounded out to match that of the actual implant and the width and length of the template equal those of the implant. That way, the surgeon by adjusting its position on the bone receives an immediate feedback on how the actual implant will fit later at the same position. Through its attached tracker, the position of the tool can be determined by the system at any time.

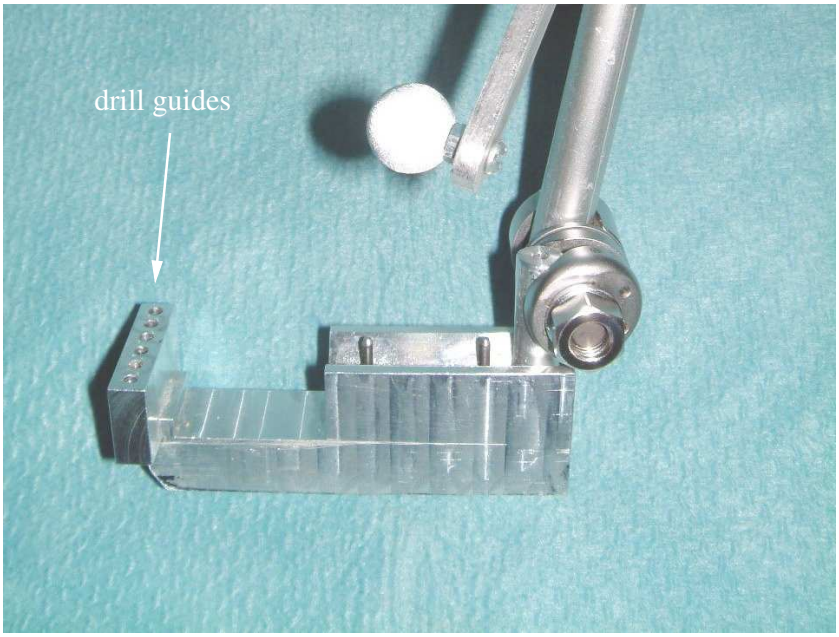

Figure 4.1. The plate dummy. The reflective sphere belongs to the affixed tracker. The holes on the left side of the template are used as drill guides for K-wires.

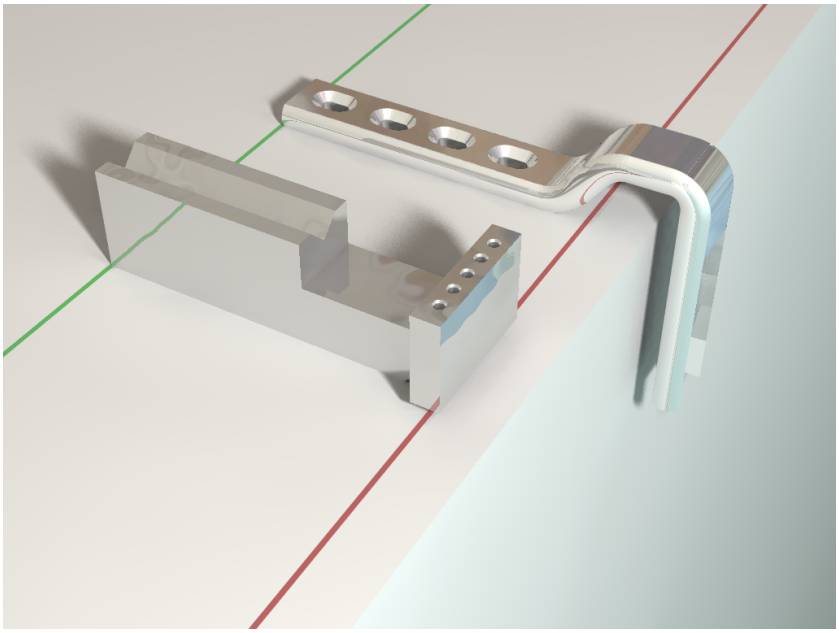

Figure 4.2. The matching geometries of the plate dummy and the implant. The green line marks the distal end of the template/implant, the red line marks the location of the osteotomy plane.

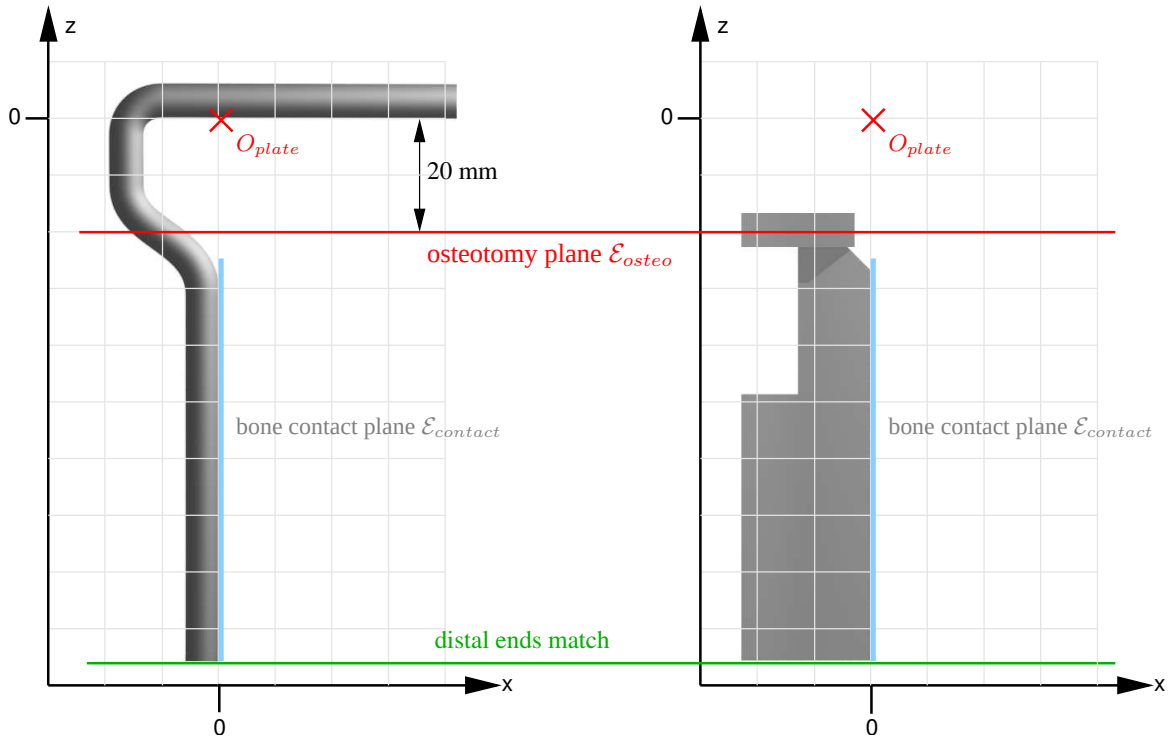

Figure 4.3. The implant and the plate dummy are defined in the same coordinate system. Note that their areas of contact with the bone match exactly (blue), so the plate dummy can be used to find the place of best fit for the implant.

The purpose of using the plate dummy is to give the surgeon the possibility to indicate the desired location and orientation of the implant directly on the bone. Inside the FEMOS system, these parameters are represented by the plate pose $\mathbf{M}_{PlateCS \to DistCS}$ (see section 3.5.4), which transforms points whose coordinates are given in the plate coordinate system *PlateCS* to their target position on the femur, given in the coordinate system of the distal reference, *DistCS*. The goal is now to determine the value of $\mathbf{M}_{PlateCS \to DistCS}$ from the current location of the plate dummy.

This can be achieved easily by calibrating the plate dummy accordingly. As discussed in section 3.1.1.1, calibration serves to determine the pose $\mathbf{M}_{ToolCS \to TrackerCS}$, which converts between the tool coordinate system and the tracker coordinate system. Since the plate dummy was designed to match the geometry of the implant, every point of the plate dummy unambiguously corresponds to a point in the implant coordinate system *PlateCS*. Thus, it is possible to define the geometry of the plate dummy itself in the implant coordinate system (see Figure 4.3), or, in other words, use the implant coordinate system as the tool coordinate system (which can be freely chosen, see section 3.1.1.1) with which the calibration is performed! Calibration now yields a pose $\mathbf{M}_{PlateCS \to TrackerCS}$, in which *ToolCS* was substituted by *PlateCS*.

As a corollary, the current plate pose $\mathbf{M}_{PlateCS \to DistCS}$ can now immediately be calculated using the pose of the plate dummy tracker and the distal reference tracker, as provided by the tracking system:

$$\mathbf{M}_{PlateCS \to DistCS} = \underbrace{\mathbf{M}^{-1}_{DistCS \to CamCS}}_{\text{Distal reference tracker}} \cdot \underbrace{\mathbf{M}_{TrackerCS \to CamCS}}_{\text{Plate dummy tracker}} \cdot \underbrace{\mathbf{M}_{PlateCS \to TrackerCS}}_{\text{Plate dummy calibration}}$$

This pose replaces the default pose of the implant, originally determined as described in section 3.5.4.

The procedure of the intervention now changes in the following way: after the surgeon has entered the osteotomy parameters, he uses the plate dummy to find the correct position of the template by moving it around directly on the bone. The template's position is detected by the tracking device and displayed on the screen, overlaid on the fluoroscopic images. The surgeon can now observe how the position of the plate changes in the images while he moves the template on the bone. As before, the proximal part of the implant is displayed with the inverse target pose applied, that is, as it will appear after the osteotomy.

If the surgeon finds that there is no position at which the implant can be fixed for the current set of planning parameters, he can go back to the planning mode and adjust the parameters accordingly.

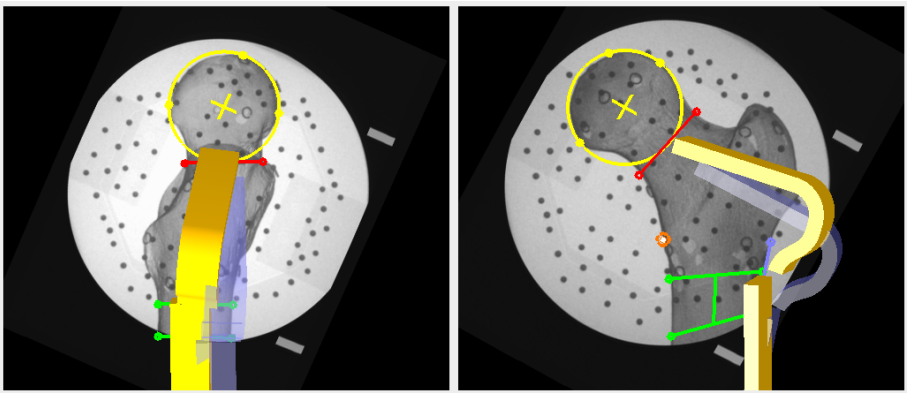

Figure 4.4. The plate dummy tracking mode of the planning system. The yellow shape represents the template at its current tracked position. The transparent blue shape is the default position of the template, as determined by the system.

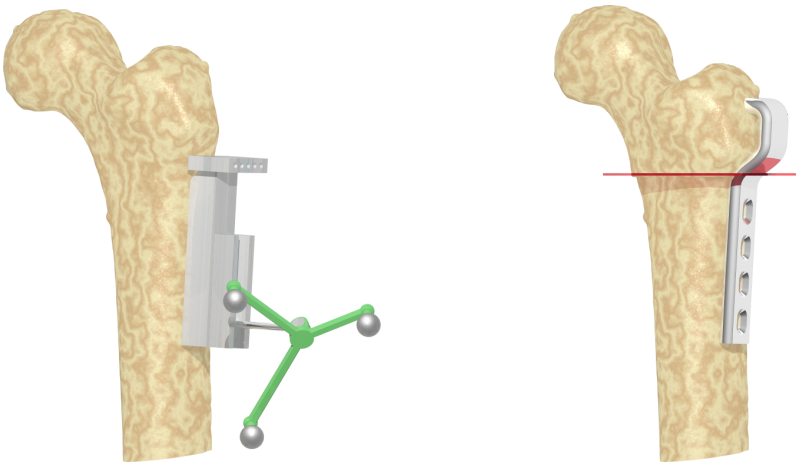

(a) Template on the femur (b) Virtual plate position

Figure 4.5. The plate dummy on the femur. It determines the position of the plate shaft. Knowing the osteotomy pose, the system can calculate the ensuing position of the implant blade.

4.1.1 Adjustment of the Osteotomy Plane

As mentioned before, the osteotomy plane calculated by the planning system is not optimal, since it is not parallel to the implant blade. In the improved version of the FEMOS system, this problem is solved by adjusting the osteotomy plane according to the position of the plate dummy. Since the position of the latter determines the subsequent position of the implant, it can be used to define an osteotomy plane which is exactly parallel to the implant blade.

This is done by defining the osteotomy plane relative to the plate dummy, so that it moves along with it. The following definitions are used to specify the osteotomy plane in the coordinate system of the plate (see 4.3):

- The osteotomy plane is perpendicular to the shaft vector $\vec{d}_{shaft}$ of the plate
- The osteotomy plane is located 20mm below the bottom face of the implant's blade

The value of 20mm is derived from the plate shape: it is the position at which the bent part of the implant meets its shaft. On the bone, this part is located slightly distal of the trochanter major, around which the plate bends.

The definition given above uniquely determines the osteotomy plane in the implant coordinate system, $\mathcal{E}_{osteo[PlateCS]}$. Together with the current pose of the plate $\mathrm{M}_{PlateCS \rightarrow DistCS}$,

obtained from the plate dummy, it is possible to calculate the osteotomy plane $\mathcal{E}_{osteo[DistCS]}$ in the distal coordinate system:

$$\mathcal{E}_{osteo[DistCS]} := \mathbf{M}_{PlateCS \rightarrow DistCS} \cdot \mathcal{E}_{osteo[PlateCS]}$$

This value serves as input parameter to the planning algorithm, and replaces the value originally determined from the model reconstruction (see section 3.5.1). The planning algorithm itself needs not to be modified in any way.

4.1.2 The Effective Wedge Size

As described in section 2.4.3, the user can specify an additional translation $\vec{t}_{add} = (t_{AP}, t_{LM}, t_{SI})$, which modifies the target pose after the fragments have been tilted and rotated relative to each other.

This translation, however, is not independent of the wedge size. In other words, specifying a translation $\vec{t}_{add}$ influences the size of the wedge, so that the desired wedge size w cannot be guaranteed.

This becomes most obvious with translations in superior/inferior direction. An additional translation $\vec{t}_{add} = (0, 0, -t_{inf})$ with $t_{inf} > 0$ corresponds to shifting the proximal femur fragment in distal direction and causes a shortening of the leg. This can only be realized by cutting out a larger portion of bone and hence increase the wedge size. Similarly, a translation $\vec{t}_{add} = (0, 0, t_{sup})$ with $t_{sup} > 0$ represents a shifting of the proximal fragment in proximal direction and causes the leg to be lengthened (relative to its length with $\vec{t}_{add} = 0$), which can only be achieved by decreasing the wedge size.

The same holds to a lesser degree for translations in medial/lateral and anterior/posterior direction. As long as the osteotomy plane is orthogonal to the femur shaft axis, this presents no problem - in this case, a translation in these directions corresponds to a shifting of the fragment on the osteotomy plane, the reason being that the vector $\vec{t}_{add}$ is given in the osteotomy coordinate system, which was defined so that its z axis is the femur shaft axis. Thus, in this case, the xy plane corresponds to the osteotomy plane and translations in medial/lateral and anterior/posterior directions are parallel to this plane.

This changes, however, if the osteotomy plane is no longer orthogonal to the femur shaft axis, and hence not the xy plane of the osteotomy coordinate system. This is what happens when the location of the osteotomy plane is determined by the plate dummy. Now, medial/lateral and anterior/posterior directions are no longer parallel to the osteotomy plane, since they are still given in the osteotomy coordinate system. Thus, translations in these di-

rections will lead either to collisions of the fragments with each other, or to a gap forming between them (see Figure 4.6). Again, this can be compensated by adjusting the size of the wedge.

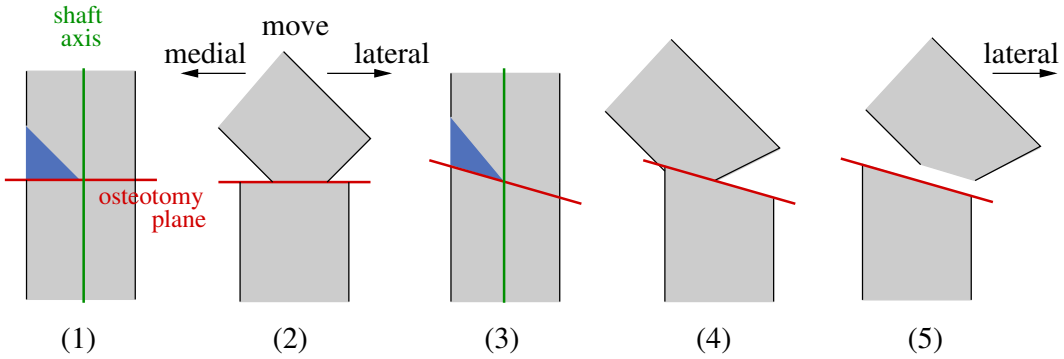

Figure 4.6. If the osteotomy plane is orthogonal to the shaft axis (1), the proximal fragment can be moved in lateral/medial direction (2). Otherwise (3), moving the proximal fragment out of the initial position (4), may cause a gap (5) or a collision between the fragments.

The above considerations show that for a translation $\vec{t}_{add}$ other than 0, the specified wedge size can not be realized in general. In practice, this effect is negligible for medial/lateral and anterior/posterior directions, since although the osteotomy plane may not be exactly orthogonal to the femur axis, it is sufficiently so to not cause large deviations in the wedge size. Also, since the femur cross section is not an ideal circle, the wedge size is a somewhat fuzzy value anyway. For superior/inferior translations, however, the effect mentioned has considerable impact on the wedge size.

The computation of the wedge plane $\mathcal{E}_{wedge}$, as discussed in section 3.5.3, takes these effects into account automatically by basing the calculation of $\mathcal{E}_{wedge}$ on the complete target pose (that is, the target pose including the additional translations). Thus, the wedge formed by $\mathcal{E}_{osteo}$ and $\mathcal{E}_{wedge}$ will have an effective size which differs from the originally specified wedge size w.

4.1.3 Guides for the Osteotomy Plane

As mentioned at the beginning of the chapter, the free-handed execution of the osteotomy proved to be inaccurate due to lack of guidance. A way to solve this problem is to create a guide for the saw by drilling two parallel Kirschner-wires into the bone in such a way that they are tangent to the plane determining the cut to be made. The saw can now slide along these wires and is thus prevented from drifting off (see Figure 4.7).

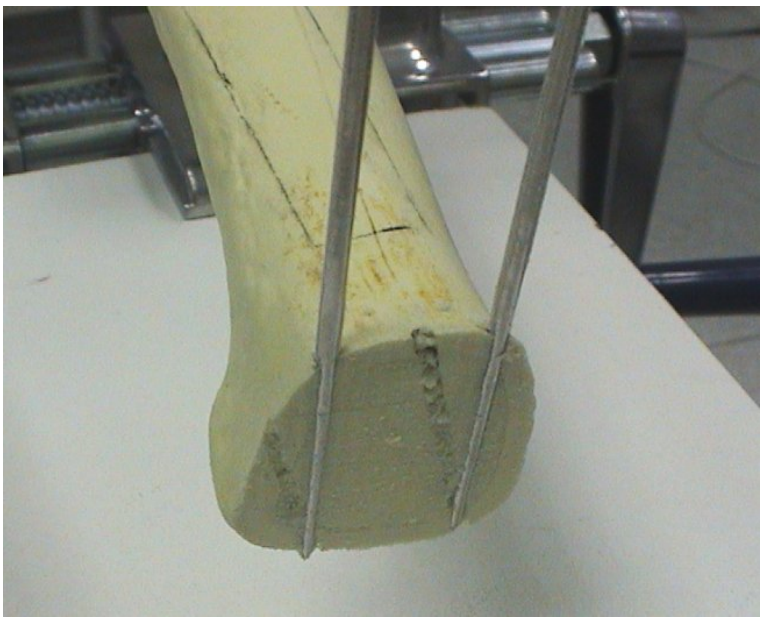

Figure 4.7. A saw cut created using K-wires. As can be seen, the K-wires provide excellent guidance for the saw blade so that the cut is very even. Although the picture shows an artificial bone, the procedure works just as well with real bones.

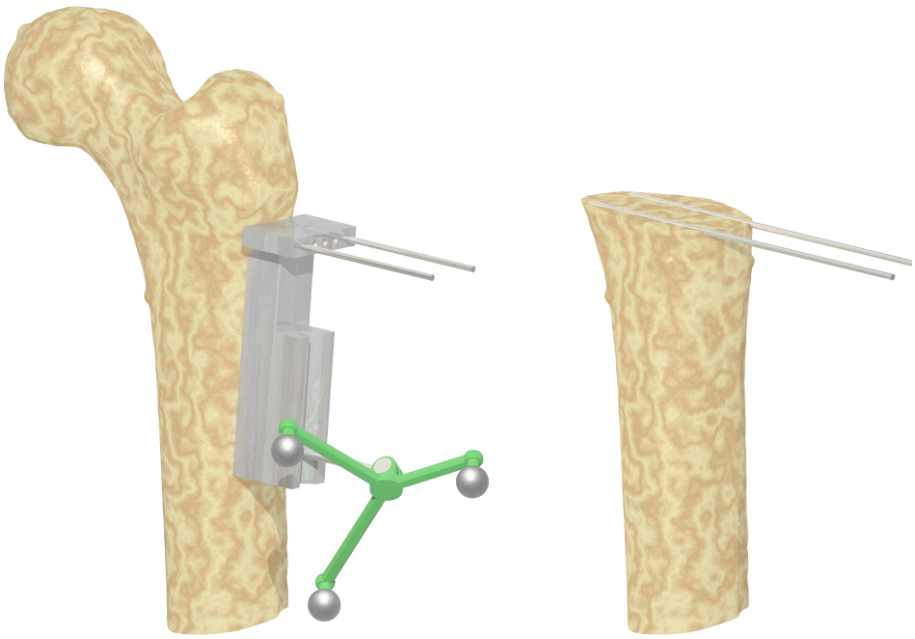

Figure 4.8. The template is used to place the K-wires, which provide a guide for the saw

However, this leaves the problem of how to drill the wires into the femur at the correct position and orientation. This problem was solved by adding drill guides to the proximal

end of the plate dummy. After the position of the template has been adjusted satisfactorily, the surgeon chooses two of the available guide holes (see Figure 4.1) and drills two K-wires through them into the bone (hence the name). These two wires now mark the osteotomy plane, providing the guides along which the saw cut is performed (see Figure 4.8).

For this to work, the holes must be placed so that they are tangent to the osteotomy plane, which is possible because the position of the osteotomy plane relative to the plate dummy is fixed (see previous chapter).

4.2 The Osteotomy Target Pose Guide

The previous chapter describes how the plate dummy is used to create drill guides for the K-wires marking the osteotomy plane. This solves the problem of how to create a precise cut along the osteotomy plane. However, the problem remains for the two other critical steps of the intervention, namely the creation of the wedge plane and the blade channel.

This section discusses how these problems were solved using a specially designed device, which enables the positioning of further K-wires to be used as guides for the wedge plane and the blade channel. The basic idea is to use the tracked plate dummy, whose position is known to the system, as basis on which to mount the so-called *pose shuttle*, a tool which carries the position of the drill guides relative to the plate dummy. The pose shuttle is essentially a small joint arm with six degrees of freedom, which can be locked in a certain position (see Figure 4.9).

4.2.1 Overview of the Procedure with the Target Pose Guide

This section gives an overview of the procedure as it is performed using the target pose guides. The various steps are discussed in detail in the following sections. The entire workflow is depicted in Figure 4.10. With the guides, the procedure works as follows:

1. The plate dummy is positioned at the bone as described in section 4.1. It is fixed to the bone with two K-wires, which will later serve as guides for the cut along the osteotomy plane. Also, the K-wires hold the plate dummy in place during the following steps of the procedure.

2. The target pose, which defines the position of both the blade channel and the wedge plane, is transferred to the pose shuttle via an external alignment device.

(a) The pose shuttle with the joints locked

(b) The shuttle docked to the plate dummy

Figure 4.9. The pose shuttle with the drill sleeves used as guide for the K-wires

3. The pose shuttle is mounted to the plate dummy on the bone. The two tools were constructed so that they can be connected in an unambiguous way.

4. Two additional K-wires are drilled into the bone using the drill guides of the pose shuttle. Let them be called K1 and K2 for later reference.

5. The pose shuttle is removed

6. A guide template is slid on the two K-wires, K1 and K2. The template features a chisel guide as well as several drill guides for drilling further K-wires (used later).

7. The blade channel is gouged, using the template's chisel guide which is constructed so that it guides the chisel in the correct direction for the blade channel.

8. Two K-wires are drilled through the guide template's holes. The holes are arranged so that they are tangent to the wedge plane, and thus the drilled K-wires can be used as saw guides for the wedge plane.

9. The guide template is removed.

10. The saw guides are used to create a cuts along the osteotomy and wedge planes.

As opposed to the conventional approach, this method requires six additional K-wires to be inserted into the bone. However, as they are quite thin they do not interfere with the healing process in any way.

> **Note:** In combination with the plate dummy, this method allows guides to be created for all the essential steps of the intervention - the removal of the wedge and the gouging of the blade channel. Furthermore, the tracking system is not involved in any of the steps beyond the initial tracking of the plate dummy. All of the remaining steps, including the final alignment of the fragments, can be performed without the tracking system.

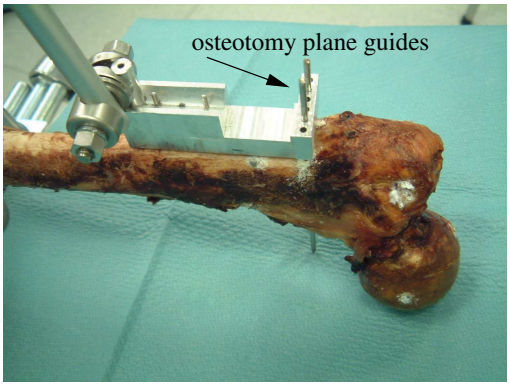

(1) The plate dummy is positioned

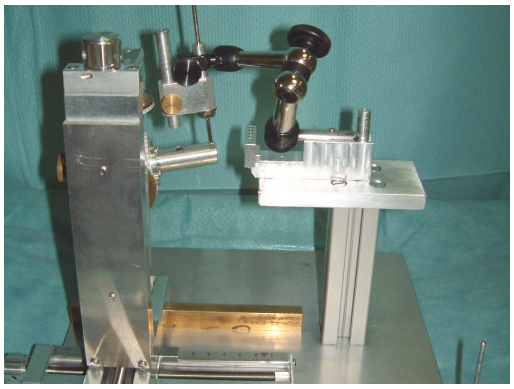

(2) The pose shuttle is adjusted to the target pose

(3) The pose shuttle on the bone

(4) Two K-wires (K1 and K2) are drilled

Figure 4.10. Workflow of the intervention with the guides

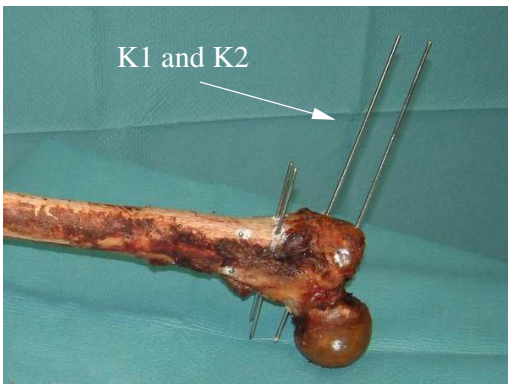

(5) The pose shuttle is removed

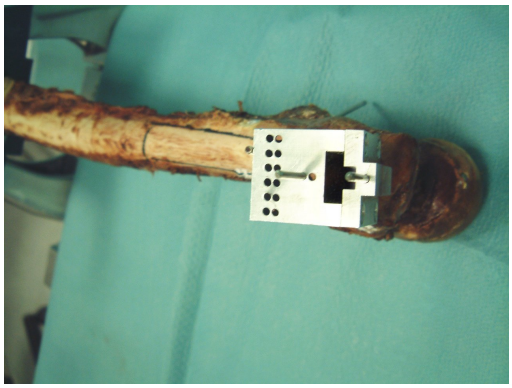

(6) The guide template is slid on K1 and K2

(7) The blade channel is gouged

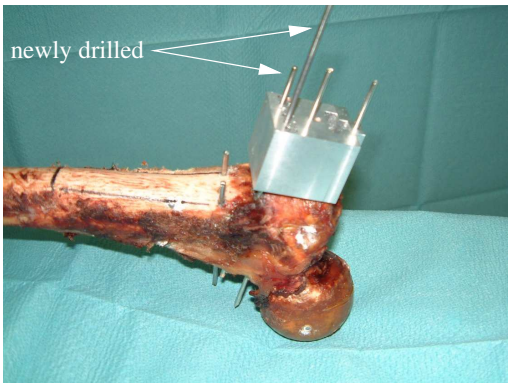

(8) Two K-wires are drilled, which serve as guides for the wedge plane

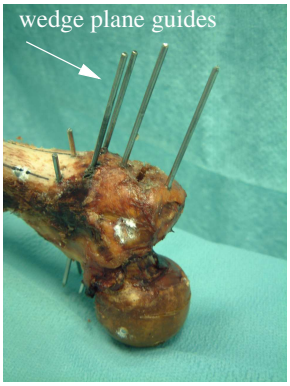

(9) The drill guide is removed

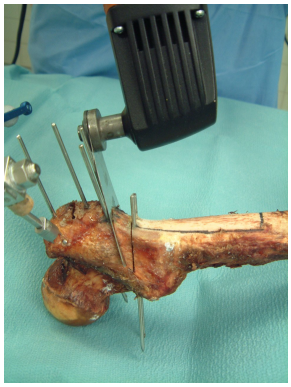

(10) The cuts are made

4.2.2 The Guide Template

In the procedure mentioned in the preceding chapter, the wedge plane and the blade channel are created using guides. The chisel guide is part of the guide template slid on the K-wires K1 and K2, and the saw guides are two K-wires drilled with the drill guides of the guide template.

Since the template is rigid, it is obvious that the positions of the blade channel and the wedge plane solely depend on K1 and K2. This is possible because the relative positions of the wedge plane and the blade channel are fixed, for the following reason: as discussed in section 4.1.1, the location of the osteotomy plane is determined by the plate dummy, so that it has a fixed distance (20mm) to the blade of the implant, to which it is parallel. Since, after the osteotomy, the wedge plane and the osteotomy plane coincide, the wedge plane is necessarily also parallel to the implant blade, and hence the blade channel. In other words: the wedge plane is always situated 20mm below the blade channel and is parallel to it. The template guide must be constructed so that these requirements are met (see Figure 4.11).

The problem to be solved now is to find the correct locations for K1 and K2, so that the guide template provides the correct guides for the blade channel and the wedge plane. K1 and K2 are positioned with the pose shuttle, which is discussed in the next chapter.

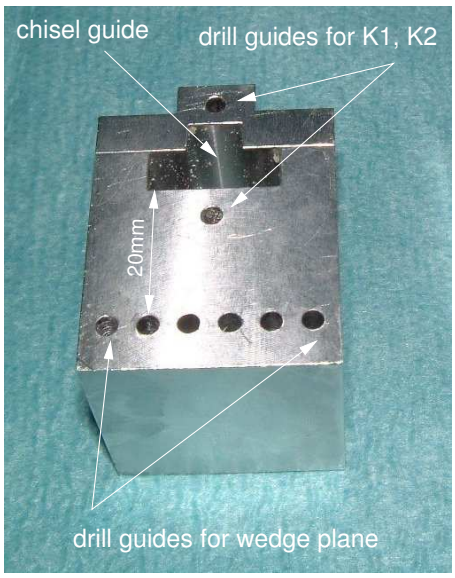

(k) The template with the chisel guide and drill guides

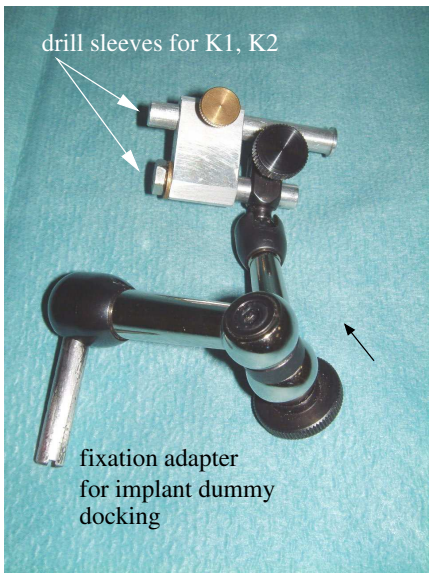

(l) The pose shuttle with the drill sleeves and the adapter for the plate dummy

Figure 4.11. The guide template and the pose shuttle

4.2.3 The Pose Shuttle

The pose shuttle is a small lockable joint arm. The joints can be manipulated in six degrees of freedom, thus allowing the drill sleeves attached to the arm's end effector to reach any given position and orientation (within the mechanical constraints of the arm). The arm can be locked, that is, the joints can be adjusted until the desired configuration has been reached and then be fixed so that they cannot be moved any more. The two drill sleeves are used to place the K-wires K1 and K2 on the bone.

The pose shuttle can be thought of as a means to transfer the target pose to the bone. The basic idea is to do this in two steps:

1. Through an external adjustment device, the pose is transferred to the pose shuttle (see section 4.2.4)

2. The pose shuttle is mounted to the plate dummy in an unambiguous way, thereby reproducing the stored pose on the bone

4.2.4 The Adjustment Fixture

This section describes the adjustment fixture, through which the target pose is transferred to the pose shuttle so that it can be reproduced on the bone. The basic idea was to construct a device which can position its end effector with six degrees of freedom, so that an arbitrary pose can be realized, adjust it depending on the target pose, and then have this pose be transferred to the pose shuttle mounted on the fixture by manipulating the shuttle's joints until its pose corresponds to that of the end effector.

As can be seen in Figure 4.12, the end effector of the adjustment fixture features two holes, which exactly match the holes of the drill sleeves (for K1 and K2) on the pose shuttle. The joints of the pose shuttle must be adjusted so that they are in line with the corresponding holes of the end effector. This can easily checked by inserting two K-wires into the holes.

> **Note:** Through the procedure of aligning the holes of the end effector with those of the pose shuttle, one degree of freedom on the pose shuttle remains undetermined (see red arrow in Figure 4.12), as the drill sleeves can be freely moved in this direction with the holes remaining perfectly aligned. This is irrelevant for the drilling, as the direction of possible translation coincides with the drilling direction. However, it loses one degree of freedom required for the unique transfer of the target pose. Section 4.3 describes how this problem is dealt with.

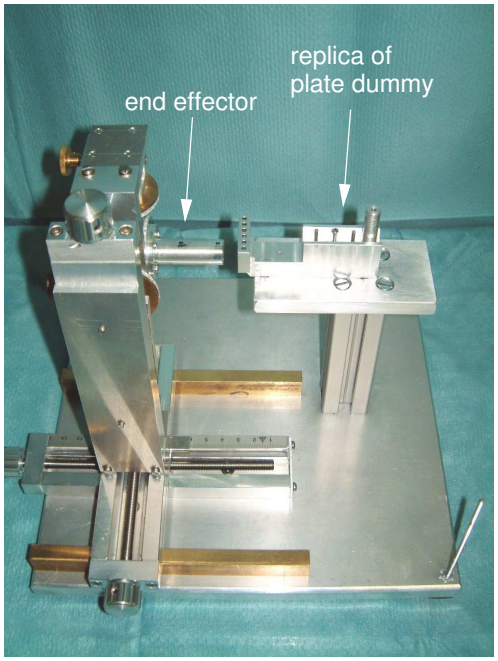

(a) The adjustment fixture in zero position. The end effector can be adjusted to any given 6D pose (within the mechanical constraints of the device).

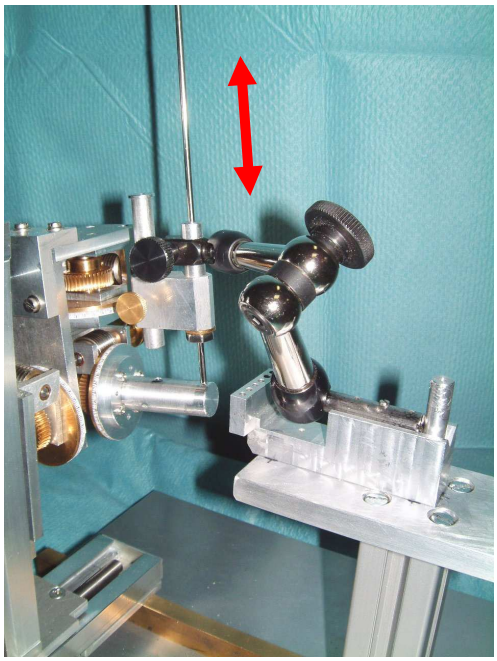

(b) The adjustment fixture with the pose shuttle mounted. The red arrow indicates the undetermined degree of freedom. The picture shows how a K-wire is used to check the alignment of the drill sleeve and the end effector.

Figure 4.12. The adjustment fixture used to align the pose shuttle to a given pose

In principle, the adjustment fixture is a passive robot with three translational and three rotational joints which are operated manually with turning knobs. Each of the joints possesses a scale, allowing it to be precisely adjusted to a given value. Taking into account the geometry of the fixture, the FEMOS system can calculate the six values needed to represent any given pose of the end effector. In the case at hand, the pose to be chosen is the one which correctly positions the drill sleeves for K1 and K2 on the pose shuttle.

Part of the adjustment fixture is a replica of the plate dummy, which serves as docking place for the pose shuttle. During adjustment, the pose shuttle sits on this replica in the same position in which it will later be mounted to the actual plate dummy on the bone (see Figure 4.9). Thus, the replica can be thought of as a reference, which enables the coordinate systems of the fixture and the bone to be correlated.

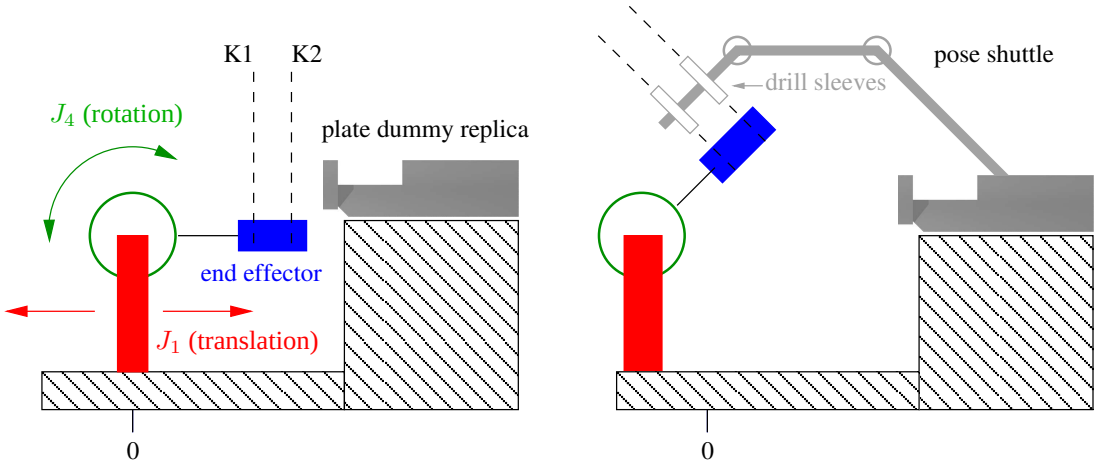

Figure 4.13. A schematic view of the fixture, drawn with two joints only (a translational joint J_1 and a rotational joint J_4). The pose of the end effector is determined by the configuration of J_1 and J_4. This pose is grabbed by the pose shuttle by aligning its drill sleeves with the holes for K1 and K2 on the end effector.

The ultimate purpose of using the fixture is to be able to create the correct blade channel and wedge plane. These depend indirectly on the current joint configuration of the fixture in the following way:

1. The joint configuration determines the position and orientation of the fixture's end effector.
2. The end effector determines the pose which is stored in the pose shuttle.
3. The pose stored in the pose shuttle determines the placement of K1 and K2.
4. K1 and K2 determine the position of the guide template.
5. The guide template determines the blade channel and the wedge plane.

4.2.4.1 The Fixture Geometry

To be able to calculate the six fixture parameters for a given pose, the system must know the geometry of the device. The device was designed as follows:

- It has three translational joints (J_1, J_2, J_3) and three rotational joints (J_4, J_5, J_6). Joint J_{n+1} is mounted to joint J_n, so that a movement of J_n affects the position or orientation of all succeeding joints in the chain.
- The rotation axes of (J_4, J_5, J_6) intersect in a single point

- All joints have a scale attached to them. The translational joints can be adjusted to a specific mm value, the rotational joints to a value given in degrees.
- The device has a zero position, in which all joints have a value of 0 mm or 0°, respectively.
- In zero position, the rotation axes of (J_4, J_5, J_6) are orthogonal to each other
- In zero position, the pose corresponds to a *null osteotomy*, which is an osteotomy which does not change the position and orientation of the proximal fragment at all.

The last point bears some elaboration: the null osteotomy is the ”osteotomy” with the parameters $(\phi_{varus}, \phi_{flexion}, \phi_{rotation}, t_{AP}, t_{LM}, t_{SI}) = (0, 0, 0, 0, 0, 0)$, which means that the target pose is identity, and no wedge is removed. In the case of a null osteotomy, the blade channel would be placed so that the implant could be inserted into the channel on the *intact* femur (because no osteotomy is performed) at the position indicated by the plate dummy(see also Figure 4.14).

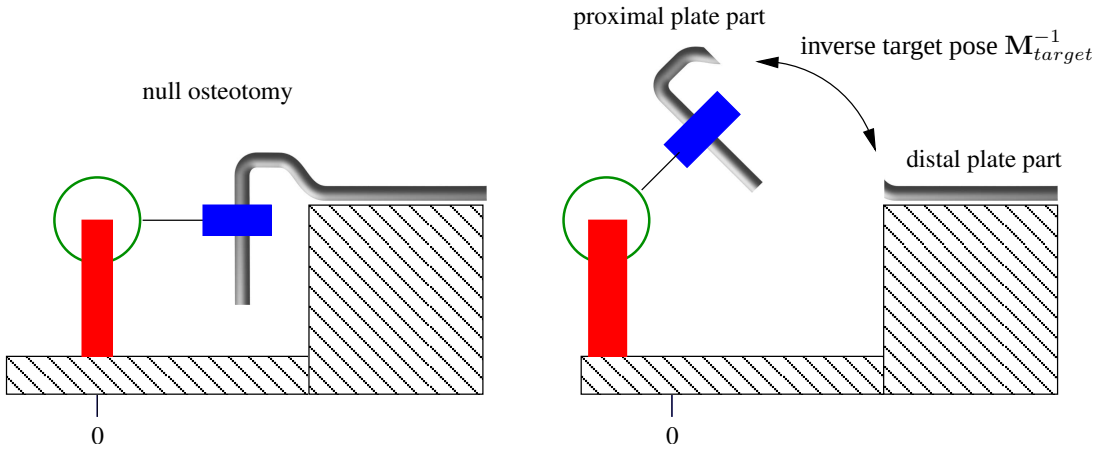

Figure 4.14. Instead of the plate dummy replica, the implant itself can be imagined mounted on the fixture at the corresponding position. The left picture shows a null osteotomy. The proximal part of the implant can be imagined as being rigidly attached to the end effector, with the two moving synchronously if the fixture configuration changes (right picture), while the distal part stays fixed. The pose between the two parts corresponds to the inverse target pose. The same principle is displayed in Figure 3.16

With respect to the adjustment fixture, this means that if the device is set to zero position, the pose shuttle will cause K1 and K2 to be placed so that the resulting blade channel and wedge plane would be in the correct position for a null osteotomy

The geometrical features of the adjustment fixture are given in the fixture coordinate system *FixtureCS*, which is defined as follows:

- The origin is the point of intersection of the rotation axes of J_4, J_5, J_6 in zero position
- The x, y and z axes are the directions of the rotation axes of J_4, J_5 and J_6 in zero position of the device. As mentioned above, these axes are mutually orthogonal.

Table 4.1 lists the features defining the fixture geometry. All values must be given in the fixture coordinate system *FixtureCS*, defined as above. They are used by the algorithm described in the next section, which determines the correct parameters to which the fixture must be adjusted for the given target pose.

Parameter	Description
$\vec{t_1}$	Translation direction of joint J_1
$\vec{t_2}$	Translation direction of joint J_2
$\vec{t_3}$	Translation direction of joint J_3
$\vec{r_4} = \vec{e_x}$	Rotation axis of rotational joint J_4
$\vec{r_5} = \vec{e_y}$	Rotation axis of rotational joint J_5
$\vec{r_6} = \vec{e_z}$	Rotation axis of rotational joint J_6
$O_{plate[FixtureCS]}$	Implant origin in the fixture coordinate system
$\vec{d}_{shaft[FixtureCS]}$	Implant shaft vector in the fixture coordinate system
$\vec{d}_{blade[FixtureCS]}$	Implant blade vector in the fixture coordinate system

Table 4.1. The essential features of the fixture geometry.

The first six parameters determine the effects caused by manipulation of a given joint. For example, manipulating J_3 causes the dependent joints $J_4..J_6$ to be translated in the direction of $\vec{t_3}$.

The parameter $O_{plate[FixtureCS]}$ is the implant origin (see section 2.5) in the fixture coordinate system *FixtureCS*. As described above, the adjustment fixture features a replica of the plate dummy. Now, imagine the plate dummy being replaced by the actual implant in the same position (see Figure 4.15). The point $O_{plate[FixtureCS]}$ is the location of the of this implant's

origin, given in the fixture coordinate system. The vectors $\vec{d}_{shaft[FixtureCS]}$ and $\vec{d}_{blade[FixtureCS]}$ are defined analogously.

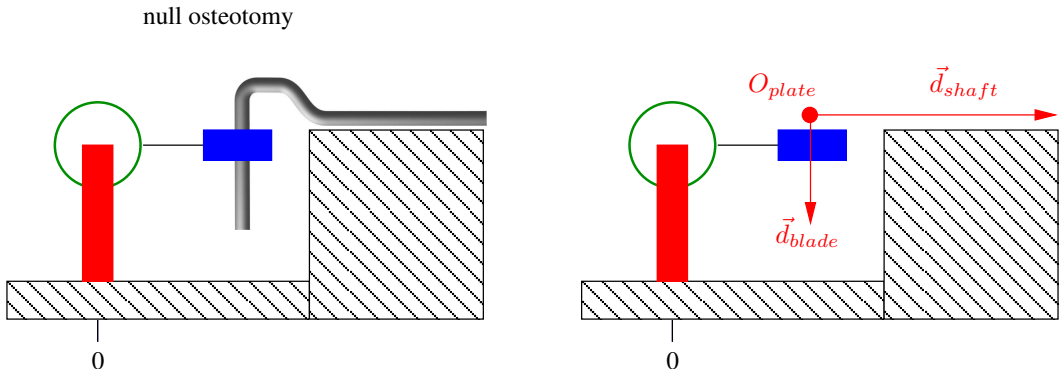

Figure 4.15. The parameters $O_{plate[FixtureCS]}$, $\vec{d}_{shaft[FixtureCS]}$ and $\vec{d}_{blade[FixtureCS]}$ define the pose of the implant on the fixture

4.2.4.2 Calculation of the Fixture Parameters

This section describes the algorithm used to calculate the six parameters $(j_1, j_2, j_3, j_4, j_5, j_6)$ to which the joints of the fixture have to be adjusted in order to yield the correct configuration for a given target pose. The values $\{j_1, j_2, j_3\}$ are translational values given in mm, the remaining values $\{j_4, j_5, j_6\}$ are angular values given in degrees.

The purpose of the algorithm is to find suitable values for the parameters which will eventually cause the correct placement of K1 and K2.

To see how the joint parameters control the position of the end effector, let P be the location of any object in the fixture coordinate system which is rigidly attached to the end effector of the fixture in zero position. If the fixture is now set to the parameters $(j_1, j_2, j_3, j_4, j_5, j_6)$, its end effector and with it the object at P moves. The object will end up at a new position P', which can be found as follows:

$$\begin{aligned} P' &= \mathbf{T}(j_1\vec{t}_1) \cdot \mathbf{T}(j_2\vec{t}_2) \cdot \mathbf{T}(j_3\vec{t}_3) \cdot \mathbf{R}(\vec{r}_4, j_4) \cdot \mathbf{R}(\vec{r}_5, j_5) \cdot \mathbf{R}(\vec{r}_6, j_6) \cdot P \\ &=: \mathbf{M}_{fixture} \cdot P \end{aligned} \tag{4.1}$$

This follows immediately from the construction of the device. In the present case, however, it is the inverse problem which needs to be solved, namely to find the parameters $(j_1, j_2, j_3, j_4, j_5, j_6)$ for a known pose $\mathbf{M}_{fixture}$. First, of course, the pose $\mathbf{M}_{fixture}$ itself needs to be determined.

To clarify again, $\mathbf{M}_{fixture}$ is the transformation in the fixture coordinate system *FixtureCS*, which is applied to objects rigidly connected to the fixture's end effector, when the configuration of the fixture is changed from its zero position to the parameters $(j_1, \ldots, j_6)$. The next few paragraphs describe how it is determined.

The end effector has two holes, corresponding to K1 and K2, which in turn determine the placement of the blade channel. In this sense, the blade channel can be regarded as rigidly attached to the end effector. Thus, the pose of the fixture's end effector directly affects the position of the blade channel. The target position of the blade channel, however, is already known through the *inverse* osteotomy target pose $\mathbf{M}^{-1}_{target[DistCS]}$ (see section 3.6.1), and can be expressed relative to the position of the plate dummy (or its replica on the fixture) by converting it to the implant coordinate system *PlateCS*:

$$\mathbf{M}_{target[PlateCS]} = \mathbf{M}^{-1}_{PlateCS \rightarrow DistCS} \cdot \mathbf{M}^{-1}_{target[DistCS]} \cdot \mathbf{M}_{PlateCS \rightarrow DistCS}$$

In this equation, the pose $\mathbf{M}_{PlateCS \rightarrow DistCS}$ is the plate pose as specified in section 4.1, which can be interpreted as a coordinate transformation from the implant coordinate system *PlateCS* to the distal coordinate system *DistCS* in which the target pose $\mathbf{M}_{target[DistCS]}$ is given.

This pose $\mathbf{M}_{target[PlateCS]}$ is the pose which needs to be transferred to the pose shuttle, because it expresses the osteotomy target pose relative to the plate dummy on the bone as well as to its replica on the fixture, both of which share a common coordinate system.

And thus, the pose $\mathbf{M}_{fixture}$ can be found: it is the pose, defined in the fixture coordinate system *FixtureCS*, which realizes the inverse target pose for the proximal part of the (imaginary) implant mounted on the fixture (see Figure 4.16). It is calculated like this:

$$\mathbf{M}_{fixture} = \mathbf{M}^{-1}_{FixtureCS \rightarrow PlateCS} \cdot \mathbf{M}^{-1}_{target[PlateCS]} \cdot \mathbf{M}_{FixtureCS \rightarrow PlateCS}$$

In this equation, the transformation $\mathbf{M}_{FixtureCS \rightarrow PlateCS}$ from the fixture coordinate system to the implant coordinate system is the pose which transforms $\vec{d}_{blade[FixtureCS]}$, $\vec{d}_{shaft[FixtureCS]}$ and $O_{plate[FixtureCS]}$, which are given according to Table 4.1, to their counterparts in the implant coordinate system (see section 2.5).

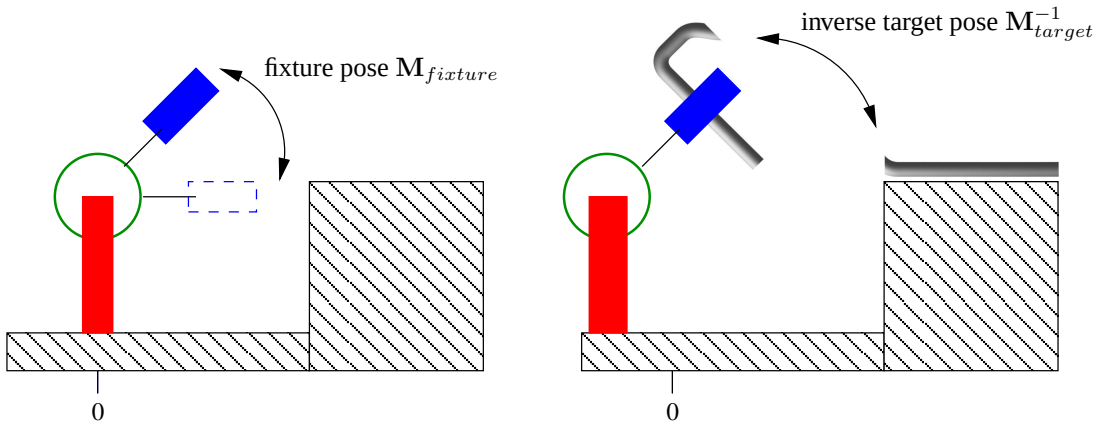

Figure 4.16. The fixture pose $\mathbf{M}_{fixture}$ describes how the end effector moves, starting at the device's zero position (left picture). It has the same effect as the inverse target pose, defined on the implant (right picture).

What remains to be done is to extract the parameters $(j_1, ..., j_6)$ which yield the fixture pose $\mathbf{M}_{fixture}$, now known. Like all rigid transformations, $\mathbf{M}_{fixture} = (\mathbf{R}_{fixture}, \mathbf{T}_{fixture})$ consists of a rotational part $\mathbf{R}_{fixture}$ and a translational part $\mathbf{T}_{fixture}$. Both of these directly appear in equation 4.1:

$$\mathbf{M}_{fixture} = \underbrace{\mathbf{T}(j_1\vec{t}_1) \cdot \mathbf{T}(j_2\vec{t}_2) \cdot \mathbf{T}(j_3\vec{t}_3)}_{\mathbf{T}_{fixture}} \cdot \underbrace{\mathbf{R}(\vec{r}_4, j_4) \cdot \mathbf{R}(\vec{r}_5, j_5) \cdot \mathbf{R}(\vec{r}_6, j_6)}_{\mathbf{R}_{fixture}}$$

Since, through $\mathbf{M}_{fixture}$, both $\mathbf{T}_{fixture} = \vec{t}_{fixture}$ and $\mathbf{R}_{fixture}$ are given, it is now possible to calculate the parameters $(j_1, \dots j_6)$. For the translational part this is straightforward:

$$\vec{t}_{fixture} = j_1\vec{t}_1 + j_2\vec{t}_2 + j_3\vec{t}_3$$

which is simply a linear equation system which can be solved for (j_1, j_2, j_3). For the rotational part $\mathbf{R}_{fixture}$, it is slightly more difficult. Since, by construction, the rotation axes of J_4, J_5 and J_6 correspond to the axes of the fixture coordinate system, $\mathbf{R}_{fixture}$ can be written as follows:

$$\mathbf{R}_{fixture} = \mathbf{R}(\vec{r}_4, j_4) \cdot \mathbf{R}(\vec{r}_5, j_5) \cdot \mathbf{R}(\vec{r}_6, j_6) =: \mathbf{R}_x \cdot \mathbf{R}_y \cdot \mathbf{R}_z$$

with

$$\mathbf{R}_x = \begin{bmatrix} 1 & 0 & 0 \\ 0 & \cos j_4 & \sin j_4 \\ 0 & -\sin j_4 & \cos j_4 \end{bmatrix}, \mathbf{R}_y = \begin{bmatrix} \cos j_5 & 0 & -\sin j_5 \\ 0 & 1 & 0 \\ \sin j_5 & 0 & \cos j_5 \end{bmatrix}, \mathbf{R}_z = \begin{bmatrix} \cos j_6 & \sin j_6 & 0 \\ -\sin j_6 & \cos j_6 & 0 \\ 0 & 0 & 1 \end{bmatrix}$$

Explicitly multiplying these matrices yields

$$\mathbf{R}_{fixture} = \mathbf{R}_x \cdot \mathbf{R}_y \cdot \mathbf{R}_z =$$

$$\begin{bmatrix} \cos j_5 \cos j_6 & \cos j_5 \sin j_6 & -\sin j_5 \\ j_4 \sin j_5 \cos j_6 - \sin j_6 \cos j_4 & \sin j_4 \sin j_5 \sin j_6 + \cos j_4 \cos j_6 & \sin j_4 \cos j_5 \\ \cos j_4 \sin j_5 \cos j_6 + \sin j_4 \sin j_6 & \sin j_6 \cos j_4 \sin j_5 - \sin j_4 \cos j_6 & \cos j_4 \cos j_5 \end{bmatrix}$$

Since the elements m_{ik} of the matrix $\mathbf{R}_{fixture} =: (m_{ik})$ are known, the remaining parameters (j_4, j_5, j_6) can now be extracted from the matrix (see [Sho94] for special cases):

$$j_4 = \text{atan2}(m_{12}, m_{22})$$

$$j_5 = \text{atan2}(-m_{02}, \sqrt{m_{22}^2 + m_{12}^2})$$

$$j_6 = \text{atan2}(m_{02}, m_{00})$$

Together with (j_1, j_2, j_3), which were already determined, this yields the complete set of parameters necessary to adjust the fixture.

4.3 Fragment Repositioning

In the procedure described above, there is no need for the tracking system beyond the fixation of the position of the plate dummy. All of the subsequent steps are performed relative to the known position of the dummy with a mechanical referencing system. Thus, the blade channel can be gouged and the wedge excised without having to use tracked instruments. The last step, the repositioning of the fragments, however, still utilizes position sensing to track the fragments themselves. As it turns out, even this can be achieved without the tracking system.

If the osteotomy has been performed accurately, the problem of positioning the fragments

is reduced to three degrees of freedom: the proximal fragment can be moved around on the osteotomy plane (2 DOF), and rotated on the plane (1 DOF). To eliminate two further degrees of freedom, observe the following: for both the sawing of the osteotomy plane and the wedge plane, two K-wires were used as guides. These guides are still in place after the fragments have been separated, and can be used to verify the fragment positioning. If the fragments are positioned correctly, the K-wires will be parallel to each other, and pairwise on top of each other. Thus, rotating the fragments until the K-wires are parallel and then translating the proximal fragment until they align, leaves only one DOF undetermined.

For this to work, both the plate dummy used for the osteotomy plane and the guide template used for the wedge plane must be designed accordingly: the holes acting as drill guides must be placed so that they are parallel and exactly on top of each other for a null osteotomy.

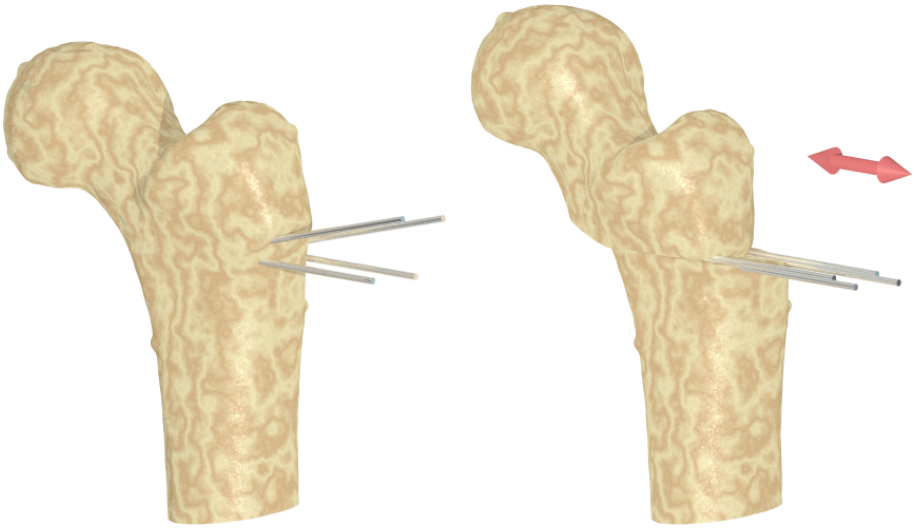

Figure 4.17. Before the osteotomy, the K-wires are drilled into the bone to be used as saw guides (left). After the osteotomy, the fragments must be positioned so that the K-wires align. The only remaining undetermined degree of freedom is a mediolateral translation, indicated by the arrow.

The remaining degree of freedom is a translation in mediolateral direction, which corresponds to the main direction of the K-wires (see also section 4.2.4). It can be fixed through the following procedure (see Figure 4.18):

1. On the adjustment fixture, measure the distance $d_{fixture}$ of the drill sleeve of the pose shuttle from the end effector of the fixture. Let $P_{effector}$ be the point on the end effector at which the distance is measured.

2. On the bone, measure the distance d_{bone} of the drill sleeve of the pose shuttle from the

bone surface. This can be done by sliding a K-wire into the drill sleeve until it touches the bone, and then measuring how far the K-wire has entered the drill sleeve. Let the point at which the K-wire touches the bone be called B (later, K1 will pierce the bone surface at B).

3. Now it is possible to calculate the distance $d_{implant}$, which B must have from the contact plane of the implant (that is, the plane at which the implant lies against the bone diaphysis) *after* the osteotomy:

$$d_{implant} := d_{fixture} - d_{bone}$$

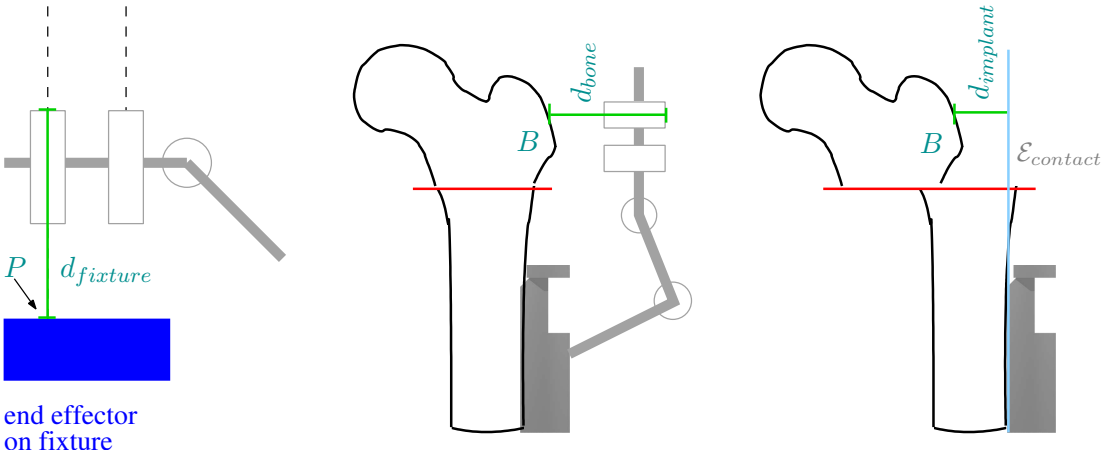

Figure 4.18. The distance $d_{fixture}$ is measured between the drill sleeves and the end effector (left). The distance $d_{fixture}$ is measured preoperatively between the drill sleeves and the bone surface (middle). The calculation yields $d_{implant}$, which determines the final distance of B from the bone contact plane of the implant/plate dummy (right).

This works if the fixture is constructed so that the point $P_{effector}$ lies on the contact plane of the replica of the implant template if the fixture is in zero position.

This procedure fixes the mediolateral translation: the proximal fragment must be positioned so that the distance of point B from the implant's contact plane is equal to $d_{implant}$.

Chapter 5 Results

In order to evaluate the different aspects of the FEMOS system, we conducted several test series. In detail, these were:

TS1 A test series with plastic femora, which was designed to investigate the maximum achievable accuracy of the system per se under optimal conditions. For these tests, only the removal of the wedge was performed. However, there was no implant used to fixate the fragments.

TS2 A test series conducted on several different anatomical specimens, which was designed to assess how well the system works with human femora. For these tests, the intervention was carried through completely, including the fixation with the implant.

TS3 A test series performed on plastic bones on a hip simulator. The simulator was designed to limit the surgeon's view of the femur under treatment, and constrain the femur's movements to those anatomically possible during a real operation. With these tests, the applicability of the general procedure under operating room conditions was evaluated.

TS4 A test series performed using the basic system as described in chapter 3, as opposed to the improved system which was used in **TS1** to **TS3**. This series served to investigate the additional benefit brought about by the system improvements as described in chapter 4. It was also performed on the hip simulator.

TS5 A test series performed *without* the FEMOS system, using the conventional operating technique on the hip simulator. These tests were conducted to be able to evaluate the differences between the conventional and the new approach with respect to obtainable accuracy and reproducibility.

The test series **TS3** to **TS5** were conducted to compare three different operating techniques under identical conditions: the full FEMOS system, including the improvements (**TS3**), the basic FEMOS system (**TS4**), and the conventional method (**TS5**).

5.1 Evaluation Procedure

All of the tests mentioned in the previous section were evaluated through the same procedure. The steps of this evaluation procedure were:

1. Prior to the operation, a number of X-ray opaque fiducials were attached to the bone. The fiducials were placed on the distal end of the bone (knee condyles), on its proximal end and around the osteotomy plane. This ensures that, after the osteotomy, on both fragments there will be a sufficient number of markers for a robust registration.

2. A preoperative CT scan of the entire bone was acquired. The CT images had a size of 512×512 pixels and a slice distance of 1mm.

3. The distal reference tracker was attached to the bone.

4. Several calibrated fluoroscopy images were taken of the prepared bone with a tracked C-arm. The images were taken so that every fiducial was visible in at least two of the images from different view directions. The same tracker later served as dynamic reference frame during the intervention, thus the camera parameters associated with the images were recorded in the *DistCS* coordinate system.

5. The intervention was performed. Information on the reconstructed femur geometry was stored for later use.

6. A postoperative CT scan of the bone was acquired with identical setup as before.

7. The metal fiducials, which were visible in the CT and the fluoroscopy images, were marked manually in both CT data sets as well as in the fluoroscopic images. As every marker was visible from different angles in two fluoroscopic images, and the images were calibrated, it was possible to determine the 3D position of every fiducial in the coordinate system in which the images had been acquired (*DistCS*). The entire procedure yielded three sets of 3D marker coordinates: two from the CT data, and one from the fluoroscopic images.

8. A rigid-body registration based on the detected fiducials was performed between the preoperative CT scan and the fluoroscopic images.

9. Two further registrations were performed between the postoperative and the preoperative CT scan: one between the fiducials on the proximal fragment, the other between the fiducials on the distal fragment

10. Based on the registration poses and the information dumped during the intervention, the osteotomy parameters could be inversely calculated (see below).

5.1.1 Preparation of the Bones

CT evaluation was chosen due to its nature as ”gold standard” with respect to imaging accuracy. For our tests, 16 fiducials were used, of which 7 were placed on the proximal fragment, and 9 on the distal fragment. To enable a robust registration, the markers were distributed across the entire femur, including the knee condyles at its distal end (see Figure 5.1). The pre-OP and post-OP CT scans were acquired with a slice distance of 1mm.

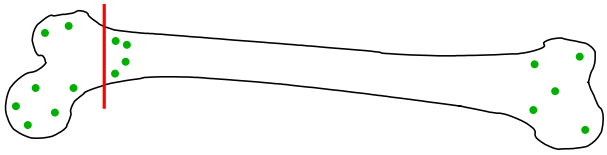

Figure 5.1. Distribution of markers for evaluation

The fiducials in the CT scans were marked manually. This procedure immediately yielded the 3D positions of the fiducials' centers. In the fluoroscopic images, the positions of the fiducials were obtained by marking the centers of the projections of each fiducial in two different images. Since the camera parameters of all images were known, the projection rays of the marked points could be calculated and intersected for corresponding projections. Thus, the 3D positions of all fiducials could be determined.

The points obtained this way were divided into multiple subsets:

Set Symbol	Source	Femur Fragment	Coordinate System	# Fiducials
$CT_{pre,prox}$	pre-OP CT	proximal	*PreCS*	7
$CT_{pre,dist}$	pre-OP CT	distal	*PreCS*	9
$CT_{post,prox}$	post-OP CT	proximal	*PostCS*	7
$CT_{post,dist}$	post-OP CT	distal	*PostCS*	9
$CT_{pre,all} = CT_{pre,prox} \cup CT_{pre,prox}$	pre-OP CT	both	*PreCS*	16
$F_{pre,all}$	fluoro images	both	*DistCS*	16

Table 5.1. The point sets used for the evaluation

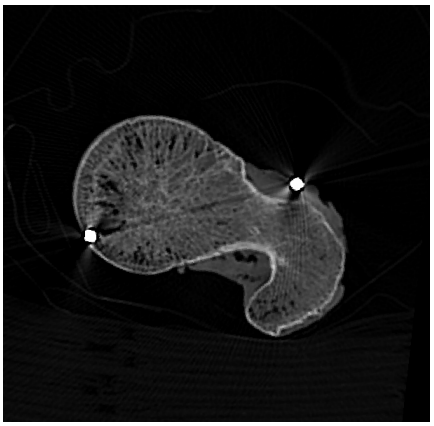

(a) CT image

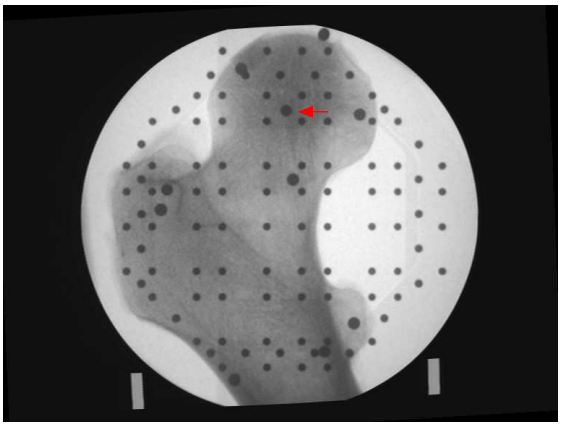

(b) Fluoro image. The larger black circles are the projections of the fiducials (the small black circles are used for C-arm calibration and have nothing to do with the evaluation)

Figure 5.2. The fiducials used are clearly visible in both the CT and the fluoro image.

5.1.2 Calculation of the Effective Osteotomy Parameters

To calculate the effective osteotomy parameters, the marker coordinates were used in the following way:

- $CT_{pre,all}$ and $F_{pre,all}$ were used to determine the transformation $\mathbf{M}_{DistCS \rightarrow PreCS}$ from *DistCS* (the coordinate system of the bone reference tracker) into *PreCS* (the coordinate system of the pre-OP CT scans)
- $CT_{pre,dist}$ and $CT_{post,dist}$ were used to determine the transformation from *PreCS* into *PostCS* (the coordinate system of the post-OP CT scans)
- $CT_{pre,prox}$ and $CT_{post,prox}$ were used to calculate the effective osteotomy pose $\mathbf{M}_{eff}$, which represents the effectively achieved realignment of the proximal fragment (as opposed to the *planned* transformation $\mathbf{M}_{target}$).

To obtain the transformations, a registration algorithm working on point sets was employed. The algorithm takes as input two sets A and B (for example, $CT_{pre,all}$ and $F_{pre,all}$ in the first case). Both sets contain an equal number of 3D points. For each point in A, there is a corresponding point in B. However, the sets are unordered, so the correspondences are not known a priori.

To find the correspondences, the centroids (the arithmetic mean of the point coordinates) C_A and C_B are calculated by the algorithm. The points in A and B are then sorted according to the distance from their respective centroid. This procedure yields two ordered sets of points $A' = (a'_1, \ldots, a'_n)$ and $B' = (b'_1, \ldots, b'_n)$, in which a'_i corresponds[1] to b'_i.

The two sets A' and B' are registered using the method described in [Hor87]. This algorithm, which works on point sets with known correspondences, yields a transformation $\mathbf{M}_{A\to B}$ which minimizes the registration error R, given as

$$R^2 = \sum_{i=1}^{n} \|(b'_i - \mathbf{M}_{A\to B} \cdot a'_i)\|^2$$

In the following, the registration function is written as

$$\mathbf{M}_{A\to B} := \text{register}(A, B)$$

With this registration algorithm, the following transformations can immediately be determined:

$$\mathbf{M}_{DistCS\to PreCS} := \text{register}(F_{pre,all}, CT_{pre,all})$$

$$\mathbf{M}_{PreCS\to PostCS,dist} := \text{register}(CT_{pre,dist}, CT_{post,dist})$$

$$\mathbf{M}_{PreCS\to PostCS,prox} := \text{register}(CT_{pre,prox}, CT_{post,prox})$$

What remains to be determined, is the effective osteotomy pose $\mathbf{M}_{eff}$. This is slightly more complicated, since, to be comparable to the planned target pose $\mathbf{M}_{target}$, the pose $\mathbf{M}_{eff}$ must be defined in the distal coordinate system *DistCS*:

$$\mathbf{M}_{eff} := \mathbf{M}^{-1}_{DistCS\to PreCS} \cdot \mathbf{M}^{-1}_{PreCS\to PostCS,dist} \cdot \mathbf{M}_{PreCS\to PostCS,prox} \cdot \mathbf{M}_{DistCS\to PreCS}$$

The pose $\mathbf{M}_{eff}$ is the effective osteotomy pose, so that the post-OP position $X'_{[DistCS]}$ of any feature $X_{[DistCS]}$ on the proximal fragment can be calculated as

[1] This method may fail if two or more points have almost the same distance to the centroid, which due to measurement inaccuracies may cause them to swap their positions in one of the lists. It can easily be fixed by leaving out these points in a preliminary registration, then determine the missing correspondences based on this preliminary result, and register again

$$X'_{[DistCS]} = \mathbf{M}_{eff} \cdot X_{[DistCS]}$$

With the algorithm described in section 3.6.4.1, it is possible to inversely determine the effective osteotomy parameters from a given transformation. The parameters thus calculated can be compared with the originally planned values to determine how accurate the intervention was performed.

5.1.3 Accuracy of the Registration Between the Point Sets

Figure 5.3 displays the registration errors of the various registrations required for the test evaluation. As described above, for each bone three separate registrations were performed: fluoro pre → CT pre, CT pre distal → CT post distal and CT pre proximal → CT post proximal. For each of the three registration poses, the mean distance after registration between corresponding markers (16 for 'all', 7 for 'proximal' and 9 for 'distal') was determined. These mean values are shown in the diagram.

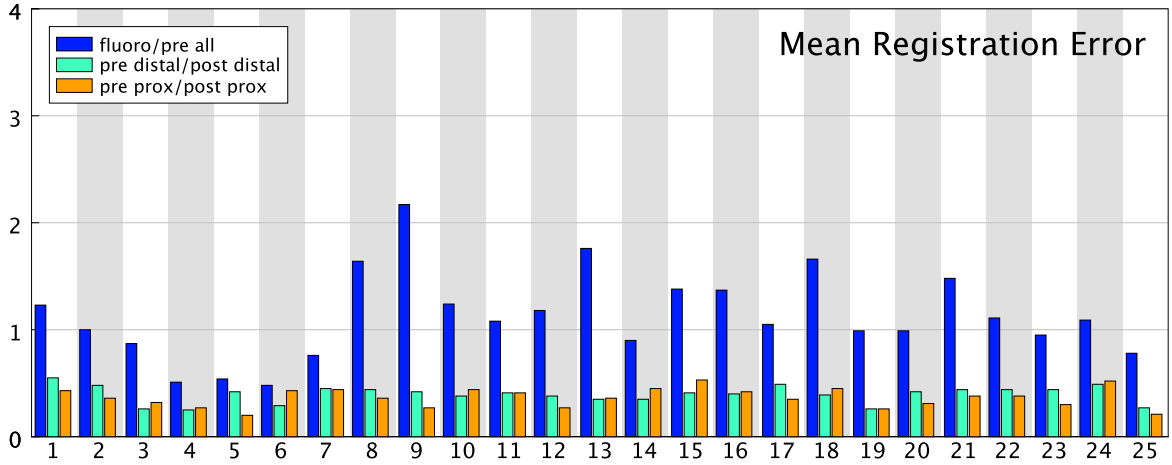

Figure 5.3. The evaluation errors of the various registrations, given in mm. For each test, three registrations were performed.

5.2 Test Setup

All of the tests were conducted with the FEMOS system, except for **TS5**, which was performed with the conventional method for comparative purposes. The software runs under Linux on a 2GHz Intel Pentium machine. We used the *Polaris* (Northern Digital Inc., Canada) camera with custom driver software to track the instruments. The trackers used were also

self-designed according to the technical requirements of the camera. The C-arm used was as *BV-21* device (Philips, Germany).

All of the tests were evaluated with the method described above. The CT scans were created with a *Cardio 64* CT scanner (Siemens, Erlangen, Germany). Every bone was scanned twice, once before the operation, once afterwards. The slice distance of the scans taken was 1 mm.

5.3 Results of the Test Series

This section describes in detail the results obtained through the test series **TS1** to **TS5**. Table 5.2 presents an overview of the different aspects of the test series.

	TS1	**TS2**	**TS3**	**TS4**	**TS5**
Operation Technique	FEMOS full	FEMOS full	FEMOS full	FEMOS basic	conventional technique
Femur	plastic	human	plastic	plastic	plastic
Metal Implant	none	dummy	real	real	real
OR Simulation	no	no	yes	yes	yes
Input Parameters	varying	varying	fixed	fixed	fixed

Table 5.2. Summary of the test series.

The following sections present the results of the test series individually. A discussion of the test series and a statistical description of the results obtained is given in section 5.4.

5.3.1 Test Series with Artificial Femur Bones (TS1)

The first test series was conducted with plastic femora (Sawbones, Sweden). The same model was used for all tests in this series. The test series consisted of five experiments, in each of which the osteotomy was performed using the improved FEMOS system, as described in chapter 4. For these tests, no blade channel was gouged and the fragments were fixated with

glue rather than with an implant. Thus, it was possible to assess the accuracy with which the actual osteotomy, that is, the excision of the wedge, was performed with the FEMOS system, leaving aside any additional errors introduced by the fixation procedure.

For this test series, the osteotomies were to be performed under ideal conditions, without taking any measures to simulate a real operating situation. This was done to minimize the errors stemming from inaccurate execution, so that the intrinsic accuracy of the system could be evaluated. There is a large number of possible error sources present within the system itself:

- calibration errors of the C-arm
- pose estimation errors of the tracking system
- errors introduced by the user during the interactive model reconstruction
- errors due to imprecise manufacturing of the adjustment fixture

Additionally to the effective osteotomy parameters, which were determined through the CT evaluation, the values displayed by the system in the fragment-tracking phase (see section 3.6.4) were recorded in order to determine the reliability of these values. Ideally, the displayed parameter values would match the values obtained from the CT evaluation.

The results of this first test series are displayed in the table below.

> **Note:** The parameter values in the tables and graphs of this chapter are given without specifying the units of measurement. Angular values (varus, flexion, rotation) were always measured in degrees, length values (translations in AP, LM and SI directions) in mm.

	planned	displayed	CT based	planned	displayed	CT based
		Femur 1			Femur 2	
varus	-15.00	-15.00	-15.69	-10.00	-9.00	-9.93
flexion	-10.00	-10.00	-10.81	-10.00	-9.00	-8.77
rotation	10.00	10.00	10.65	5.00	3.00	4.52
AP	5.00	6.00	7.02	5.00	3.00	2.83
SI	-10.00	-9.00	-10.31	0.00	1.00	-0.23
LM	5.00	4.00	4.74	5.00	4.00	4.27
		Femur 3			Femur 4	
varus	10.00	10.00	10.20	10.00	10.00	9.75
flexion	-10.00	-10.00	-10.03	-5.00	-5.00	-5.22
rotation	-5.00	-5.00	-5.76	5.00	4.00	4.79

AP	0.00	0.00	-0.86	3.00	3.00	2.67
SI	0.00	0.00	-1.48	0.00	0.00	0.71
LM	0.00	0.00	-0.68	5.00	5.00	5.20
		Femur 5				
varus	-10.00	n/a[2]	-9.67			
flexion	10.00	n/a	10.30			
rotation	-5.00	n/a	-6.52			
AP	-10.00	n/a	-10.90			
SI	0.00	n/a	-0.74			
LM	3.00	n/a	2.18			

Table 5.3. Evaluation results for the test series TS1, showing the planned values (”planned”), the values displayed during fragment tracking (”displayed”), and the values obtained from the CT evaluation (”CT based”).

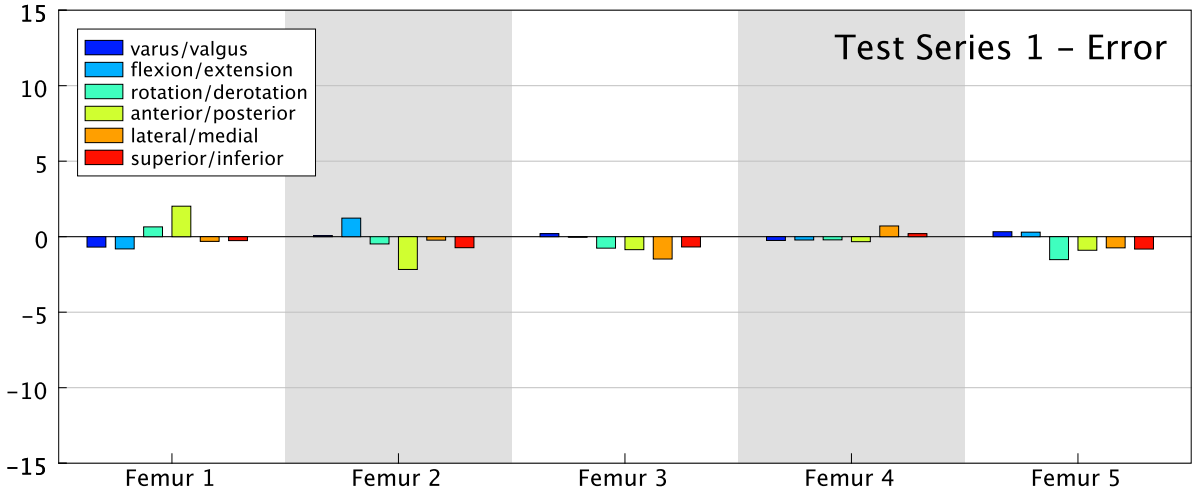

Figure 5.4. Difference of the CT-evaluated result compared to the planned values of **TS1**. For any parameter X (varus, flexion, ...), the graph depicts the value $\Delta = X_{evaluated} - X_{planned}$.

[2]Due to an error unrelated to the system the values were not recorded

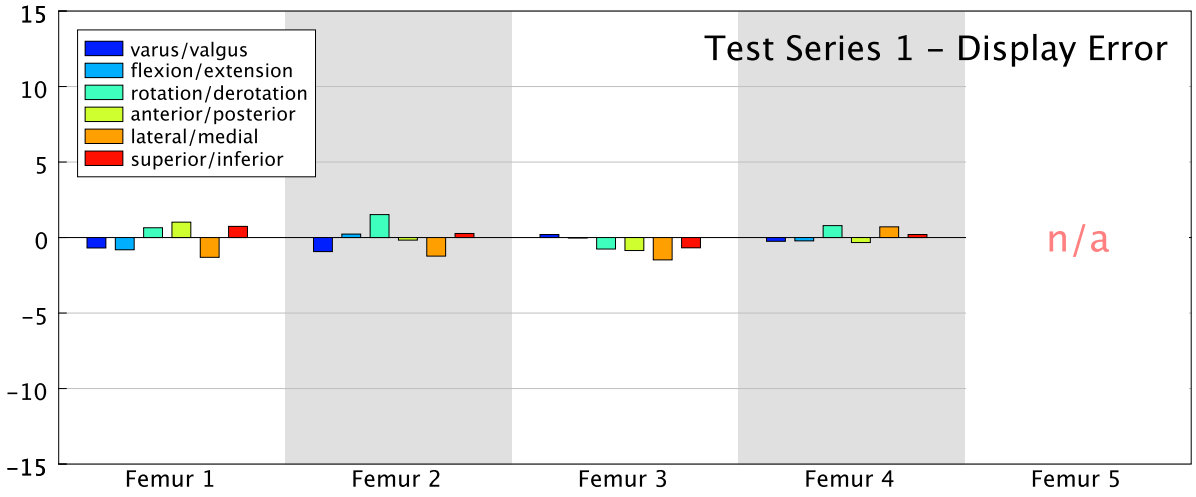

Figure 5.5. Difference of the CT-evaluated result compared to the values which were displayed during fragment tracking. For any parameter X (varus, flexion, ...), the graph depicts the value $\Delta = X_{evaluated} - X_{displayed}$.

5.3.2 Test Series with Anatomical Specimens (TS2)

The second test series (TS2) was conducted with anatomical specimens. For each of these, the intervention was completely carried through, including the gouging of the blade channel and fixation with an implant. To reduce CT artifacts caused by the metal implant, we used a set of identical custom-built implants made from aluminum[3]. These were constructed so that they exactly matched the measurements of the actual implants. As these dummys were not rigid enough to sustain the corrected fragments on their own, the corrected femur was additionally stabilized intramedullary with bone cement. With this procedure, it was possible to evaluate the accuracy with which the plates were fixed at their planned positions, which depends on both the accuracy with which the blade channel was gouged as well as the accuracy of the osteotomy.

For **TS2**, the planning parameters were varied with every specimen. These parameters, along with the results obtained from the CT evaluation, are displayed in Table 5.4.

Additionally, for this test series, the placement of the fixation plate was evaluated. In the postoperative CT scans, four points on the plate shaft were marked (see Figure 5.7). Together with the known plate geometry, it was thus possible to determine the effective plate pose. Two values were calculated for the evaluation: the angle between the real and effective central lines of the plate shaft (green line in Figure 5.7), as well as the displacement of the displacement of

[3]Later, it turned out that even the real implants caused very little artifacts, so it was possible to use these for the remaining test series **TS3** to **TS5**

the distal shaft end. The results are displayed in Table 5.5.

	planned	CT based	planned	CT based	planned	CT based
	Femur 1		Femur 2		Femur 3	
varus	-11.00	-10.90	-8.00	-8.78	-9.00	-9.47
flexion	-4.00	-4.32	5.00	6.02	4.00	4.25
rotation	-15.00	-16.27	0.00	-0.52	6.00	3.21
AP	-4.00	-4.32	-5.00	-5.88	-3.00	-2.85
SI	0.00	1.13	0.00	0.93	0.00	0.51
LM	-4.00	-4.60	-3.00	-5.20	-3.00	-2.95
	Femur 4		Femur 5			
varus	8.00	7.24	-6.00	-6.47		
flexion	-5.00	-5.84	6.00	4.53		
rotation	-12.00	-12.54	-12.00	-12.77		
AP	-8.00	-8.90	-3.00	-2.64		
SI	0.00	-0.42	0.00	-0.46		
LM	-3.00	-3.01	-3.00	-4.56		

Table 5.4. Evaluation results for the test series **TS2**, showing the planned values (”planned”), and the values obtained from the CT evaluation (”CT based”).

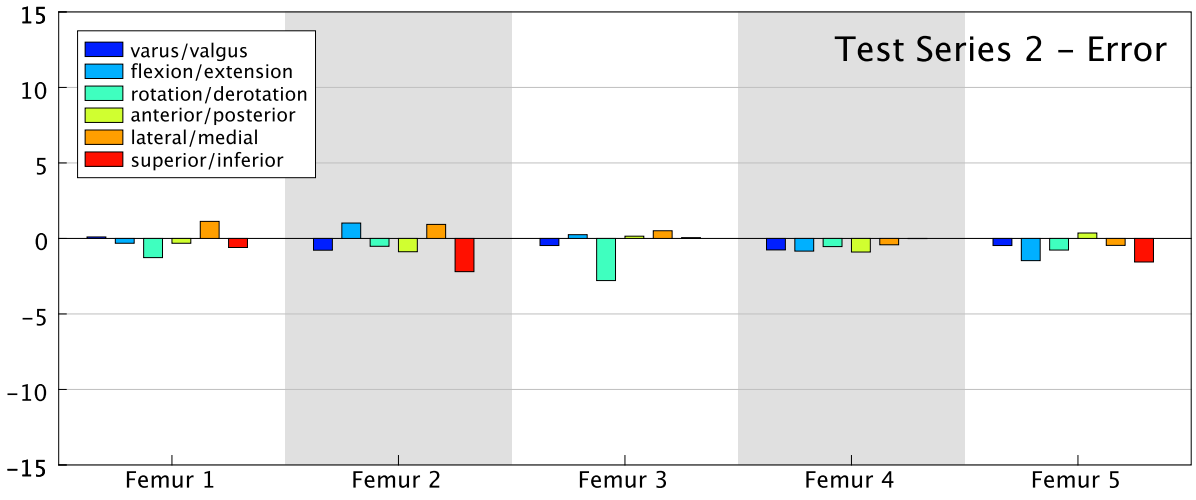

Figure 5.6. Difference of the CT-evaluated result compared to the planned values of **TS2**. For any parameter X (varus, flexion, ...), the graph depicts the value $\Delta = X_{evaluated} - X_{planned}$.

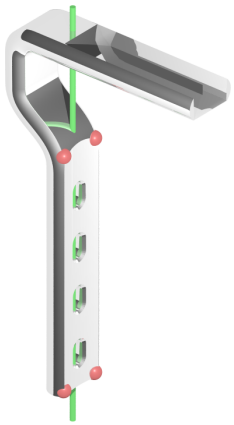

(a) The four points (red) of the plate which were marked in the post-OP CT scans. The central line of the shaft axis is marked green.

(b) The dummy plates used in **TS2** are clearly visible in the CT scans

Figure 5.7. The evaluation of the implant position.

	Femur 1	**Femur 2**	**Femur 3**	**Femur 4**	**Femur 5**
Δ distal end (mm)	3.55	7.16	2.69	2.37	5.57
Δ shaft angle (deg)	1.36	4.43	1.17	1.98	2.86

Table 5.5. Deviations of the measured plate end and shaft angle from the planned values

5.3.3 The Hip Simulator

For the remaining test series, **TS3** to **TS5**, we had a ”hip simulator” built (see Figure 5.8), which allowed the assessment of the system under conditions similar to those in an actual operation. The simulator consisted of the following parts:

- An artificial femur bone, on which the intervention was performed. The simulator was constructed so that the bone could easily be exchanged with every new experiment.
- An artificial pelvis, to which the bone was attached with rubber bands in such a way to allow pivoting movements of the bone inside the acetabulum, thus simulating the functioning of the hip joint. The pelvis itself was mounted to the operating table, simulating an immobilized patient.

- A foam rubber tube which was put over the bone, simulating the soft parts of the leg. The tube had a diameter corresponding to a human leg, and covered the entire proximal part of the femur, including the hip joint.

As opposed to the previous experiments, the test series conducted with the simulator were more realistic in the following ways:

- The visible portion of the femur was reduced to the area which is typically laid open during an operation. This was achieved by making an appropriate incision in the foam rubber. In particular, this measure prevented the surgeon from being able to see the femur neck, thus making the task of gouging the blade channel without perforating the neck isthmus more difficult.
- Through the simulated hip joint, which was additionally fixed to the table, the movements of the femur were restricted to those anatomically possible. Thus, the surgeon's freedom of adjusting the position of the femur to the current task was limited.

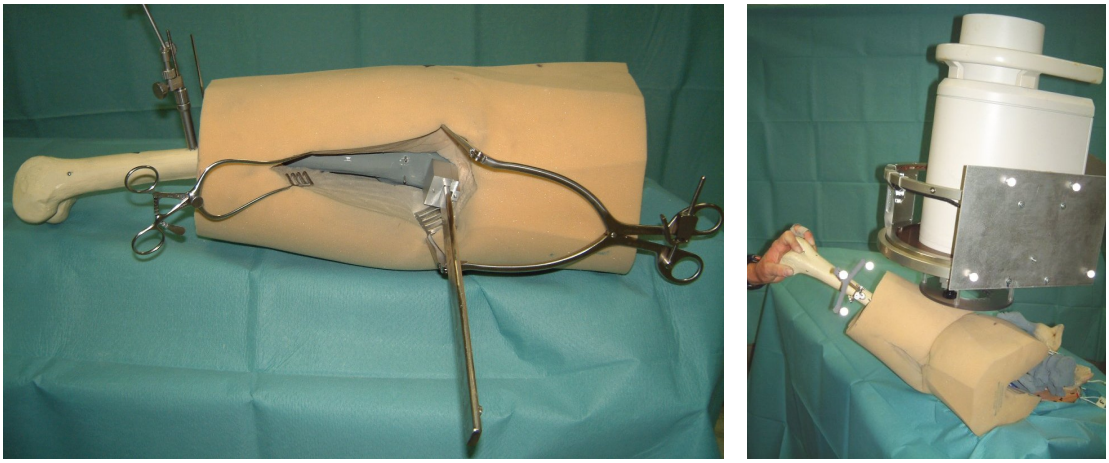

(a) Lateral view of the surgeon onto the simulator (b) Taking of the axial image

Figure 5.8. The hip simulator

5.3.4 Test of the Improved System on the Simulator (TS3)

These tests were performed with the full FEMOS system, including the improvements described in chapter 4. The results of the tests are shown in Table 5.6 and Figure 5.9.

	planned	CT based	planned	CT based	planned	CT based
	Femur 1		Femur 2		Femur 3	
varus	-10.00	-10.93	-10.00	-10.96	-10.00	-10.83
flexion	12.00	11.38	12.00	10.54	12.00	11.02
rotation	-12.00	-15.30	-12.00	-14.80	-12.00	-15.70
AP	-8.00	-9.67	-8.00	-7.66	-8.00	-9.38
SI	-4.00	-5.13	-4.00	-4.00	-4.00	-4.22
LM	0.00	-1.61	0.00	-2.37	0.00	-3.12
	Femur 4		Femur 5			
varus	-10.00	-11.58	-10.00	-9.98		
flexion	12.00	10.20	12.00	11.11		
rotation	-12.00	-14.81	-12.00	-14.31		
AP	-8.00	-8.81	-8.00	-9.71		
SI	-4.00	-5.80	-4.00	-6.38		
LM	0.00	0.38	0.00	-1.82		

Table 5.6. Evaluation results for the test series **TS3**, showing the planned values (”planned”) and the values obtained from the CT evaluation (”CT based”).

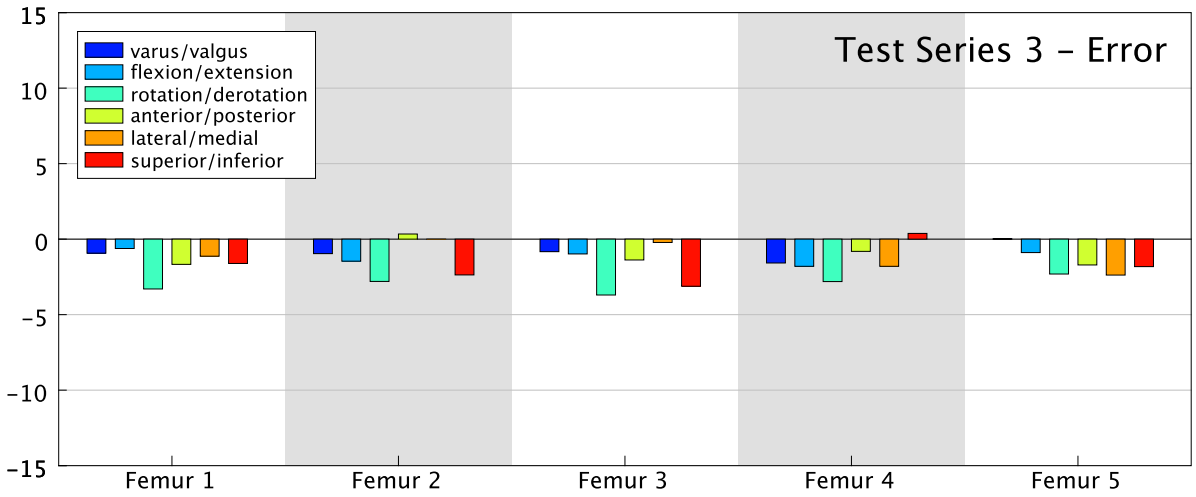

Figure 5.9. Difference of the CT-evaluated result compared to the planned values of **TS3**. For any parameter X (varus, flexion, ...), the graph depicts the value $\Delta = X_{evaluated} - X_{planned}$.

5.3.5 Test of the Basic System on the Simulator (TS4)

These tests were performed with the basic FEMOS system, as described in chapter 3. The results of the tests are shown in Table 5.7 and Figure 5.10.

	planned	CT based	planned	CT based	planned	CT based
	Femur 1		Femur 2		Femur 3	
varus	-10.00	-9.25	-10.00	-9.15	-10.00	-9.93
flexion	12.00	12.77	12.00	12.84	12.00	6.95
rotation	-12.00	-11.14	-12.00	-19.48	-12.00	-13.36
AP	-8.00	-5.87	-8.00	-10.03	-8.00	-5.92
SI	-4.00	-7.52	-4.00	1.53	-4.00	-3.91
LM	0.00	-2.61	0.00	-0.06	0.00	-4.15
	Femur 4		Femur 5			
varus	-10.00	-9.73	-10.00	-10.21		
flexion	12.00	8.94	12.00	13.67		
rotation	-12.00	-6.52	-12.00	-18.79		
AP	-8.00	-5.79	-8.00	-10.15		
SI	-4.00	-6.23	-4.00	-1.19		
LM	0.00	-2.38	0.00	2.32		

Table 5.7. Evaluation results for the test series **TS4**, showing the planned values (”planned”) and the values obtained from the CT evaluation (”CT based”).

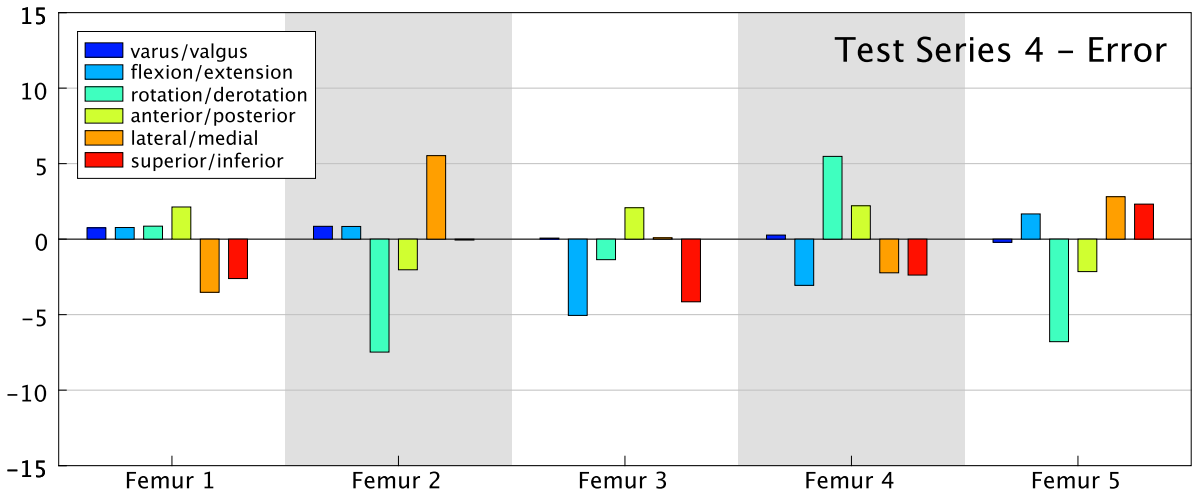

Figure 5.10. Difference of the CT-evaluated result compared to the planned values of **TS4**. For any parameter X (varus, flexion, ...), the graph depicts the value $\Delta = X_{evaluated} - X_{planned}$.

5.3.6 Test Series with the Conventional Method on the Simulator (TS5)

For **TS5**, we had the intervention performed by an experienced surgeon with the conventional technique. This experiment was conducted to be able to assess the improvements regarding accuracy and reproducibility of the FEMOS system as opposed to the conventional approach. Like **TS3** and **TS4**, this test series was performed on the simulator. The operating surgeon, who had not been involved in the development of the system, had a large experience with intertrochanteric osteotomies and related operations, having routinely performed these interventions several hundred times.

In **TS5**, only the rotational parameters were evaluated, as the translations are handled qualitatively with the conventional technique (for example with the goal of leaving the biomechanical axis unchanged), but are never specified numerically.

In contrast to the other test series **TS1..4**, the inverse calculation of the effective osteotomy parameters was done in *sequential mode*, to account for the different way in which the parameters are interpreted with the conventional operating technique (see section 2.4.2 for the difference). Table 5.8 displays the results thus obtained.

	planned	**CT based**	**planned**	**CT based**	**planned**	**CT based**
	Femur 1		Femur 2		Femur 3	
varus	-10.00	-23.06	-10.00	-23.73	-10.00	-18.65
flexion	12.00	10.34	12.00	5.01	12.00	14.94
rotation	-12.00	-9.00	-12.00	-8.47	-12.00	-13.68
	Femur 4		Femur 5			
varus	-10.00	-23.83	-10.00	-19.67		
flexion	12.00	15.12	12.00	14.77		
rotation	-12.00	-17.41	-12.00	-16.62		

Table 5.8. Evaluation results for the test series **TS5**, showing the planned values (”planned”) and the values obtained from the CT evaluation (”CT based”).

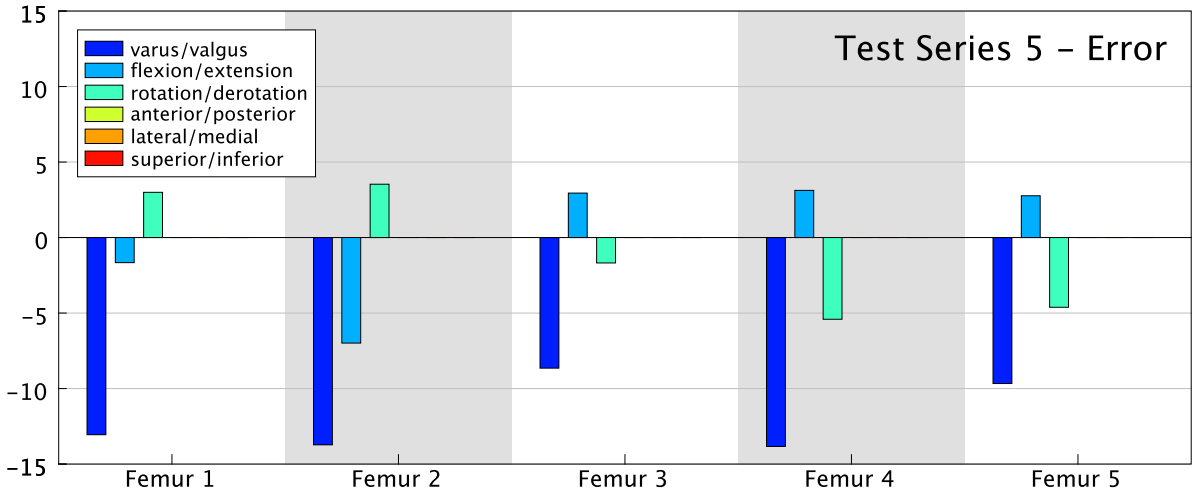

Figure 5.11. Difference of the CT-evaluated result compared to the planned values of **TS5**. For any parameter X (varus, flexion, ...), the graph depicts the value $\Delta = X_{evaluated} - X_{planned}$.

5.4 Discussion of the Results

The tests in this section were evaluated based on CT scans and fluoroscopic images, which were rigidly registered via fiducials. As Figure 5.3 shows, the registration of the CT data sets among themselves was very accurate with a mean error[4] of 0.4mm ($\pm$ 0.08mm, range 0.25mm-0.55mm) for CT pre distal $\rightarrow$ CT post distal and 0.37mm ($\pm$ 0.08mm, range 0.2mm-0.53mm) for CT pre proximal $\rightarrow$ CT post proximal. The registration of the pre CT scan with the fluoroscopic images is somewhat less accurate, with a mean error of 1.14mm ($\pm$ 0.41mm, range 0.48mm-2.17mm). However, as the markers used for registration were distributed over the entire femur, this error is in practice negligible.

Table 5.9 displays a comparison of the results of all test series. Although the various osteotomy parameters (varus/valgus, flexion/extension etc.) are mutually interdependent, it still makes sense to compare them separately, as there are error sources which specifically affect individual parameters (and influence the others, but to a lesser degree). For each test series, the mean error[5] (ME), the standard deviation (SD), the average absolute deviation[6] (AAD), and the absolute error range (AMIN/AMAX) were calculated.

Owing to the costly nature of the tests, it was not possible to conduct more than five individual experiments per test series. Due to the small size of the test series, only a limited

[4]The values given are the means of the values (which are means themselves) shown in Figure 5.3
[5]Note that the mean error has little meaning here, as two errors with different signs may cancel out.
[6]The mean of the absolute error values.

statistical analysis of the test results is possible, so the following discussion focuses mainly on examining some trends observable in the test data.

As can be seen from the diagrams in Figures 5.13, 5.14, 5.15 and 5.16, the overall best results were reached in **TS1**. This was to be expected, as **TS1** was performed under ideal conditions. This proves that the accuracy and precision of the system in itself are very high. The long chain of steps, which involves a number of potential error sources such as calibration of the fluoroscopy device and plate dummy, manual construction of the model, adjustment of the pose shuttle on the adjustment fixture, excision of the wedge and gouging of the channel using the guide templates, and fragment repositioning can be performed accurately enough, so that the result deviates from the plan by a magnitude of less than a degree for the rotational values and around 1mm for the translational ones.

The results of **TS2** are comparable to those of **TS1**, with the mean and maximum absolute error slightly higher for the rotational parameters. Again, the mean absolute error is still below 1 mm/degree for all parameters except one (rotation/derotation). This shows that the very good results of **TS1** could be reproduced with human bones.

Additionally, through the evaluation of the implant position in **TS2** (see Table 5.5), it was demonstrated that the implant matched the predicted position quite well, with an average error of 4.27mm (± 1.83mm) in the position of the distal end of the shaft and an average angular error of 2.36° ($\pm 1.19°$) in the shaft direction. This shows that the use of the plate dummy to indicate the position of the plate on the bone works well.

Comparing the test series **TS3** to **TS4**, which were conducted with the simulator, it becomes obvious that the average absolute deviation of the basic FEMOS system (**TS4**) is about 1.5 to 2 times higher than that of the improved system (**TS3**) in most parameters. The difference in the standard deviations between the two test series is even higher (up to 10 times, with the rotation parameter), which means that the results of **TS3** were much less scattered than those of **TS4**. This probably is an effect of the improved guidance the surgeon received from the templates used in **TS3**, as opposed to the free-handed execution in **TS4**.

For the test conducted with the conventional method (**TS5**), only the rotational parameters were evaluated, as no translational values were specified. Figure 5.13 shows a very high average absolute error for the varus/valgus parameter (11.79°), with a low standard deviation (2.44°). The errors in the other two parameters are comparable in magnitude to those of the test series with the basic FEMOS system (**TS4**).

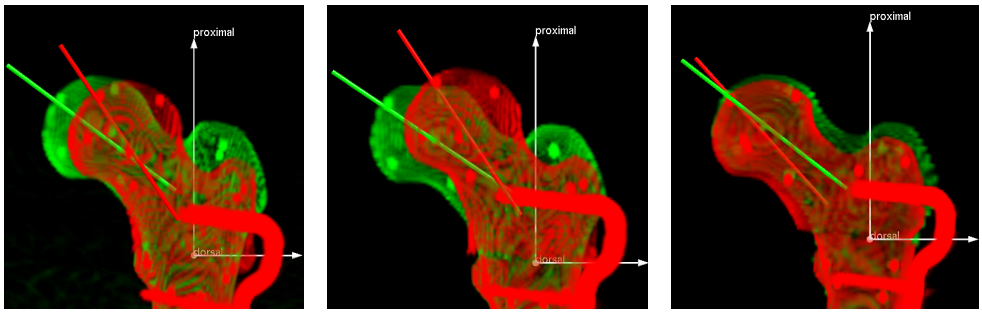

(a) Femur 1 (**TS5**) (b) Femur 2 (**TS5**) (c) Femur 5 (**TS3**)

Figure 5.12. Every image shows the preoperative (green) and the postoperative femur (red) in AP view. Both data sets were registered at their distal parts prior to rendering. The green/red lines are the projected femur neck axes, enclosing the varus/valgus angle.

For a verification of these results, renderings showing the preoperative and postoperative femur in AP view were created from the CT data sets. Figure 5.12 shows the varus/valgus angle of the first two femora of **TS5** (Figure 5.12a and 5.12b). Although the angle, which appears between the red and green lines, is displayed in projection (which, for the conventional method, does not exactly correspond to the value used in the operation, see section 2.4.2), it is nevertheless far too large for a 10° valgization. Figure 5.12c shows a femur from test series **TS3** for comparison, in which the projected angle corresponds exactly to the specified one (10°).

The standard deviation of the rotational values of **TS5** is somewhat higher than that in **TS4** for varus/valgus and flexion/extension, and a bit lower for rotation/derotation. However, by comparing it to the values of **TS3**, it becomes obvious that the use of the FEMOS system makes the intervention much more reproducible with a standard deviation 5 to 8 times lower.

Examining the mean absolute deviation of the results of test series **TS3** and **TS4**, it can be seen that, in both cases, the error in rotation/derotation parameter is the highest. This corresponds well to the observation made during the execution of the tests. While, in spite of the use of the simulator, the handling of the plate dummy and the guide templates in **TS3** did not much differ from that in **TS1** and **TS2**, the final step of fixating the bone fragments in **TS3** proved to be much more difficult. The reason was that, as opposed to **TS1** and **TS2**, the movement of the fragments was constrained by the simulator, and keeping the fragments in correct position was problematic. The main difficulty was maintaining the correct relative rotation during the fixation process, which is reflected in the values as mentioned.

The varus/valgus and flexion/extension angles of **TS1** to **TS3**, on the other hand, display

a rather low mean absolute error of less than 1mm (except for flexion in **TS3** with 1.15mm). Also, the corresponding standard deviations are low with less than 1° in all cases. The reason for this is probably that these two values (as opposed to rotation/derotation) are determined nearly exclusively by the shape of the wedge, which in turn was created using the guide templates in **TS1** to **TS3**.

Finally, as discussed in section 2.2, a critical point of the procedure is the gouging of the blade channel for the implant, with respect to avoiding a perforation of the femur neck corticalis with the chisel from the inside. During the test series conducted with the conventional operating technique (**TS5**), the neck was perforated two in five times. With the FEMOS system, however, no perforation occurred in any of the 20 experiments in which the system was used (**TS1** to **TS4**).

	ME	SD	AAD	AMIN	AMAX	ME	SD	AAD	AMIN	AMAX
			TS1					**TS2**		
varus	-0.07	0.41	0.31	0.07	0.69	-0.48	0.36	0.52	0.10	0.78
flexion	0.09	0.75	0.52	0.03	1.23	-0.27	0.96	0.78	0.25	1.47
rotation	-0.46	0.79	0.72	0.21	1.52	-1.18	0.95	1.18	0.52	2.79
ap	-0.45	1.54	1.26	0.33	2.17	-0.32	0.58	0.52	0.15	0.90
lm	-0.41	0.80	0.69	0.23	1.48	0.34	0.74	0.69	0.42	1.13
si	-0.46	0.43	0.54	0.20	0.82	-0.86	0.99	0.88	0.01	2.20
			TS3					**TS4**		
varus	-0.86	0.57	0.86	0.02	1.58	0.35	0.45	0.43	0.07	0.85
flexion	-1.15	0.47	1.15	0.62	1.80	-0.97	2.93	2.28	0.77	5.06
rotation	-2.98	0.53	2.98	2.31	3.70	-1.86	5.42	4.39	0.86	7.48
ap	-1.05	0.85	1.18	0.34	1.71	0.45	2.32	2.12	2.03	2.21
lm	-1.11	1.01	1.11	0.00	2.38	0.54	3.69	2.84	0.09	5.53
si	-1.71	1.31	1.86	0.38	3.12	-1.38	2.53	2.30	0.06	4.15
			TS5							
varus	-11.79	2.44	11.79	8.65	13.83					
flexion	0.04	4.41	3.50	1.66	6.99					
rotation	-1.04	4.17	3.65	1.68	5.41					
ap	n/a	n/a	n/a	n/a	n/a					
lm	n/a	n/a	n/a	n/a	n/a					
si	n/a	n/a	n/a	n/a	n/a					

Table 5.9. A comparison of the results of the test series. The columns display the mean error (ME), standard deviation of the errors (SD), average absolute deviation (AAD), and minimal/maximal absolute error (AMIN/AMAX) of the test results.

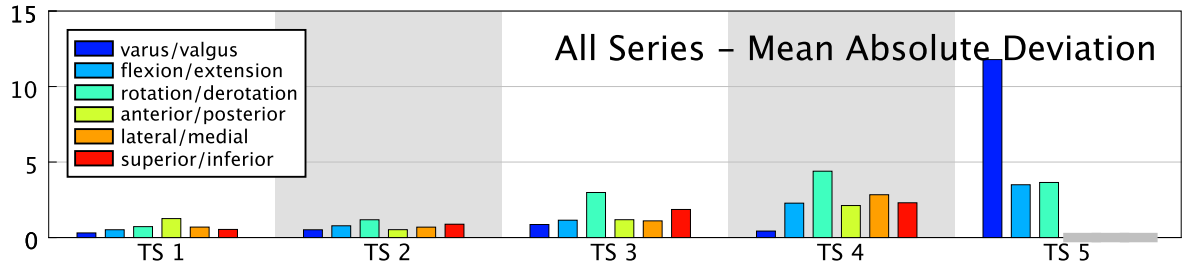

Figure 5.13. The average absolute error (=mean of absolute errors) of the test results.

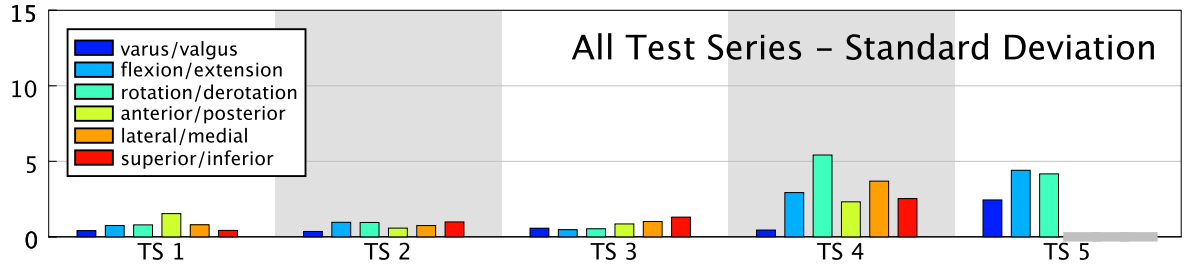

Figure 5.14. The standard deviations of the test series.

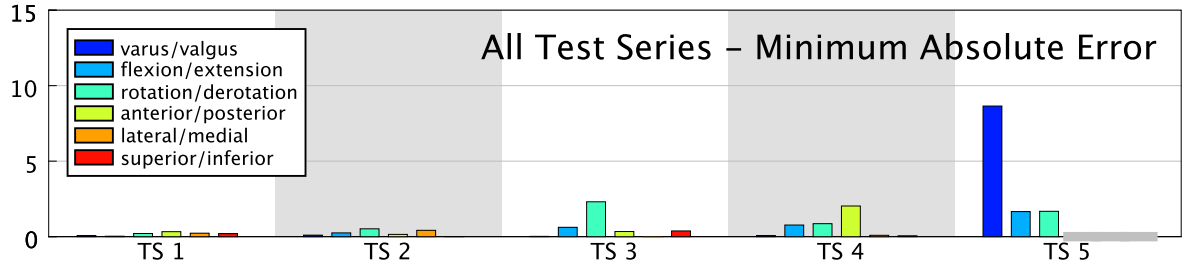

Figure 5.15. The minimum absolute error of the test series.

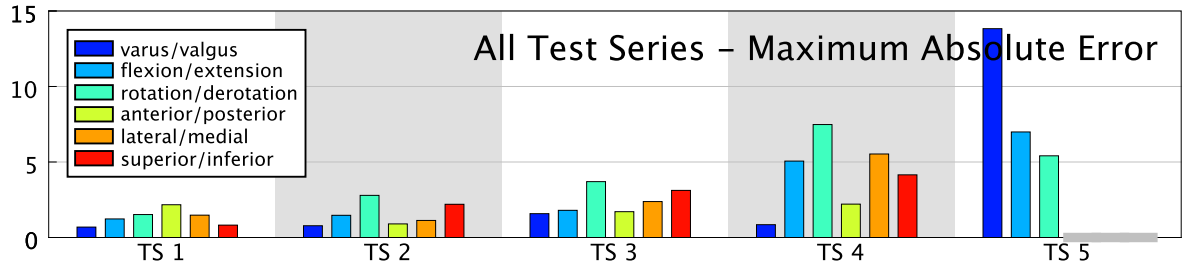

Figure 5.16. The maximum absolute error of the test series.

Chapter 6 Summary and Conclusion

In this thesis, a novel approach for performing intertrochanteric osteotomies of the proximal femur was proposed and evaluated. With the FEMOS system, it is possible to plan an osteotomy solely based on two intraoperatively acquired fluoroscopic images, and perform the intervention accurately with the help of a tracking system. The use of the tracking system was minimized so that the essential parts of the operation can be carried out without depending on the localizer, thereby avoiding problems commonly associated with optical tracking, such as marker occlusion or loosening of the reference tracker. Furthermore, the procedure was designed so as to deviate as little as possible from the conventional method, so that the intervention can be continued without the FEMOS system at any point, if necessary.

The system was tested in-vitro with respect to various aspects, including a comparison with the conventional method performed under identical conditions. The tests demonstrated a significant increase in accuracy and reproducibility over the conventional technique. They also demonstrated that the essential parts of the intervention — the gouging of the blade channel and the cutting of the excision planes — can be performed with very high accuracy, which, however, decreases somewhat with the final step in the procedure, the fixation of the fragments. More work may be needed to secure the highest precision overall, for example an optimization of the instruments used intraoperatively to position the fragments might be helpful.

The system, as described in this thesis, is focused on fluoroscopic images acquired intraoperatively. However, since the amount of information which can be gained from these images is somewhat limited, this may not be sufficient for some cases. Some attempts in this direction are already worked on, but have not yet been developed far enough to be included in this thesis. They shall be briefly mentioned here:

- For the correction of complex multilevel deformities, it may be desirable to plan the intervention based on CT images of the patient. A 3D planning tool with which this can be done was developed in [Bur03a]. The target pose and resection planes determined by

this tool could be imported into the FEMOS system, with which the surgery could then be performed. Of course, this poses the problem of registering the CT data set with the intraoperatively reconstructed model. One idea, yet to be tested, would be to construct an analogous primitive model (femur head, neck shaft axis) from the CT images, and perform the registration through a matching of the two models.

- In case of an aseptic necrosis of the femoral head, an intertrochanteric osteotomy is performed to change the position of the affected area on the femoral head with respect to the acetabulum, so that stress on this area is decreased. For this kind of intervention, it would be useful to visualize the position of the affected area in the planning phase. As this kind of damage is normally not clearly visible in the fluoroscopic images, a solution to this problem would be to mark the affected areas preoperatively in an MR data set, where they are visible, and import their locations into the FEMOS system. Again, it should be possible to solve the problem of registration via constructing the primitive femur model from the MR images.

While these extensions may help to make the system even more versatile, this thesis has demonstrated that the approach realized is already powerful enough to handle a large number of cases, which can be treated with much higher accuracy and reproducibility through the FEMOS system than through any comparative method.

Appendix A Notational Conventions and Mathematical Basics

The FEMOS system is primarily a geometric planning system, which reconstructs a primitive 3D model of the femur bone and performs operations on this model, thereby changing its geometry. This involves a large number of calculations with objects in Euclidean space, such as points, vectors, lines and planes. This section presents the mathematical notation used throughout this thesis for the representation and manipulation these geometrical entities.

A.1 Geometric Primitives

Geometric primitives in this context are objects like points, vectors, planes and lines which are used to specify geometric features. For example, the femur head is represented by a point and its shaft axis by a line.

A.1.1 Vectors

Vectors in 3D space $\mathbb{R}^3$ are denoted by lowercase letters, for example $\vec{a}, \vec{b}, \vec{t}, \vec{u}$ or $\vec{v}$. They represent a direction or a displacement in space, and hence are inherently different from points, which represent locations. This difference has a practical effect on the way transformations are applied to vectors and points (see section A.2). Vector operations such as addition and subtraction are defined as usual.

The vectors $\vec{e}_x := (1,0,0)^{\mathrm{T}}$, $\vec{e}_y := (0,1,0)^{\mathrm{T}}$ and $\vec{e}_x := (0,0,1)^{\mathrm{T}}$ are called *canonical unit vectors*.

A.1.2 Points

Points in 3D space are denoted by uppercase letters such as A, B, C, P, Q, H or N. They represent a location in space.

The point $O = (0, 0, 0)$ is called *origin*.

The addition of a point P and a vector $\vec{v}$ are performed component-wise and yields a point Q, which is the displacement of the original point P by $\vec{v}$, written as follows:

$$Q = P + \vec{v}$$

Subtraction of a vector from a point is defined analogously. Similarly, the subtraction of one point from another point yields the displacement vector $\vec{v}$, equivalent to the above equation:

$$\vec{v} = Q - P$$

The addition of two points is undefined.

A.1.3 Lines

Lines in 3D space are denoted by the letter ℓ and are defined by a pair $(P, \vec{v})$, consisting of the line's base point P and its direction vector $\vec{v}$. The line defined by P and $\vec{v}$ is written $\ell(P, \vec{v})$.

A.1.4 Planes

The letter $\mathcal{E}$ denotes planes, which are typically represented by a 3-tuple $\mathcal{E}(P, \vec{u}, \vec{v})$, consisting of a base point P and two direction vectors $\vec{u}$ and $\vec{v}$, spanning the plane. Alternatively, a plane can be defined by a base point P and its normal vector $\vec{n}$, written as $\mathcal{E}(P, \vec{n})$.

The compound entities like lines and planes are distinguished by their subscripts, for example $\mathcal{E}_{osteo}$ (the osteotomy plane) or ℓ_{shaft}, the shaft axis.

A.2 Geometric Transformations

Geometric transformations are applied to the primitive types like points, vectors, lines and planes. Although the concept of geometric transformations is rather general, only rigid transformations consisting of a translation and a rotation in 3D space are used in the FEMOS system. They can also be interpreted as transformations between two coordinate systems.

For any transformation $\mathbf{X}$, where $\mathbf{X}$ can be a translation, rotation or general pose, the application to one of the primitive types is written using the operator "$\cdot$":

$$P' = \mathbf{X} \cdot P$$

A.2.1 Rotations

The letter $\mathbf{R}$ denotes 3D rotations, which are usually represented as matrices from $\mathbb{R}^{3,3}$. A rotation can be applied to points and vectors by using the common rules for matrix multiplications:

$$P' = \mathbf{R} \cdot P$$

$$\vec{v}' = \mathbf{R} \cdot \vec{v}$$

Three common ways to specify a rotation are:

$\mathbf{R}(\vec{a}, \phi)$ Every rotation can be represented by a pair consisting of a vector $\vec{a}$, defining the axis about which to rotate, and an angle ϕ, specifying the rotation amount. The sense of rotation is usually defined so that rotations by a positive angle appear in clock-wise direction when looked at in the direction of $\vec{a}$.

$\mathbf{R}(\vec{v_1}, \vec{v_2}, \vec{v_3})$ This implicitly specifies a rotation by giving an orthonormal base $\{\vec{v_1}, \vec{v_2}, \vec{v_3}\}$ to which the unit vectors $\{\vec{e_1}, \vec{e_2}, \vec{e_3}\} = \{(1,0,0)^{\mathrm{T}}, (0,1,0)^{\mathrm{T}}, (0,0,1)^{\mathrm{T}}\}$ are mapped so that $\mathbf{R} \cdot \vec{e_i} = \vec{v_i}$ for $i \in \{1,2,3\}$

$\mathbf{R}(\phi, \theta, \psi, d)$ Euler angles, given by the three angular values (ϕ, θ, ψ) and the axis specification $d \in \{\mathbf{X}, \mathbf{Y}, \mathbf{Z}\}^3$, for example $d = \mathbf{XZX}$. The rotation is performed by rotating consecutively by ϕ, θ and ϕ about the axes specified by d, in the given order[1] given by d). For example, the rotation $R(10°, 20°, 30°, \mathbf{XYX})$ defines a rotation about the x axis by $10°$, followed by a rotation about the y axis by $20°$ and a rotation about x (again) by $30°$.

> **Note:** Rotations in the sense used here, denoted by the letter $\mathbf{R}$, always rotate about the origin of the coordinate system. Rotations about arbitrary points can be achieved by combining a "pure" rotation with a translation (see A.2.3).

[1] Traditionally, Euler angles were defined to have the order $\mathbf{ZXZ}$. However, the concept can easily be extended to allow the use of an arbitrary order.

A.2.2 Translations

The letter $\mathbf{T}$ denotes a translational transformation, which can be identified with a vector $\mathbf{T} = \vec{t}$. Thus, $\mathbf{T}$ represents the translation by a vector $\vec{t}$. It should be kept in mind that $\vec{t}$ and $\mathbf{T}$, although closely related, represent two different concepts: $\vec{t}$ is a vector and $\mathbf{T}$ is a transformation which can be applied to geometric primitives using the operator "$\cdot$"[2]

Translations can be applied to points by adding the translation vector using the common rules for vector addition.

$$P' = \mathbf{T} \cdot P := P + \vec{t}$$

> **Note:** Applying a translation to a vector does not change the vector, because a vector represents a direction rather than a location:
>
> $$\vec{v'} = \mathbf{T} \cdot \vec{v} := \vec{v}$$

A.2.3 General Transformations

The letter $\mathbf{M}$ designates a pose, that is, a rigid transformation in 3D space. Every such transformation can be represented uniquely as a pair $\mathbf{M} = (\mathbf{R}, \mathbf{T}) = (\mathbf{R}, \vec{t})$ consisting of a rotation and a translation.

A pose given through its constituent parts $\mathbf{R}$ and $\mathbf{T}$ is applied to points and vectors by consecutively applying the rotation and translation:

$$P' = \mathbf{M} \cdot P = \mathbf{T} \cdot (\mathbf{R} \cdot P) = \mathbf{R} \cdot P + \vec{t}$$

$$\vec{v'} = \mathbf{M} \cdot \vec{v} = \mathbf{T} \cdot (\mathbf{R} \cdot \vec{v}) = \mathbf{R} \cdot \vec{v}$$

As can be seen, the translational part of the pose is ignored when the pose is applied to a vector instead of a point. This makes it easy to define the application of a pose to a plane and a line:

$$\mathcal{E}' = \mathbf{M} \cdot \mathcal{E}(P, \vec{v}, \vec{u}) = \mathcal{E}(\mathbf{M} \cdot P, \mathbf{M} \cdot \vec{v}, \mathbf{M} \cdot \vec{u})$$

[2] While using the dot operator "$\cdot$" in connection with translation may be a bit uncommon, this notation was chosen to be able to conveniently express the concatenation of multiple transformations, for example $\mathbf{T}_1 \cdot \mathbf{R}_1 \cdot \mathbf{T}_2$. Also, this notation is consistent with the idea that a translation is just a special case of a general 6D transformation (see next section).

$$\ell' = \mathbf{M} \cdot \ell(P, \vec{v}) = \ell(\mathbf{M} \cdot P, \mathbf{M} \cdot \vec{v})$$

Rotations and translations themselves can be regarded as special cases of a pose, namely $\mathbf{M}_R = (\mathbf{R}, \mathbf{I})$ and $\mathbf{M}_T = (\mathbf{I}, \mathbf{T})$ with $\mathbf{I}$ being the identity transformation.

A.2.4 Chaining and Inverting Transformations

Transformations can be chained by consecutively applying them in a given order, so that in every step the current transformation is applied to the result of the preceding transformation. For every sequence of transformations $\mathbf{M}_1, \ldots, \mathbf{M}_n$, there exists a single transformation $\mathbf{M}_\Pi(\mathbf{R}_\Pi, \vec{t}_\Pi)$, consisting of one translation and rotation, which has the same effect as the combined sequence (note that the order in which the transformations are applied to P is from rightmost to leftmost):

$$P' = \mathbf{M}_\Pi \cdot P = \mathbf{M}_1 \cdot \mathbf{M}_2 \cdot \ldots \cdot \mathbf{M}_n \cdot P$$

That such a transformation $\mathbf{M}_\Pi$ exists, can easily be verified by observing that, given $\mathbf{M}_1(\mathbf{R}_1, \vec{t}_1)$ and $\mathbf{M}_2(\mathbf{R}_2, \vec{t}_2)$, the following holds for any point P:

$$P' = \mathbf{M}_2 \cdot (\mathbf{M}_1 \cdot P) = \mathbf{R}_2 \cdot (\mathbf{R}_1 \cdot P + \vec{t}_1) + \vec{t}_2 = \underbrace{\mathbf{R}_1 \cdot \mathbf{R}_2}_{\mathbf{R}_\Pi} \cdot P + \underbrace{\mathbf{R}_2 \cdot \vec{t}_1 + \vec{t}_2}_{\vec{t}_\Pi}$$

Also, for any rigid transformation $\mathbf{M}$, there exists an inverse transformation $\mathbf{M}^{-1}$ with the following property ($\mathbf{I}$ is the identity transformation):

$$\mathbf{M}^{-1} \cdot \mathbf{M} = \mathbf{I}$$

A translation $\mathbf{T} = \vec{t}$ is inverted by inverting the vector defining it, $\mathbf{T}^{-1} = -\vec{t}$. For a rotation matrix $\mathbf{R}$, the inverse is the transposed matrix $\mathbf{R}^{-1} = \mathbf{R}^{\mathrm{T}}$. From this it follows that a general transformation $\mathbf{M}$ can be inverted like this:

$$\mathbf{M}(\mathbf{R}, \vec{t})^{-1} = \mathbf{M}(\mathbf{R}^{-1}, -\mathbf{R}^{-1} \cdot \vec{t})$$

A.2.5 Coordinate Systems

A pose can be interpreted in two ways:

- As a transformation *within* a coordinate system which changes the orientation or position of an object. For example, the point P could be translated and rotated in space by the pose $\mathbf{M}$ and end up at the new position $P' = \mathbf{M} \cdot P$. The object now occupies a new location in space.

- As a transformation *between* coordinate system, which converts the coordinates of an object from one coordinate system to another. For example, the point P could be converted from coordinate system CS1 to coordinate system CS2 by the transformation $\mathbf{M}$ so that $P_{[CS2]} = \mathbf{M} \cdot P_{[CS1]}$. In this case, P's location in space has not changed, but the reference frame in which its coordinates are given.

Both interpretations are just two aspects of the same concept. In this thesis, both notions frequently occur. If the location-transforming aspect is to be emphasized, the transformed version of a feature X is written as X', for example

$$H' = \mathbf{M}_{target} \cdot H$$

Poses converting between coordinate systems are written as $\mathbf{M}_{CS1 \to CS2}$. If a feature X is to be converted from coordinate system CS1 to coordinate system CS2, this is indicated in the variable's index, for example

$$P_{[CS2]} = \mathbf{M}_{CS1 \to CS2} \cdot P_{[CS1]}$$

The coordinate system in which a feature is defined can usually be inferred from the context in which it is used. Should this not be the case, the coordinate system will be explicitly given in the index, such as $H_{[CS1]}$ or $\mathcal{E}_{osteo[CS2]}$.

A special case are poses themselves: interpreted as a location-changing transformation, a pose $\mathbf{M}_{foo[CS1]}$ operates in a given coordinate system CS1, that is, can be applied to objects themselves specified in CS1. Sometimes, however, it is necessary to express the same pose in another coordinate system, CS2, so that it operates on objects given in CS2. The sought-after pose $\mathbf{M}_{foo[CS2]}$ can be constructed as follows:

$$\mathbf{M}_{foo[CS2]} = \mathbf{M}_{CS1 \to CS2} \cdot \mathbf{M}_{foo[CS1]} \cdot \mathbf{M}_{CS2 \to CS1}$$

That is, an entity X given in CS2, to which the pose $\mathbf{M}_{foo[CS2]}$ is applied, will first be converted from CS2 to CS1, then the pose $\mathbf{M}_{foo[CS1]}$ is applied, and the transformed object is converted back from CS1 to CS2.

A.3 Functions

This section defines a few functions, which are later used in the calculations.

- The dot product of two vectors:

$$<,>: \quad (\vec{u},\vec{v}) \quad \rightarrow \quad <\vec{u},\vec{v}>= u_1v_1 + u_2v_2 + u_3v_3$$

- The cross product of two vectors. The cross product $\vec{w} := \vec{v} \times \vec{u}$ has the property of being perpendicular to both $\vec{u}$ and $\vec{v}$:

$$\times: \quad (\vec{u},\vec{v}) \quad \rightarrow \quad \vec{u} \times \vec{v} = \begin{pmatrix} u_2v_3 - u_3v_2 \\ u_3v_1 - u_1v_3 \\ u_1v_2 - u_2v_1 \end{pmatrix}$$

- Vector normalization:

$$\text{normalize}: \quad v \quad \rightarrow \quad \tfrac{1}{|v|}v$$

- Angle between two vectors:

$$\text{angle}: \quad (u,v) \quad \rightarrow \quad \text{angle between } u \text{ and } v$$

- Determine an angle from its known sine and cosine (this function guarantees that $\text{atan2}(\sin\phi, \cos\phi) = \phi$ in the entire range $\phi \in [-\pi;\pi[$, as opposed to $\arcsin$ or $\arccos$ alone, where for example $\arcsin\sin\pi = 0 \neq \pi$, by taking into account the quadrant of the result by inspecting the signs of its arguments).

$$\text{atan2}: \quad (sin\phi, cos\phi) \quad \rightarrow \quad \phi$$

- Intersection of two objects.

$$\text{intersect}: \quad (X_1, X_2) \quad \rightarrow \quad \text{intersection of } X_1 \text{ and } X_2$$

This function is meant to work on a pair of geometrical objects X_1 and X_2, such as two planes, two lines, one line and one plane or two otherwise defined objects. If relevant, special cases are mentioned in the text (like skew lines in 3D or two planes being parallel or identical). However, this function is assumed to work for the ”normal” case, like a line and a plane intersecting in one point etc.

The types of intersections occurring in this thesis can all be solved with elementary analytical geometry. Their solution is not discussed in detail.

- General projection of a vector $\vec{v}$ onto a plane $\mathcal{E}$ given through a point and a normal vector:

$$\text{proj}: \quad (\vec{v}, (P, \vec{n})) \quad \rightarrow \quad \vec{v} - < \vec{n}, \vec{v} > \cdot \vec{n}$$

- Rotation about an arbitrary axis. Rotations as described in section A.2.1 are ”pure” rotations, in that their axis of rotation always contains the origin. Rotations by an angle ϕ about an arbitrary axis in 3D space $\ell_{axis} = (A, \vec{d})$, given through a base point A and a direction vector $\vec{d}$, must be constructed by combining a pure rotation with two translations, which is done by the function ”axisrotate”:

$$\text{axisrotate}: \quad (A, \vec{d}, \phi) \quad \rightarrow \quad \mathbf{T}(A - O) \cdot \mathbf{R}(\vec{d}, \phi) \cdot \mathbf{T}(O - A)$$

The ”axisrotate” function yields a general transformation, consisting of the following components:

  - The translation $\mathbf{T}(O - A)$ by a vector $\vec{t} := O - A$, which maps the base point of the rotation axis to the origin
  - The pure rotation $\mathbf{R}(\vec{d}, \phi)$, which rotates by ϕ about an axis defined by the origin and the direction vector $\vec{d}$
  - The translation $\mathbf{T}(A - O)$, by the vector $-\vec{t}$, which maps the origin back to the original base point

Bibliography

[Ami00] LP. Amiot, K. Lang, M. Putzier, H. Zippel & H. Labelle. *Comparative Results Between Conventional And Computer-Assisted Pedicle Screw Installation in the Thoracic, Lumbar, And Sacral Spine.* Spine., vol. 25, 2000.

[Bat04] H. Bathis, L. Perlick, M. Tingart, C. Luring, D. Zurakowski & J. Grifka. *Alignment in Total Knee Arthroplasty. A Comparison of Computer-Assisted Surgery with the Conventional Technique*. Journal of Bone and Joint Surgery, vol. 86, 2004.

[Bau86] R. Baumgartner, P. E. Ochsner & A. Schreiber. *Checkliste Orthopädie*. 1986.

[Bra99] Christian Brack. *Röntgenbasierte Navigation von chirurgischen Werkzeugen in der Orthopädie*. PhD thesis, Technische Universität München, 1999.

[Bur03a] R. Burgkart, C. Brossmann, M. Layer, E. Bartels, J. Dreer, A. Schweikard & R. Gradinger. *A New Method for an Intuitive Surgical Planning System for 3D Correction- Osteotomies of Bony Deformations*. Medicine Meets Virtual Reality, vol. 11, 2003.

[Bur03b] Stefan Burkhardt. *Orthopädische Navigation auf Basis von Kernspin-Datensätzen*. PhD thesis, Technische Universität München, 2003.

[Bur05] R. Burgkart, H. Gottschling, M. Roth, R. Gradinger & A. Schweikard. *Fluoroskopie-basierte 3D-Navigation komplexer Korrekturosteotomien des proximalen Femurs*. Der Orthopäde, vol. 34, pages 1137–1143, 2005.

[Cro00] H. Croitoru, Randy E. Ellis, Carolyn F. Small & David R. Pichora. *Fixation-Based Surgery: A New Technique for Distal Radius Osteotomy.* In MICCAI, pages 1126–1135, 2000.

[Eyk02] J. C. Eyke, J. E. Ricciardi, W. Roesch & T. Whitecloud. *Computer-Assited Virtual Fluoroscopy*. The University of Pennsylvania Orthopaedic Journal, vol. 15, 2002.

[Got05] H Gottschling, M Roth, A Schweikard & R Burgkart. *Intraoperative, Fluoroscopy-Based Planning for Complex Osteotomies of the Proximal Femur*. The International Journal of Medical Robotics and Computer Assisted Surgery, vol. 1, no. 3, 2005.

[Gun00] A. R. Gunkel, W. F. Thumfahrt & W. Freysinger. *Computerunterstützte 3D-Navigationssysteme*. HNO, vol. 48, 2000.

[Han99] H. Handels, J. Ehrhardt, W. Plotz & S. J. Poppl. *Computer-Assisted Planning and Simulation of Hip Operations Using Virtual Three-Dimensional Models*. Studies in Health Technology and Informatics, vol. 68, 1999.

[Har00] Richard Hartley & Andrew Zisserman. *Multiple-View Geometry in Computer Vision*. Cambridge University Press, 2000.

[Has02] J. Hassenpflug & M. Prymka. *Navigation und Robotik in der Gelenk- und Wirbelsäulenchirurgie,* chapter "Valgisierende Tibiakopfosteotomie - Möglichkeiten für den Einsatz eines Navigationssystems", pages 351–355. Springer, Berlin, 2002.

[Haz03] Eric Hazan & Leo Joskowicz. *Computer-Assisted Image-Guided Intramedullary Nailing of Femoral Shaft Fractures*. Techniques in Orthopaedics, vol. 18, 2003.

[Hof99] R. Hofstetter, M. Slomczykowski, M. Sati & L.-P. Nolte. *Fluoroscopy as Imaging Means for Computer-Assisted Surgical Navigation*. Computer Aided Surgery, vol. 4, 1999.

[Hor87] B. Horn. *Closed-Form Solution of Absolute Orientation Using Unit Quaternions*. Journal of the Optical Society of America, vol. 4, pages 629–641, 1987.

[Hub03] R. Hube, A. Birke, W. Hein & S. Klima. *CT-based and fluoroscopy-based navigation for cup implantation in total hip arthroplasty*. Surgical Technology International, vol. 11, 2003.

[Imh57] G. Imhaeuser. *Zur Pathogenese und Therapie der jugendlichen Hüftkopflösung*. Zeitschrift für Orthopädie, vol. 88, pages 3–41, 1957.

[Jos98] Leo Joskowicz, Charles Milgrom, Ariel Simkin, Lana Tockus & Ziv Yaniv. *FRACAS: A System for Computer-Aided Image-Guided Long Bone Fracture Surgery*. Computer Aided Surgery, vol. 3, 1998.

[Kep04] P. Keppler, F. Gebhard, PA. Grutzner, G. Wang, G. Zheng, T. Hufner, S. Hankemeier & LP. Nolte. *Computer Aided High Tibial Open Wedge Osteotomy.* Injury, vol. 35, 2004.

[Kha00] Rasool Khadem, Clement C. Yeh, Mohammad Sadeghi-Tehrani, Michael R. Bax, Jeremy A. Johnson, Jacqueline Nerney Welch, Eric P. Wilkinson & Rahmih Shahidi. *Comparative Tracking Error Analysis of Five Different Optical Tracking Systems*. Computer Aided Surgery, vol. 5, pages 98–107, 2000.

[Kor00] J. Kordelle, C. Mamisch, R. Kikinis & R. Seipel zand J. Richolt. *Anatomical Analysis and Preoperative Planning of Correctional Osteotomies*. Minimally Invasive Therapy and Allied Technologies, vol. 9, pages 269–276, 2000.

[Kra76] W. G. Kramer, W. A. Craig & S. Noel. *Compensating Osteotomy at the Base of the Femoral Neck for Slipped Capital Femoral Epiphysis*. Journal of Bone and Joint Surgery, vol. 58(6), pages 796–800, 1976.

[Lai00] T. Laine, T. Lund, M. Ylikoski, J. Lohikoski & D. Schlenzka. *Accuracy of Pedicle Screw Insertion with And Without Computer Assistance: a Randomised Controlled Clinical Study in 100 Consecutive Patients.* European Spine Journal, vol. 9, 2000.

[Lan02] Frank Langlotz. *State-of-the-art in Orthopaedic Surgical Navigation with a Focus on Medical Image Modalities*. The Journal of Visualization and Computer Animation, vol. 13, 2002.

[Ma 99] B. Ma, R. E. Ellis & David J. Fleet. *Spotlights: A Robust Method for Surface-Based Registration in Orthopedic Surgery*. In MICCAI, pages 936–944, 1999.

[Men97] F. Menschik. *The Hip Joint as a Conchoid Shape*. Journal of Biomechanics, vol. 30, no. 9, pages 971–973, 1997.

[Mer98] P. Merloz, J. Tonetti, L. Pittet, M. Coulomb, S. Lavallee & P. Sautot. *Pedicle Screw Placement Using Image Guided Techniques.* Clin Orthopaedics and Related Research, vol. 354, 1998.

[Moc95] Jose Luis Moctezuma de la Barrera. *Ein durchgängiges System zur computer- und roboterunterstützten Chirurgie*. PhD thesis, Technische Universität München, 1995.

[Nis89] K. Nishiyama, T. Sakamaki & Y. Ishii. *Follow-up Study of the Subcapital Wedge Osteotomy for Severe Chronic Slipped Capital Femoral Epiphysis*. Journal of Pediatric Orthopaedics, vol. 9, pages 412–416, 1989.

[Nol00] L. P. Nolte, M. A. Slomczykowski, U. Berlemann, M. J. Strauss, R. Hofstetter, D. Schlenzka, T. Laine & T. Lund. *A New Approach To Computer-aided Spine Surgery: Fluoroscopy-based Surgical Navigation.* European Spine Journal, vol. 9, 2000.

[Pal02] Dror Paley. *Principles of Deformity Correction*. Springer, 2002.

[Sch01] Sebastien Schmerber & Fabrice Chassat. *Accuracy Evaluation of a CAS System: Laboratory Protocol and Results with 6D Localizers, and Clinical Experiences in Otorhinolaryngology*. Computer Aided Surgery, vol. 6, 2001.

[Sho94] Ken Shoemake. *Graphic Gems IV*, chapter III.5, pages 222–229. Morgan Kaufmann, San Francisco, 1994.

[Sim97] David Simon. *Intra-Operative Position Sensing and Tracking Devices*. In Proceedings of the First Joint CVRMed / MRCAS Conference, pages 62–64, June 1997.

[Spa03] M. Sparmann, B. Wolke, H. Czupalla, D. Banzer & A.Zink. *Positioning of Total Knee Arthroplasty with And Without Navigation Support. A Prospective, Randomised Study.* Journal of Bone and Joint Surgery, vol. 85, 2003.

[Suh] N. Suhm, A. L. Jacob, L.-P. Nolte, P. Regazzoni & P. Messmer. *Surgical Navigation Based on Fluoroscopy - Clinical Application for Computer-Assisted Distal Locking of Intramedullary Nails*. Computer Aided Surgery, vol. 5.

[Tso98] C. Y. Tso, R. E. Ellis, J. Rudan & M. M. Harrison. *A Surgical Planning and Guidance System for High Tibial Osteotomies*. In MICCAI '98: Proceedings of the First International Conference on Medical Image Computing and Computer-Assisted Intervention, pages 39–50, London, UK, 1998. Springer-Verlag.

[Via95] W. Viant & R. Phillips. *A Computer Assisted Orthopaedic System for Distal Locking of Intramedullary Nails*, 1995.

[Wan04] Gongli Wang, Guoyan Zheng, Paul Alfred Grützner, Jan von Recum & Lutz-Peter Nolte. *A CT-Free Intraoperative Planning and Navigation System for High Tibial Dome Osteotomy.* In MICCAI (2), pages 610–620, 2004.

[Wes04] Jay B. West & Calvin R. Maurer Jr. *Designing Optically Tracked Instruments for Image-Guided Surgery.* IEEE Trans. Med. Imaging, vol. 23, no. 5, pages 533–545, 2004.

[Woo97] M. Woo, J. Neider & T. Davis. *OpenGL Programming Guide, Second Edition*, 1997.

[Zhe02] G. Zheng, A. Marx, U. Langlotz, K. H. Widmer, M. Buttaro & L. P. Nolte. *A Hybrid CT-Free Navigation System for Total Hip Arthroplasty*. Computer Aided Surgery, vol. 7, 2002.